2011

COMPUTER SIMULATION OF A HOLLOW-FIBER BIOREACTOR: HEPARAN REGULATED GROWTH FACTORS-RECEPTORS BINDING AND DISSOCIATION ANALYSIS

Changjiang Zhang
University of Kentucky, changjiang_z@hotmail.com

ABSTRACT OF DISSERTATION

Changjiang Zhang

The Graduate School

University of Kentucky

2011

COMPUTER SIMULATION OF A HOLLOW-FIBER BIOREACTOR: HEPARAN REGULATED GROWTH FACTORS-RECEPTORS BINDING AND DISSOCIATION ANALYSIS

ABSTRACT OF DISSERTATION

A dissertation submitted in partial fulfillment of the
requirements for the degree of Doctor of Philosophy in the
College of Engineering
at the University of Kentucky

By

Changjiang Zhang

Lexington, Kentucky

Director: Jun Zhang, Ph.D., Professor of Computer Science

Lexington, Kentucky

2011

ABSTRACT OF DISSERTATION

COMPUTER SIMULATION OF A HOLLOW-FIBER BIOREACTOR: HEPARAN REGULATED GROWTH FACTORS-RECEPTORS BINDING AND DISSOCIATION ANALYSIS

This thesis demonstrates the use of numerical simulation in predicting the behavior of proteins in a flow environment.

A novel convection-diffusion-reaction computational model is first introduced to simulate fibroblast growth factor (FGF-2) binding to its receptor (FGFR) on cell surfaces and regulated by heparan sulfate proteoglycan (HSPG) under flow in a bioreactor. The model includes three parts: (1) the flow of medium using incompressible Navier-Stokes equations; (2) the mass transport of FGF-2 using convection-diffusion equations; and (3) the cell surface binding using chemical kinetics. The model consists of a set of coupled nonlinear partial differential equations (PDEs) for flow and mass transport, and a set of coupled nonlinear ordinary differential equations (ODEs) for binding kinetics. To handle pulsatile flow, several assumptions are made including neglecting the entrance effects and an approximate analytical solution for axial velocity within the fibers is obtained. To solve the time-dependent mass transport PDEs, the second order implicit Euler method by finite volume discretization is used. The binding kinetics ODEs are stiff and solved by an ODE solver (CVODE) using Newton's backward differencing formula. To obtain a reasonable accuracy of the biochemical reactions on cell surfaces, a uniform mesh is used. This basic model can be used to simulate any growth factor-receptor binding on cell surfaces on the wall of fibers in a bioreactor, simply by replacing binding kinetics ODEs.

Circulation is an important delivery method for natural and synthetic molecules, but microenvironment interactions, regulated by endothelial cells and critical to the molecule's fate, are difficult to interpret using traditional approaches. Growth factor capture under flow is analyzed and predicted using computer modeling mentioned above and a three-dimensional experimental approach that includes pertinent circulation characteristics such as pulsatile flow, competing binding interactions, and limited bioavailability. An understanding of the controlling features of this process is desired. The experimental module consists of a bioreactor with synthetic endothelial-lined hollow fibers under flow. The physical design of the system is incorporated into the model parameters. FGF-2 is used for both the experiments and simulations. The

computational model is based on the flow and reactions within a single hollow fiber and is scaled linearly by the total number of fibers for comparison with experimental results. The model predicts, and experiments confirm, that removal of heparan sulfate (HS) from the system will result in a dramatic loss of binding by heparin-binding proteins, but not by proteins that do not bind heparin. The model further predicts a significant loss of bound protein at flow rates only slightly higher than average capillary flow rates, corroborated experimentally, suggesting that the probability of capture in a single pass at high flow rates is extremely low. Several other key parameters are investigated with the coupling between receptors and proteoglycans shown to have a critical impact on successful capture. The combined system offers opportunities to examine circulation capture in a straightforward quantitative manner that should prove advantageous for biological or drug delivery investigations.

For some complicated binding systems, where there are more growth factors or proteins with competing binding among them moving through hollow fibers of a bioreactor coupled with biochemical reactions on cell surfaces on the wall of fibers, a complex model is deduced from the basic model mentioned above. The fluid flow is also modeled by incompressible Navier-Stokes equations as mentioned in the basic model, the biochemical reactions in the fluid and on the cell surfaces are modeled by two distinctive sets of coupled nonlinear ordinary differential equations, and the mass transports of different growth factors or complexes are modeled separately by different sets of coupled nonlinear partial differential equations. To solve this computationally intensive system, parallel algorithms are devised, in which all the numerical computations are solved in parallel, including the discretization of mass transport equations and the linear system solver Stone's Implicit Procedure (SIP). A parallel SIP solver is designed, in which pipeline technique is used for LU factorization and an overlapped Jacobi iteration technique is chosen for forward and backward substitutions. For solving binding equations ODEs in the fluid and on cell surfaces, a parallel scheme combined with a sequential CVODE solver is used. The simulation results are obtained to demonstrate the computational efficiency of the algorithms and further experiments need to be conducted to verify the predictions.

KEYWORDS: Numerical simulation, laminar convection diffusion flow, mass transport, fibroblast growth factor and receptor binding, parallel computing

Changjiang Zhang

September 15, 2011

COMPUTER SIMULATION OF A HOLLOW-FIBER BIOREACTOR: HEPARAN REGULATED GROWTH FACTORS-RECEPTORS BINDING AND DISSOCIATION ANALYSIS

By

Changjiang Zhang

Jun Zhang, Ph.D.

Director of Dissertation

Raphael Finkel, Ph.D.

Director of Graduate Studies

September 15, 2011

Date

RULES FOR THE USE OF DISSERTATIONS

Unpublished dissertations submitted for the Doctor's degree and deposited in the University of Kentucky Library are as a rule open for inspection, but are to be used only with due regard to the rights of the authors. Bibliographical references may be noted, but quotations or summaries of parts may be published only with the permission of the author, and with the usual scholarly acknowledgements.

Extensive copying or publication of the dissertation in whole or in part also requires the consent of the Dean of the Graduate School of the University of Kentucky.

A library that borrows this dissertation for use by its patrons is expected to secure the signature of each user.

Name	Date

DISSERTATION

Changjiang Zhang

The Graduate School

University of Kentucky

2011

COMPUTER SIMULATION OF A HOLLOW-FIBER BIOREACTOR: HEPARAN REGULATED GROWTH FACTORS-RECEPTORS BINDING AND DISSOCIATION ANALYSIS

DISSERTATION

A dissertation submitted in partial fulfillment of the
requirements for the degree of Doctor of Philosophy in the
College of Engineering
at the University of Kentucky

By

Changjiang Zhang

Lexington, Kentucky

Director: Jun Zhang, Ph.D., Professor of Computer Science

Lexington, Kentucky

2011

ACKNOWLEDGEMENTS

It took five years for me to finish this dissertation. During these five years of study at the University of Kentucky, I encountered many difficulties in my academic study. Thanks to all kinds of support, help, and encouragement from my advisor, collaborators, and friends around me, I managed to finish this dissertation.

First, I would like to thank my academic advisor, Dr. Jun Zhang, who has inspired and encouraged me to conduct research in computer modeling and simulation, and led me to the area of bioinformatics and computational biology, a totally new area to me. Dr. Zhang has been a great mentor on every account, and his broad knowledge and constructive suggestions to this dissertation are sincerely appreciated.

Second, I would like to thank other faculty members of my Advisory Committee: Dr. Zongming Fei (Department of Computer Science), Dr. Jerzy W. Jaromczyk (Department of Computer Science), and Dr. Fuqian Yang (Department of Chemical and Materials Engineering), for their insightful comments and invaluable suggestions on this work. I would also like to thank the outside examiner Dr. Daniel Lau (Department of Electrical and Computer Engineering) for taking the time to review this document and his helpful comments on this dissertation.

Third, I would like to express my appreciation to my research collaborators, Dr. Wensheng Shen, Department of Computational Science, SUNY Brockport, for his outstanding work for the modeling of this research and initial basic program, Dr. Michael Fannon, Department of Ophthalmology and Visual Sciences, University of Kentucky, for his invaluable comments on this dissertation and interesting introduction in biology, Dr. Kimberly Forsten-Williams, Department of Chemical Engineering, Virginia Polytechnic Institute and State University, for her great mentor on building binding kinetics models, invaluable comments and suggestions on conducting the simulations, and Dr. Bing Zhao, Department of Ophthalmology and Visual Sciences, University of Kentucky, for her collaboration in providing all the experimental data and verifi-

cations.

Fourth, I would like to thank all members during my study in the Laboratory for High Performance Scientific Computing & Computer Simulation, Dr. Yin Wang, Dr. Jie Wang, Dr. Xuwei Liang, Mr. Ning Cao, Mr. Dianwei Han, Mr. Qi Zhuang, Mr. Lian Liu, Mr. Pengpeng Lin, Ms. Ruxin Dai, Mr. Nirmal Thapa, and Mr. Xiwei Wang, for creating a friendly working environment together and their helpful discussions and suggestions.

Finally, I would like to thank my family members. I thank my parents for their long lasting support of my education. Most importantly, I thank my dear wife, Mou Zhou, and my two lovely sons, Jeffrey Zhang and Eric Zhang, for their endless love, ever-lasting support, and great patience during my graduate study at Lexington, KY toward my Ph.D. degree in Computer Science.

The research work with this dissertation was fully supported by:

- U.S. National Institutes of Health (NIH-HL086644).

I would like to express my gratitude to this funding agency that has provided the financial support.

Table of Contents

List of Tables

List of Figures

List of Files

1 Introduction

The purpose of this chapter is to state the motivation of the proposed dissertation research and give an introduction to computer modeling and simulation in the areas of fluid dynamics, mass transfer, chemical reaction, cellular and molecular biochemistry. Simulation models are usually described by coupled nonlinear partial differential equations (PDEs) for fluid dynamics and mass transfer, and ordinary differential equations (ODEs) for chemical reaction and cellular and molecular biochemistry.

By Moore's law, the number of transistors that can be placed inexpensively on an integrated circuit doubles approximately every two years. This trend has continued for more than half a century, and it is expected to continue until 2015 or 2020 or later [42, 51]. Today, computer capacity (processing speed, memory capacity, etc.) is growing much more rapidly. High performance desktop computers, even laptops with multi-core processors and graphics processing unit (GPU) technology, are commonly used in homes, offices and research laboratories. These computers have more powerful computational capacity than most middle-sized mainframe computers from the 1970's and 80's. Problems that take a few minutes or even seconds of CPU time using today's computers would have taken years to complete using computers available two decades ago [1]. In the meantime, computational cost has been reduced constantly and substantially. According to current investigation, expenses for a given task have been reduced by a factor of ten every eight years [8].

A direct consequence of this trend is that the modeling and simulation of complex phenomena, such as multi-dimensional molecular binding that couples fluid flow and chemical reactions, is made possible in practice. Most costly computer simulations and visualizations running on high performance computers (cluster machines or even personal computers) have become a reality. Technological advancement in computer science had led to the rapid development of bioinformatics and computational system

biology.

1.1 Motivation

Traditionally, research on fluid dynamics, mass transfer, chemical reaction, cellular and molecular biochemistry has depended heavily on experimental and theoretical approaches. The advantages of these two approaches are that the experimental approach produces more realistic results and the theoretical approach gives a clean solution in formula form. However, both of these have some drawbacks. For the experimental approach, test equipment is required and expensive in some cases. For example, measurement in wind tunnel experiments is difficult and costly. Sometimes, it is even impractical to perform experiments or measurements, like *in vivo* diagnostics related to human beings or drug delivery research in human blood vessels or capillaries. Instead, *in vitro* experiments and/or numerical simulations are used as alternatives. The theoretical approach is usually restricted to simple geometries and linear problems, and therefore it is not possible to obtain a theoretical solution for most complicated geometries and nonlinear problems.

The numerical method, however, can overcome many of the drawbacks related to experimental and theoretical approaches. It can cut the cost of experiments, apply it to complicated nonlinear problems, and obtain a transient solution. Although it may have some drawbacks, such as modeling issues, numerical errors, convergence and stability issues, boundary conditions, etc. [1], these issues are easily recognized and can be avoided in most cases.

One of the most important topics of this dissertation is the numerical simulation of laminar convection-diffusion-reaction pulsatile flow in a bioreactor, an *in vitro* experimental apparatus for cellular study. Since the flow in human blood vessels or capillaries has similar properties, it can be used as a complementary tool to simulate biochemical reactions *in vitro*. Examples of the applications include drug delivery and

tumor therapy research in human blood vessels or capillaries, which are beneficial to the health care of human beings.

Though there are several commercial software packages on the market that could be used for similar research purposes, such as COMSOL®, these packages are either too costly or too general, and can not be used for specific needs. In this research work, we develop a software package to complement experiments, in order to study biochemical processes, such as growth factors-receptors binding and dissociation analysis in a bioreactor flow environment.

1.2 Modeling Procedure

The procedures involved in modeling and simulation usually include four steps [74]:
(1) set up a mathematical model;
(2) rewrite the mathematical model for computer simulation;
(3) develop a computer program;
(4) verify simulation results.
Generally, computer simulation often incurs a very low cost, though an initial cost is required to develop a simulation program or purchase commercial simulation software. It should be recognized that once a simulation program is created, the cost in subsequent studies is usually negligible. Also, it is easy to modify the simulation program to handle different situations.

This research focuses on the modeling and simulation of physical, biochemical and cellular binding kinetics processes in flow conditions, which are governed by partial differential equations (PDEs) and ordinary differential equations (ODEs). So, the first step in the modeling procedure is to derive a set of PDEs or ODEs as the mathematical model.

For flow dynamics and mass transport equations, they are usually defined by a set of second-order partial differential equations. A general second-order partial

differential equation in a standard form in a 2D Cartesian coordinate system can be written as [1]:

$$a(x,y)u_{xx} + b(x,y)u_{xy} + c(x,y)u_{yy} + d(x,y)u_x + e(x,y)u_y + f(x,y)u = g(x,y) \quad (1.1)$$

where $a(x,y)$, $b(x,y)$, $c(x,y)$, $d(x,y)$, $e(x,y)$, and $f(x,y)$ are functions of (x,y).

Eq. (1.1) can be classified as hyperbolic, parabolic and elliptic, based on the values of a, b and c. The PDE is hyperbolic if $b^2 - 4ac > 0$, parabolic if $b^2 - 4ac = 0$ and elliptic if $b^2 - 4ac < 0$. Hyperbolic or parabolic PDEs govern initial value or initial boundary value problems, which are frequently called marching or propagation problems. Elliptic PDEs govern boundary value problems, or equilibrium problems, which include steady-state temperature distributions, incompressible inviscid flow, and equilibrium stress distributions in solids.

The mathematical model of PDEs is not suitable for direct computer simulation. The PDEs in the continuous domain must be discretized, so that the dependent variables exist only at discrete points. Frequently-used discretization techniques in numerical simulation include finite difference, finite element and finite volume methods. The finite difference method is easy to apply to discretizing differential equations directly, easy to obtain higher order accuracy by using higher order difference, and the coefficient matrix of the linear system obtained from implicit discretization is easy to solve, but difficult to apply it to irregular domains. For finite volume and finite element methods, the differential equations have to be written in integral form. The major advantage of finite volume and finite element methods is their application in irregular domains and use of fully unstructured grids composed of triangles and/or quadrilaterals [4]. The finite volume method has an inherent flux conservation, which is a desired feature in numerical simulation of fluid flow and mass transfer. This explains why the finite volume method is so popular in applications of computational fluid dynamics (CFD). However, both finite volume and finite element methods have the drawback of higher computational cost in implicit discretization, due to a denser

coefficient matrix. The selection of a discretization method depends on actual applications. For simple geometry, the finite difference method can be used for simplicity. In the case of complex geometry with irregular boundaries, the finite volume or the finite element method can be applied.

Biochemical reaction and cellular binding kinetics equations are usually defined by a set of nonlinear ordinary differential equations. A general nonlinear ordinary differential equation can be expressed in vector form as:

$$\frac{d\vec{y}}{dt} = f(\vec{y}, t) \tag{1.2}$$

Eq. (1.2) can be solved by the finite difference method by using backward differencing formulation.

$$\vec{y}^n = \vec{y}^{n-1} + \Delta t f(\vec{y}^n) \tag{1.3}$$

Newton's method is used to solve Eq. (1.3) and the solution is

$$\vec{y}^n = \vec{y}^{n-1} + \Delta t (I - \Delta t J)^{-1} \vec{y}^{n-1} \tag{1.4}$$

where $J = \partial f / \partial y$ is the Jacobian matrix. This nonlinear system can be solved by a ODE solver. For example, The CVODE solver [6] can be used with a user-supplied Jacobian matrix.

Normally, the whole simulation system is a complicated one, with coupled PDEs and ODEs, which should be calculated in a planned order. For example, in order to calculate mass transport equations for growth factors competitive binding to their receptors in capillaries or fibers of a bioreactor, two steps are needed. First, flow velocities and binding kinetics equations are calculated separately; second, mass transport equations are calculated by using velocities obtained in the first step. The solution of binding kinetics in the first step is used as an initial solution for mass transport equations, if binding kinetics occur in the whole domain, or as boundary conditions, if binding kinetics only occur on cell surfaces lined on the walls of fibers.

1.3 Numerical Methods for PDEs

Numerical schemes, which are employed to convert governing PDEs to discrete algebraic expressions, are very important for the solution of equations in terms of accuracy, stability and efficiency, and are usually problem dependent. Hyperbolic equations can be solved very efficiently using explicit methods, in which only one unknown appears in each equation. High resolution schemes have been developed using explicit discretization and flux limiters [81], such as the second order total variation diminishing (TVD) scheme [62], second order Monotone Upstream-centered Schemes for Conservation Laws (MUSCL) type TVD scheme [86], third order piecewise parabolic method (PPM) [9], Runge-Kutta methods, and higher order weighted essentially non-oscillatory (WENO) scheme [72]. For these explicit schemes, there exists a common drawback. They are not unconditionally stable. The stability of explicit numerical schemes is confined by the Courant−Friedrichs−Lewy (CFL) condition [11].

For problems governed by elliptic PDEs, such as the steady-state heat conduction equation, simultaneous equations have to be solved, which involves inversion of the coefficient matrix. Such a matrix is usually sparse, and its detailed structure depends on the dimensions of the problem and the discretization strategy. For parabolic equations, such as the transient heat conduction equation, the simple explicit method is highly dissipative. The commonly used method is the implicit treatment of temporal terms, and again, simultaneous algebraic equations have to be solved.

For one dimensional applications in fluid dynamics, such as 1D diffusion problems, the coefficient matrix of the discrete algebraic equations is frequently tridiagonal or block tridiagonal. A very efficient numerical algorithm, the tridiagonal matrix algorithm (TDMA), also known as the Thomas algorithm (named after Llewellyn Thomas), exists, running in linear time. It is a simplified form of the Gaussian elimination method that can be used to solve tridiagonal systems of equations [10]. For multidimensional cases, however, the coefficient matrix is very difficult to invert

directly. Due to the attractive features of the Thomas algorithm, a multi-dimensional problem is frequently solved with multi-steps, such that a tridiagonal matrix is formed for each step. Algorithms related to this technique include the alternating-direction-implicit (ADI) method and fractional-step methods.

The ADI method is a finite difference method for solving parabolic and elliptic PDEs, and most notably, it is used to solve the problem of heat conduction, or solve diffusion equations, in two or more dimensions [1]. The advantage of the ADI method is that the equations in every iteration have a simpler structure and are thus easier to solve than traditional methods, such as the Crank-Nicolson method. The disadvantage is that the splitting techniques of the ADI method and the fractional-step method do not work well in situations that are highly nonlinear, such as the strongly coupled chemical reactions in flow conditions. Therefore, this research is focused on the Krylov subspace iterative methods and incomplete LU factorization methods to solve linear systems in simulation of various physical and biological phenomena which are modeled by PDEs in a flow environment.

This dissertation is organized as follows. Chapter 2 gives a brief review of some different methods of solving linear systems related to PDEs in computational fluid dynamics and mass transfer, which are very important parts of this research. Iterative Methods and Preconditioners are also discussed. Chapter 3 describes basic models and numerical methods for performing simulations of pulsatile flow moving through a hollow fiber cartridge, as well as methods used to analyze growth factor-receptor binding and dissociation processes. Chapter 4 describes in detail how to combine experiments and simulations, in order to study the endothelial cell capture of heparin-binding growth factors under flow condition. Chapter 5 presents a parallel system to simulate multiple proteins moving through a bioreactor coupled with competitive binding in the fluid and on cell surfaces, in order to mimic complex bioreactions in human blood vessels or capillaries. A novel parallel, Stone's strongly implicit

procedure solver, is introduced in Chapter 6. Conclusions, contributions and future work are presented in Chapter 7.

2 Iterative Methods and Preconditioners

The purpose of this chapter is to give a brief review of some different methods for solving linear systems related to solving PDEs in computational fluid dynamics and mass transfer, which are very important parts of this research. It will review direct methods, stationary iterative methods, Krylov subspace-based iterative methods, preconditioners, and Stone's strongly implicit procedure (SIP) [80].

2.1 Direct Methods

2.1.1 Gaussian Elimination

The Gaussian elimination method is used for solving general linear systems of algebraic equations, $Ax = b$, where A is a square matrix and has the following form:

$$A = \begin{bmatrix} a_{11} & a_{12} & \cdots & a_{1n} \\ a_{21} & a_{22} & \cdots & a_{2n} \\ \cdots & \cdots & \cdots & \cdots \\ a_{n1} & a_{n2} & \cdots & a_{nn} \end{bmatrix}$$

The algorithm of Gaussian elimination has two parts, forward elimination and backward substitution. Forward elimination reduces a given system to either triangular or echelon form, or results in a degenerate equation with no solution, indicating the system has no solution. This is accomplished through the use of elementary row operations. Backward substitution finds the solution of the linear system above.

For a linear system of n equations for n unknowns, the number of arithmetic operations required by Gaussian elimination is on the order of $O(n^3)$. The Gaussian elimination method is numerically stable for diagonally dominant or positive-definite matrices. For general matrices, Gaussian elimination is usually considered to be stable in practice if partial pivoting is used, even though some unstable examples exist [30].

2.2 Stationary Iterative Methods

Stationary iterative methods are methods for solving a linear system of equations

$$Ax = b$$

where A is a given matrix and b is a given vector.

Stationary iterative methods are based on the relaxation of coordinates. Beginning with an initial approximate solution, these methods modify the components of approximation, one or a few at a time and in a certain order, until convergence is reached and the criteria of relative errors are met. Each of these modifications, called relaxation steps, is aimed at eliminating one or a few components of the residual vector [66].

Stationary iterative methods can be expressed in the simple form:

$$x^k = Bx^{k-1} + C$$

where neither B nor C depends upon the iteration count k [43].

Four main stationary methods are the Jacobi method, the Gauss-Seidel (GS) method, the successive overrelaxation (SOR) method, and the symmetric successive overrelaxation (SSOR) method.

The Jacobi method is based on solving for every variable locally, with respect to the other variables. One iteration corresponds to solving for every variable once. It is easy to understand and implement, but convergence is slow. The GS method is similar to the Jacobi method, except that it uses updated values as soon as they are available. The GS method generally converges faster than the Jacobi method, but it is still relatively slow. The SOR method can be derived from the GS method by introducing an extrapolation parameter. This method can converge faster than the GS method by an order of magnitude. The SSOR method is useful as a preconditioner for nonstationary methods. However, it has no advantage over the SOR method as a stand-alone iterative method.

2.2.1 Jacobian Iteration

Let x_i^k denote the ith component of the kth iteration; therefore the Jacobi iteration can be expressed as:

$$x_i^{k+1} = a_{ii}^{-1}\left(b_i - \Sigma_{j\neq i} a_{ij} x_j^k\right)$$

This is a component-wise form of the Jacobi iteration. The Jacobi iteration uses splitting in the following way:

$$A = D + (L + U)$$

where D is the diagonal component of A. L and U are the strictly lower and upper triangular components of A.

The Jacobi iteration can be rewritten in vector form as:

$$x^{k+1} = -D^{-1}(L + U)x^k + D^{-1}b$$

The Jacobi iteration matrix is:

$$M_J = -D^{-1}(L + U)$$

Note that D is diagonal and hence trivial to invert.

2.2.2 Gauss-Seidel Iteration

Similarly, the GS iteration overwrites the approximate solution with the new value as soon as it is computed. For forward GS iteration, the new value can be expressed as:

$$x_i^{k+1} = a_{ii}^{-1}\left(b_i - \Sigma_{j<i} a_{ij} x_j^{k+1} - \Sigma_{j>i} a_{ij} x_j^k\right)$$

The forward GS iteration uses the following splitting:

$$A = (D + L) + U$$

Note that $D + L$ is a lower triangular, hence $(D + L)^{-1}$ is easy to compute. The forward GS iteration can be rewritten in a vector form as:

$$x^{k+1} = -(D + L)^{-1}Ux^k + (D + L)^{-1}b$$

The forward GS iteration matrix is:

$$M_{FGS} = -(D + L)^{-1}U$$

The backward GS iteration begins the update of x with the nth coordinate, rather than the 1st, resulting in the splitting:

$$A = (D + U) + L$$

$D + U$ is an upper triangular, and its inverse is also easy to compute. The backward GS iteration can be rewritten in matrix form as:

$$x^{k+1} = -(D + U)^{-1}Lx^k + (D + U)^{-1}b$$

The backward GS iteration matrix is:

$$M_{BGS} = -(D + U)^{-1}L$$

A symmetric GS iteration is a forward GS iteration followed by a backward GS iteration. This leads to the iteration matrix:

$$M_{SGS} = M_{BGS}M_{FGS} = (D + U)^{-1}L(D + L)^{-1}U.$$

When A is symmetric, or $U = L^T$, we have:

$$M_{SGS} = (D + U)^{-1}L(D + L)^{-1}U = (D + L^T)^{-1}L(D + L)^{-1}L^T.$$

2.2.3 Successive Overrelaxation Iteration

The SOR iteration modifies the GS iteration by adding a relaxation factor ω to the linear system [66, 93]. The system of linear equations is rewritten as:

$$(D + \omega L)x = \omega b + ((1 - \omega)D - \omega U)x$$

where $\omega > 1$ is a constant. The iteration matrix of SOR is:

$$M_{SOR} = (D + \omega L)^{-1}((1 - \omega)D - \omega U).$$

The performance can be dramatically improved with ideal values of ω, but it still can not compete with the Krylov methods. Another disadvantage of the SOR is that it is often difficult to make the choice of relaxation factor ω, which depends on the properties of the coefficient matrix A.

2.2.4 Symmetric Successive Overrelaxation Iteration

If the coefficient matrix A is symmetric, the SSOR method can produce an iteration matrix similar to a symmetric matrix. The SSOR includes a forward SOR sweep and a backward SOR sweep. This method is usually used as a preconditioner to other iterative methods for symmetric matrices. The iteration matrix of the SSOR is:

$$M_{SSOR} = (D + \omega U)^{-1}((1-\omega)D - \omega L)(D + \omega L)^{-1}((1-\omega)D - \omega U).$$

2.3 Krylov Subspace Based Iterative Methods

Krylov subspace iteration methods are considered to be the most useful iterative techniques available for solving large linear systems. These techniques are based on projections, both orthogonal and oblique, onto Krylov subspaces, which are subspaces spanned by vectors of the form $p(A)v$, where p is a polynomial. In short, these techniques approximate $A^{-1}b$ by $p(A)b$, where p is a "good" polynomial [66].

2.3.1 Conjugate Gradient

The Conjugate Gradient (CG) method is intended to solve symmetric positive definite (SPD) linear systems. A matrix A is symmetric if $A = A^T$ and positive definite if its eigenvalues are all positive, i.e., $x^T Ax > 0$ for all $x \neq 0$. For a positive definite matrix, solving the system of equations $Ax = b$ is equivalent to finding the minimum of the following equation, with respect to all the x_i [19].

$$\phi(x) = \frac{1}{2}x^T Ax - x^T b = \frac{1}{2}\sum_{j=1}^{n}\sum_{i=1}^{n} a_{ij}x_i x_j - \sum_{i=1}^{n} x_i b_i$$

Note that if $\phi(x)$ is the minimal value of R^n then

$$\nabla\phi(\tilde{x}) = A\tilde{x} - b = 0$$

and hence $\tilde{x} = x$.

One of the conjugate gradient algorithms is presented in Algorithm 1 [66].

Algorithm 1 Conjugate Gradient Algorithm

1: Initialization: $r_0 = b - Ax_0$, $p_0 = r_0$
2: **for** $j = 0, \cdots$, until convergence or $j < j_{max}$ **do**
3: $\alpha_j = (r_j, r_j)/(Ap_j, p_j)$
4: $x_{j+1} = x_j + \alpha_j p_j$
5: $r_{j+1} = r_j - \alpha_j A p_j$
6: if r_{j+1} is sufficiently small then exit for loop
7: $\beta_j = (r_{j+1}, r_{j+1})/(r_j, r_j)$
8: $p_{j+1} = r_{j+1} + \beta_j p_j$
9: **end for**
10: the result is x_{k+1}

This is the most commonly used algorithm. In Algorithm 1, only four vectors need to be stored, x, p, r, and Ap. There are several alternative formulations [43, 66], such as the Preconditioned Conjugate Gradient (PCG) and the Split Preconditioned Conjugate Gradient (SPCG) algorithms.

The conjugate gradient method can be applied to an arbitrary n-by-m matrix by applying it to normal equations A^TA and right-hand side vector A^Tb, since A^TA is a symmetric positive-semidefinite matrix for any A. The result is a conjugate gradient on the normal equations (CGNR):

$$A^TAx = A^Tb$$

As an iterative method, it is not necessary to form A^TA explicitly in memory but only to perform the matrix-vector and transposed matrix-vector multiplications. Therefore CGNR is particularly useful when A is a sparse matrix, since these operations are usually extremely efficient. However, the drawback is that the condition number $\kappa(A^TA) = \kappa^2(A)$, so the rate of convergence of CGNR may be slow and the quality of the approximate solution may be sensitive to roundoff errors.

2.3.2 Bi-Conjugate Gradient Stabilized (BiCGStab)

The BiCGStab method was proposed by van der Vorst [85], with the purpose of extending the CG algorithm to solve nonsymmetric linear systems. It is a variant of the biconjugate gradient (BiCG) method, and it has faster and smoother convergence than the original BiCG, as well as other variants such as the conjugate gradient squared (CGS) method . The BiCGStab algorithm is summarized in Algorithm 2 [43].

Algorithm 2 Unpreconditioned BiCGStab

$r_0 = b - Ax_0$
Choose an arbitrary vector $\hat{r}_0 = r_0$
$\rho_0 = \alpha = \omega_0 = 1$
$v_0 = p_0 = 0$
for $j = 0, \cdots$, until convergence or $j < j_{max}$ **do**
  $\rho_j = (\hat{r}_0, r_{j-1})$
  $\beta = (\rho_j/\rho_{j-1})(\alpha/\omega_{j-1})$
  $p_j = r_{j-1} + \beta(p_{j-1} - \omega_{j-1}v_{j-1})$
  $v_j = Ap_j$
  $\alpha = \rho_j/(\hat{r}_0, v_j)$
  $s = r_{j-1} - \alpha v_j$
  $t = As$
  $\omega_j = (t, s)/(t, t)$
  $x_j = x_{j-1} + \alpha p_j + \omega_j s$
  $r_j = s - \omega_j t$
end for

In Algorithm 2, seven vectors need to be stored, x, b, r, $\hat{r}_0$, p, v and t. Four matrix-vector products are required in each iteration of the algorithm.

2.3.3 General Minimum Residual (GMRES)

The GMRES method is a projection method that minimizes the residual norm over all vectors in $x_0 + \mathcal{K}_k$, where x_0 is the initial value and $\mathcal{K}_k$ is the k-th Krylov subspace with $v_1 = r_0/\|r_0\|_2$ [66]. The k-th Krylov subspace is:

$$\mathcal{K}_k(A, r_0) = \text{span}(r_0, Ar_0, \cdots, A^{k-1}r_0)$$

where $r_0 = b - Ax_0$.

This method seeks an approximate solution x_k from the affine subspace $x_0 + \mathcal{K}_k$ of dimension k by imposing the Galerkin condition:

$$b - Ax_m \perp \mathcal{K}_k$$

The kth GMRES iteration is equivalent to the least squares problem:

$$\text{minimize}_{x \in x_0 + \mathcal{K}_k} \|b - Ax\|_2.$$

One implementation of the GMRES can be written as Algorithm 3 [66].

Algorithm 3 GMRES

1: Compute $r_0 = b - Ax_0$, $\beta = \|r_0\|_2$, and $v_1 = r_0/\beta$
2: Define the $(m+1) \times m$ matrix $\bar{H}_m = h_{i,j}(1 \le i \le m+1, 1 \le j \le m)$
3: Set $\bar{H}_m = 0$
4: **for** $j = 1, \cdots, m$ **do**
5: Compute $w_j = Av_j$
6: **for** $i = 1, \cdots, j$ **do**
7: $h_{i,j} = (w_j, v_i)$
8: $w_j = w_j - h_{i,j} v_i$
9: **end for**
10: $h_{j+1,j} = \|w_j\|_2$
11: If $h_{j+i,j} = 0$ set $m = j$ and goto 14
12: $v_{j+1} = w_j / h_{j+1,j}$
13: **end for**
14: Compute y_m, the minimizer of $\|\beta e_1 - \bar{H}_m y\|_2$
15: Compute $x_m = x_0 + V_m y_m$

2.4 Preconditioners

A preconditioner to a given linear system can be any form of explicit or implicit modifications of the original system that makes it easier and faster to solve by an iterative method [66]. For the original system $Ax = b$, a preconditioned system $M^{-1}Ax = M^{-1}b$ can be formed, where the preconditioning matrix M^{-1} can be inexpensively applied to a matrix-vector product. The construction of M^{-1} can be performed in different ways depending on a variety of applications.

2.4.1 Jacobi, GS, SOR, and SSOR Preconditioners

A fixed-point iteration for the linear system $Ax = b$ has the form [66]:

$$x^{k+1} = M^{-1}Nx^k + M^{-1}b = Gx^k + f$$

where $A = M - N$, M and N are the splitting of A,$f = M^{-1}b$, and $G = M^{-1}N = I - M^{-1}A$.

For the Jacobian iteration, the preconditioning matrix is $M = D$, where D is the diagonal of A.

For the GS iteration, the preconditioning matrix is $M = (D + L)$ for a forward sweep and $M = D + U$ for a backward sweep, where L and U are the strict lower and upper parts of A, respectively.

For the SOR iteration, the preconditioning matrix is in the form of $M = (D + \omega L)$ or $M = (D + \omega U)$.

The preconditioning matrix for the SSOR iteration is $M = (D+\omega L)D^{-1}(D+\omega U)$.

2.4.2 ILU(0) Preconditioner

The ILU(0) Preconditioner is an incomplete LU factorization of A with no fill-in, i.e., the zero pattern of matrix $M = LU$ is precisely the same as that of matrix A. For a 2D Laplace' equation, the coefficient matrix A is five-diagonal, but matrix M is seven-diagonal. The entries in these extra diagonals are called fill-in elements. The ILU(0) factorization can be stated as any pairs of matrices L (unit lower triangular) and U (upper triangular), such that the elements of $A - LU$ are zero in locations where the elements of A are not zero. For any arbitrary matrix A, let $NZ(A)$ denote any nonzero elements in A, i.e., the set of pairs (i, j), such that $a_{i,j} \neq 0$, where $1 \leq i, j \leq n$. The algorithm of ILU(0) factorization can be written as Algorithm 4 [66].

Algorithm 4 ILU(0)

```
for i = 2, ··· , n do
  for k = 1, ··· , i − 1 do
    if (i, k) ∈ NZ(A) then
      Compute a_{i,k} = a_{i,k}/a_{k,k}
      for j = k + 1, ··· , n do
        if (i, j) ∈ NZ(A) then
          Compute a_{i,j} = a_{i,j} − a_{i,k}a_{k,j}
        end if
      end for
    end if
  end for
end for
```

2.4.3 ILU(p) Preconditioner

The accuracy of the ILU(0) incomplete LU factorization may be insufficient to yield an adequate rate of convergence. More accurate Incomplete LU factorizations are often more efficient, as well as more reliable. These more accurate factorizations will differ from ILU(0) in that they allow some fill-ins [66].

The ILU(p) Preconditioner allows some fill-ins to increase the accuracy and improve the rate of convergence, where p is the level of fill.

In an ILU(p), all fill-in elements with a level of fill less than p are kept. The higher the level, the smaller the elements. The initial level of fill of an element $a_{i,j}$ of a sparse matrix A is defined by $lev_{i,j} = 0$ if $a_{i,j} \neq 0$ or $i = j$, and $lev_{i,j} = \infty$ otherwise. During the construction, the level of fill is updated by $lev_{i,j} = \min(lev_{i,j}, lev_{i,k} + lev_{k,j} + 1)$. Let $a_{i,*}$ indicate the ith row of A, and let $a_{i,j}$ indicate the entry of A. The algorithm for ILU(p) factorization can be written as Algorithm 5 [66].

2.4.4 ILUT Preconditioner

Incomplete factorizations, which rely on the levels of fill, are blind to numerical values because elements that are dropped depend only on the structure of A. This can cause some difficulties for realistic problems. A few alternative methods are available which

Algorithm 5 ILU(p)

```
Initialization
for a_{i,j} ≠ 0 do
    lev(a_{i,j}) = 0
end for
for i = 2, ··· , n do
    for k = 1, ··· , i − 1 do
        if lev(a_{i,k}) ≤ p then
            Compute a_{i,k} = a_{i,k}/a_{k,k}
            Compute a_{i,*} = a_{i,*} − a_{i,k}a_{k,*}
            lev_{i,j} = min(lev_{i,j}, lev_{i,k} + lev_{k,j} + 1)
        end if
    end for
    for each a_{i,j} in row i do
        if lev(a_{i,j}) > p then
            a_{i,j} = 0
        end if
    end for
end for
```

are based on dropping elements in the Gaussian elimination process, according to their magnitude rather than their locations. The ILUT Preconditioner algorithm has two dropping steps with two parameters, p and τ. The first step is to drop any element w_k such that $w_k < \tau_i$, where w is a full length working row and w_k is the k-th entry of this row. τ_i is relative tolerance, obtained by multiplying τ by the 2-norm of the i-th row. The second step is to drop any element in the row that is less than the relative tolerance τ_i, keeping only the p largest elements in the L part, and p largest elements in the U part of the row, in addition to the diagonal element. Therefore, p can be viewed as a parameter that helps control memory usage, while τ helps to reduce computational cost. An algorithm of ILUT factorization can be written as Algorithm 6 [66].

2.5 Stone's SIP Method

LU decomposition is an excellent general purpose linear equation solver. The biggest disadvantage is that it fails to take advantage of coefficient matrix A as a sparse

Algorithm 6 ILUT

Initialization
for $i = 1, \cdots, n$ **do**
  $w = a_{i,*}$
  for $k = 1, \cdots, i-1$ **do**
    if $w_k \neq 0$ **then**
      $w_k = w_k / a_{k,k}$
      if $w_k < \tau \|w\|_2$ **then**
        $w_k = 0$
      end if
      if $w_k \neq 0$ **then**
        $w = w - w_k u_{k,*}$
      end if
    end if
  end for
  Apply dropping rule to row w
  for $j = 1, \cdots, i-1$ **do**
    $l_{i,j} = w_j$
  end for
  for $j = i, \cdots, n$ **do**
    $u_{i,j} = w_j$
  end for
  $w = 0$
end for

matrix. The LU decomposition of a sparse matrix is usually not sparse; thus, for large system of equations, LU decomposition may require a prohibitive amount of memory and arithmetical operations.

In preconditioned iterative methods, if the preconditioner matrix M is a good approximation of coefficient matrix A, then the convergence is faster. Thus, it may be a good idea to use approximate factorization LU of A as iteration matrix M.

Stone proposed a version of an incomplete lower-upper decomposition method for solving such a sparse linear system of equations in 1968, also known as the strongly implicit procedure (SIP) [80]. The method uses an incomplete LU decomposition, which approximates the exact LU decomposition, in order to generate an iterative solution. This method is designed for an equation system arising from the discretization of partial differential equations, and it was first used as a pentadiagonal system obtained while solving an elliptic partial differential equation in a two dimensional space by a finite difference method. This method does not apply to a general system of equations, but it does apply to a sparse linear system of equations arising in computational fluid dynamic problems.

An algorithm of SIP can be written as Algorithm 7 [19, 80].

Algorithm 7 Ston's Strongly Implicit Procedure(SIP)

For the sparse linear system $Ax = b$
calculate Incomplete LU factorization of matrix A
  $Ax = (M - N)x = (LU - N)x = b$
  $Mx^{k+1} = Nx^k + b \quad , with \ \|M\| \gg \|N\|$
  $Mx^{k+1} = LUx^{k+1} = c^k$
  $LUx^k = L(Ux^{k+1}) = Ly^k = c^k$
set a guess
  $k = 0, x^k$
  $r^k = b - Ax^k$
while $\|r^k\|_2 > \epsilon$ **do**
   evaluate new right hand side
     $c^k = Nx^k + b$
   solve $Ly^k = c^k$ by forward substitution
     $y^k = L^{-1}c^k$
   solve $Ux^{k+1} = y^k$ by back substitution
     $x^{k+1} = U^{-1}y^k$
end while

3 A Numerical Study of Pulsatile Flow Through a Hollow Fiber Cartridge: Growth Factor-Receptor Binding and Dissociation Analysis

3.1 Introduction

The binding of fibroblast growth factor-2 (FGF-2) to its cell surface receptor (FGFR) and the role of heparan sulfate proteoglycans (HSPG) in regulating the process for endothelial cells has been of interest for many years because of their roles in cell signaling and cellular proliferation, processes which are important for angiogenesis. Certainly control of these cells which line blood vessels is likely to be important in being able to control tumor growth and wound healing. In the past two decades, with the development of high performance computers, several computational models of FGF-2 binding to its receptor FGFR and regulated by HSPG have been proposed [13, 17, 20, 26, 27, 38, 48, 55]. Nugent and Edelman were among the earliest researchers, developing a simple model, involving these three species, FGF-2, FGFR and HSPG. They measured kinetic binding rate constants experimentally and their results provided a foundation for investigating the complexity of FGF-2 binding. Nugent, Forsten-Williams and coworkers introduced more complexity into their models with dimerization and formation of higher order species. Filion and Popel proposed a model of FGF-2 interactions with cell surface receptors including diffusive transport within the culture dish [20]. Ibrahimi and coworkers proposed a simple model for the stepwise assembly of a ternary FGF-2-FGFR-HSPG complex [38]. Not like the previous models for the kinetic assembly of a ternary complex in which binary FGF-2-FGFR or FGFR-HSPG complexes are intermediates, they claimed that FGFR and HSPG are unbound in the absence of FGF-2 ligand, and the availability of FGF-2 results in formation of initial FGF-2-HSPG complexes, which promotes the rapid binding of FGFR and creates ternary complexes capable of undergoing dimerization and subsequent FGFR activation. Forsten-Williams and coworkers took their model a step further by linking their model to experimental activation of ERK 1/2, an

important intracellular signaling pathway component [27]. These previous modeling systems are based on culture environment.

This chapter addresses the competitive binding of some basic models, in which only one growth factor (such as FGF-2) binds to its receptors (such as FGFR, HSPG, etc.) in a flow environment to mimic kinetics occur on cell surfaces in blood capillaries. No competitive binding occurs in the solution. The whole model consists of three coupled parts [71, 96]: (1) the medium flow part uses the incompressible Navier-Stoke equations; (2) the convective and diffusive mass transport of a growth factor in the flow uses transport equations; (3) the binding kinetics on cell surfaces uses a set of ordinary differential equations.

3.2 Simulation Environment

In order to investigate the quantitative properties of the growth factor (FGF-2) binding, one-pass experiments (i.e., no recycling of the fluid through the cartridge) and simulations have been set up. Fig. 3.1 is a diagram of the hollow fiber cartridge system used in the experiments [50]. The growth factor (FGF-2) is injected into the left sampling port and the pump is turned on. The fluid is pumped into the cartridge and the growth factor (FGF-2) enters into twenty hollow-fiber capillaries, which are coated with endothelial cells on the wall. Fluid from the capillaries is pooled in the right outlet reservoir and collected in tubes approximately every ten seconds during one-pass experiments.

3.3 Modeling Process

The geometric model is based on the experimental one and illustrated in Fig. 3.2. The flow is pulsatile. So, the simulation cost can be greatly reduced by finding some analytical solution to the velocity, instead of calculating it numerically. The walls of the hollow-fiber capillaries are assumed to be rigid and nonporous. In addition, the

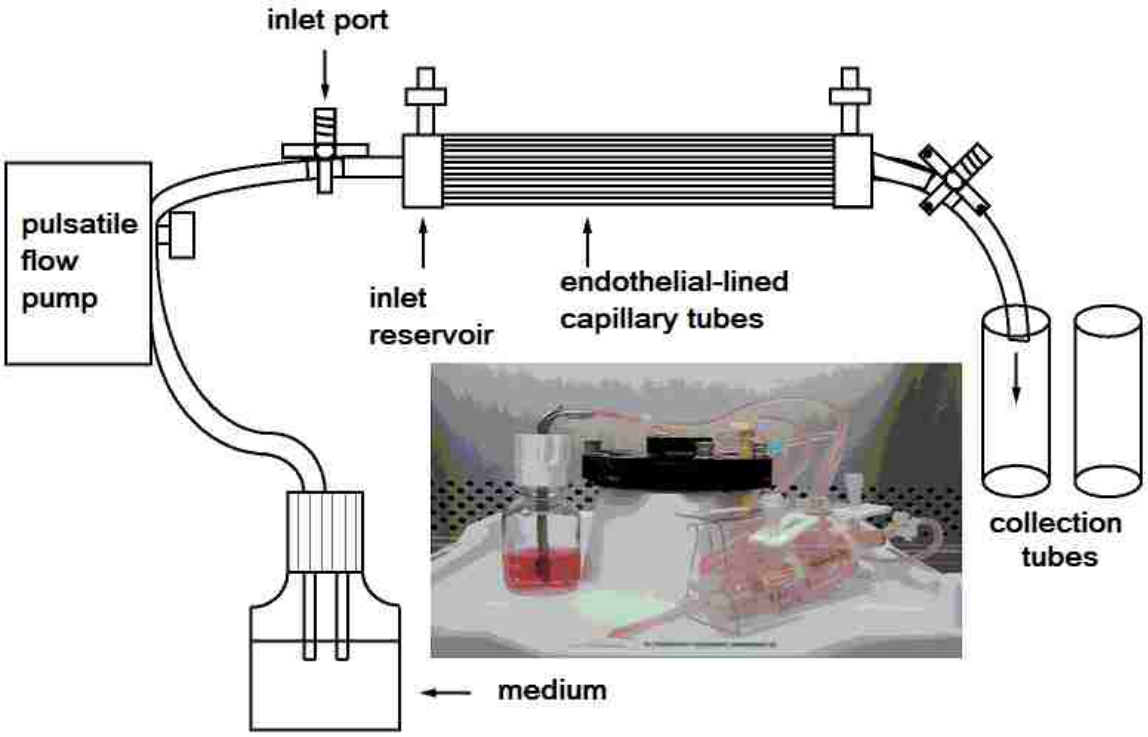

Figure 3.1: Hollow fiber cartridge system from FiberCell®.

following assumptions are made: (1) All of the twenty hollow-fiber capillaries have the same dimensions, flow, and cell densities; (2) The flow is steady, axisymmetric and laminar, for simplicity, entrance effects are ignored [35]; (3) The fluid is incompressible, Newtonian, viscous and isothermal; (4) The endothelial cells are distributed evenly on the wall of the hollow-fiber capillaries and tightly packed.

The model consists of three coupled parts: (1) the medium flow equations; (2) the convective and diffusive mass transport equations of the growth factor (FGF-2) in the flow; (3) the competitive binding kinetics equations [71, 96]. The binding kinetics of the simulation is based on Forsten-Williams et al. 2005 model [27].

3.3.1 Medium Flow Equations

Because of the axis-symmetry of the hollow-fiber capillaries, the model can be simplified from 3D to 2D. Based on the above assumptions, the governing equations of

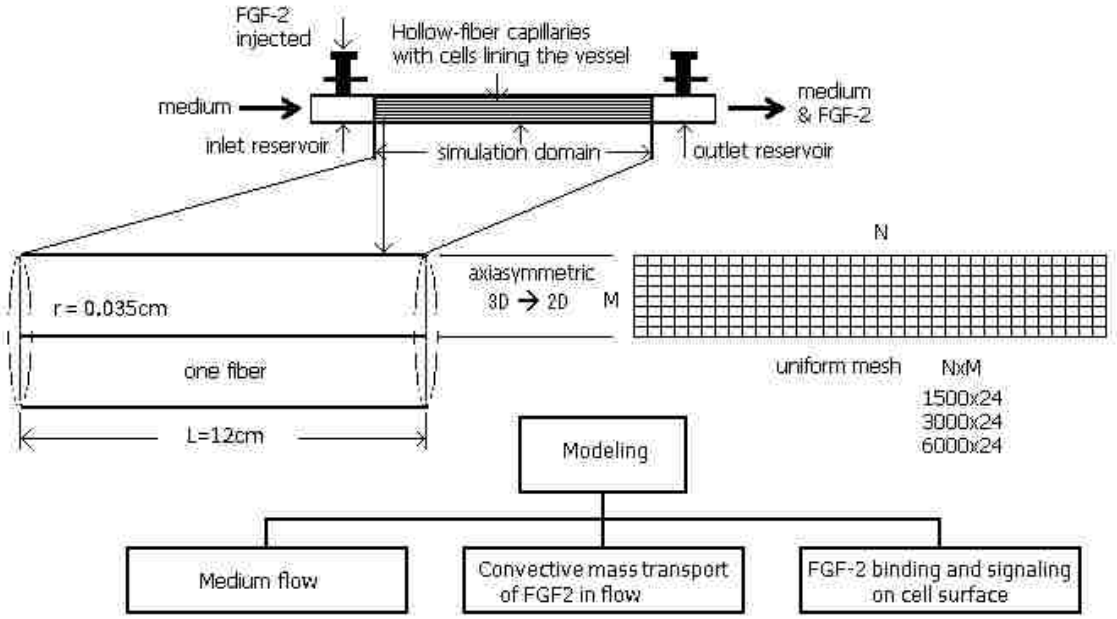

Figure 3.2: The diagram of modeling process.

the model are given by [19, 71, 94]:

The mass conservation equation:

$$\frac{\partial u}{\partial x} + \frac{v}{r} + \frac{\partial v}{\partial r} = 0 \tag{3.1}$$

The radial momentum equation:

$$\rho(\frac{\partial v}{\partial t} + u\frac{\partial v}{\partial x} + v\frac{\partial v}{\partial r}) + \frac{\partial p}{\partial r} = \mu(\frac{1}{r}\frac{\partial v}{\partial r} + \frac{\partial^2 v}{\partial x^2} + \frac{\partial^2 v}{\partial r^2} - \frac{v}{r^2}) \tag{3.2}$$

The axial momentum equation:

$$\rho(\frac{\partial u}{\partial t} + u\frac{\partial u}{\partial x} + v\frac{\partial u}{\partial r}) + \frac{\partial p}{\partial x} = \mu(\frac{1}{r}\frac{\partial u}{\partial r} + \frac{\partial^2 u}{\partial x^2} + \frac{\partial^2 u}{\partial r^2}) \tag{3.3}$$

where ρ is the density, μ is the viscosity of the medium and it is a constant due to Newtonian incompressible flow, p is the dynamic pressure, u is the axial velocity, and v is the radial velocity.

The above PDEs can be computed numerically, as described in [71]. They can also be calculated theoretically in some special cases, such as described below.

If these equations are restricted to only fully developed region of the flow, Eq. (3.1) reduces to:

$\frac{v}{r} + \frac{\partial v}{\partial r} = 0$, so $v \equiv 0$, and $\frac{\partial p}{\partial r} \equiv 0$

Eq. (3.2) can be eliminated. Eq. (3.3) reduces to:

$$\rho\frac{\partial u}{\partial t} + \frac{\partial p}{\partial x} = \mu(\frac{1}{r}\frac{\partial u}{\partial r} + \frac{\partial^2 u}{\partial r^2}) \tag{3.4}$$

Eq. (3.4) is the simplified form on which the classical solution for fully developed, steady, and pulsatile flow is based.

If the fiber is assumed to be rigid, the velocity of u is a function of r and t only, and pressure p is a function of x and t only, that is, u=$u(r,t)$,p=$p(x,t)$. For oscillatory flow, if the steady and oscillatory parts of velocity and pressure are identified by subscripts "s" and "ϕ", respectively, to isolate the oscillatory flow problem, we write

$u(r,t) = u_s(r) + u_\phi(r,t)$ and $p(x,t) = p_s(x) + p_\phi(x,t)$

Substituting these into Eq. (3.4), we obtain:

$$\frac{\partial p_s}{\partial x} - \mu(\frac{1}{r}\frac{\partial u_s}{\partial r} + \frac{\partial^2 u_s}{\partial r^2}) + \rho\frac{\partial u_\phi}{\partial t} + \frac{\partial p_\phi}{\partial x} - \mu(\frac{1}{r}\frac{\partial u_\phi}{\partial r} + \frac{\partial^2 u_\phi}{\partial r^2}) = 0 \tag{3.5}$$

Suppose pressure gradient is $\frac{\partial p}{\partial t} = k_s + k_\phi(t)$. Eq. (3.5) can be separated into the steady and oscillatory parts.

For steady part equation:

$$\frac{\partial p_s}{\partial x} - \mu(\frac{1}{r}\frac{\partial u_s}{\partial r} + \frac{\partial^2 u_s}{\partial r^2}) = 0 \tag{3.6}$$

The solution is $u_s = \frac{k_s}{4\mu}(r^2 - R^2)$.

The volumetric flow rate $q_s = N_f \int u_s 2\pi r dr = -\frac{k_s N_f \pi R^4}{8\mu}$, or $k_s = -\frac{q_s 8\mu}{N_f \pi R^4}$, thus, $u_s = \frac{2q_s}{N_f \pi R^4}(R^2 - r^2) = \frac{2q_s}{N_f \pi R^2}(1 - \frac{r^2}{R^2})$,

where N_f $(= 20)$ is the number of fibers in the cartridge.

For oscillatory part equation:

$$\mu(\frac{1}{r}\frac{\partial u_\phi}{\partial r} + \frac{\partial^2 u_\phi}{\partial r^2}) - \rho\frac{\partial u_\phi}{\partial t} = k_\phi(t) \tag{3.7}$$

Let $k_\phi(t) = k_s e^{j\omega t} = k_s(cos\omega t + isin\omega t) = k_{\phi R} + ik_{\phi I}$ and $u_\phi(r,t) = U_\phi(r)e^{i\omega t}$, Eq. (3.7) becomes:

$$\frac{1}{r}\frac{dU_\phi}{dr} + \frac{d^2U_\phi}{dr^2} - \frac{i\alpha}{R^2}U_\phi = \frac{k_s}{\mu} \tag{3.8}$$

where $\alpha = \sqrt{\frac{\rho\omega}{\mu}}R$.

Combining boundary conditions $U_\phi(R) = 0$ and $|U_\phi(0)| < \infty$, the solution is $U_\phi(r) = \frac{ik_sR^2}{\mu\alpha^2}(1 - \frac{J_0(\zeta)}{J_0(\Lambda)})$ where $\Lambda = (\frac{i-1}{\sqrt{2}})\alpha$, $\zeta = \Lambda\frac{r}{R}$, and $J_0(Z)$ is the Bessel functions of the first kind of order zero.

Therefore,

$$u_\phi(r,t) = \frac{ik_sR^2}{\mu\alpha^2}(1 - \frac{J_0(\zeta)}{J_0(\Lambda)})e^{i\omega t} \tag{3.9}$$

or

$$u_\phi(r,t) = \frac{-k_sR^2}{4\mu}((1 - \frac{r^2}{R^2}) - \frac{i\alpha^2}{16}(3 - \frac{4r^2}{R^2} + \frac{r^4}{R^4}))e^{i\omega t} \tag{3.10}$$

When oscillatory flow is at low frequency, that is $\alpha < 1.0$, the second part in Eq. (3.10) can be ignored and it becomes:

$$u_\phi(r,t) = \frac{-k_sR^2}{4\mu}(1 - \frac{r^2}{R^2})e^{i\omega t} \tag{3.11}$$

Let $k_\phi(t) = k_{\phi R}$, then:

$$u(r,t) = u_s(r) + u_\phi(r,t) = \frac{2q_s}{N_f\pi R^2}(1 - \frac{r^2}{R^2})(1 + cos\omega t) \tag{3.12}$$

The distance downstream from the fiber entrance to where flow becomes fully developed is called the entrance length, symbolized L_e. The entrance length required for a fully developed velocity profile to form in laminar flow has been expressed by Langhaar according to [89]:

$$L_e = 0.0575 \times Re \times D = 0.0575 \times \frac{\rho D^2 V}{\mu} \tag{3.13}$$

where D represents the inside diameter of the fiber, R_e is the Reynolds number, ρ is the density of the fluid, μ is the viscosity of the fluid, and V is the mean fluid velocity.

When the average volumetric flow rate q is 0.67 ml/min for the whole cartridge, the mean fluid velocity for one fiber V will be 0.001451 m/s. In the current study, $\rho = 1000kg/m^3$, and $\mu = 0.001Pa \cdot s$, L_e is around 0.004 cm, which is much less than one percent of the length of the fiber (12 cm). Even for some higher flow rates, such as q=6.7 ml/min, $L_e \approx 0.04$ cm, it is still less than one percent of the length of the fiber. Thus, the flow in the whole fiber is treated as fully developed, and the entrance effects are ignored.

Eq. (3.12) is used as an approximate analytical solution of u during the simulation, and Eq. (3.10) can be used as a general solution to a pulsatile pressure gradient function.

3.3.2 Mass Transport Equations

The mass transport equation for the growth factor (FGF-2) consists of two mechanisms: *convection* and *dissipation*. Convection describes the transport of local components along the streamlines of the flow. Dissipation describes the diffusive transport of components due to concentration gradient. The mass must be conserved. Generally, the mass transport equation can be expressed as [71]:

$$\frac{\partial \rho\phi}{\partial t} + \nabla \cdot (\rho\vec{u}\phi) = \nabla \cdot (K_d \nabla\phi) + S(\phi) \tag{3.14}$$

where ϕ is the concentration, K_d is the diffusion coefficient, $\frac{\partial \rho\phi}{\partial t}$ is the transient term, $\nabla \cdot (\rho\vec{u}\phi)$ is the convection term, $\nabla \cdot (K_d \nabla\phi)$ is the diffusion term, and $S(\phi)$ is the source term.

In the model, the density ρ is constant due to incompressible flow. The mass transport of the growth factor (FGF-2) in a circular hollow-fiber can be described by the following equation [71]:

$$\frac{\partial \phi}{\partial t} + \frac{1}{r}\frac{\partial (rv\phi)}{\partial r} + \frac{\partial (u\phi)}{\partial x} = \frac{1}{r}\frac{\partial}{\partial r}(rK_d\frac{\partial \phi}{\partial x}) + \frac{\partial}{\partial x}(K_d\frac{\partial \phi}{\partial x}) + F(\phi, t, x) \tag{3.15}$$

where ϕ is the concentration of the growth factor (FGF-2), u and v are the axial and the radial velocities, respectively, K_d is the molecular diffusion coefficient and

treated as a constant in both radial and axial directions, and $F(\phi, t, x)$ is the rate of change due to the kinetic transformation of the growth factor (FGF-2) binding to its receptors on cell surfaces.

If the flow in the fiber is assumed to be fully developed, Eq. (3.15) can be simplified as:

$$\frac{\partial \phi}{\partial t} + \frac{\partial (u\phi)}{\partial x} = \frac{1}{r}\frac{\partial}{\partial r}(rK_d\frac{\partial \phi}{\partial x}) + \frac{\partial}{\partial x}(K_d\frac{\partial \phi}{\partial x}) + F(\phi, t, x) \tag{3.16}$$

The boundary conditions of Eq. (3.16) are:

(1) $\frac{\partial \phi}{\partial r} = 0$ at $r = 0$, reflecting symmetry of the flow along the fiber centerline.

(2) $\frac{\partial \phi}{\partial r} = F(\phi, t, x)$ at $r = R$, reflecting binding rate of the growth factor (FGF-2) on cell surfaces on the wall of the fiber.

(3) $\phi(t) = \phi_{ent}(t)$ at $x = 0$, assuming well mixed entrance flow, with uniform concentration along the fiber radius.

The Mass Transport Equation Discretization

The mass transport equation is the most critical part of the whole computational model. It is preferable to solve it with a reasonable accuracy. In the current study, the second order accuracy is enough considering the accuracy of the experimental results. To achieve the second order time accuracy, a quadratic backward approximation for the time derivative term is used. To maintain numerical stability as well as to achieve second order spatial accuracy, a deferred correction numerical strategy is used [19, 71]. This is a combination of the first order upwind differencing and the second order central differencing, as shown in the following formula:

$$F = F^L + \lambda(F^H - F^L)^{old} \tag{3.17}$$

where F is the approximation of surface integrals or the net flux through the control volume boundary, F^L stands for the approximation by some lower-order scheme, such as the first order upwind differencing scheme (UDS) in this research, F^H is the higher-order approximation, such as the second order central differencing scheme (CDS), and

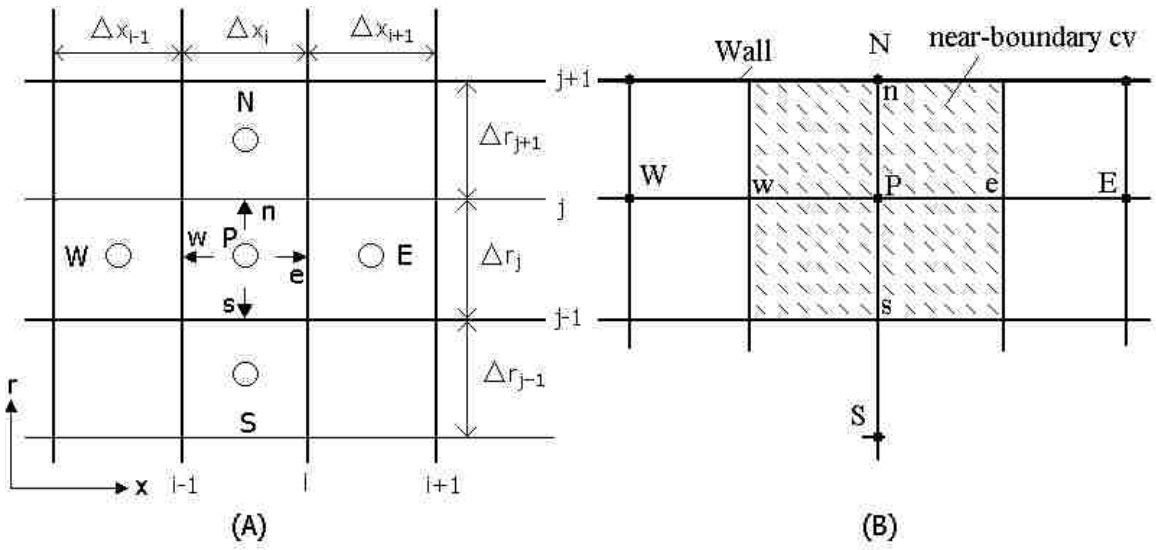

Figure 3.3: The finite volume notation of control volumes in axisymmetric coordinates, (A) the control volume, (B) the north boundary control volume.

λ is the blending factor ($0 \leq \lambda \leq 1$). The term in brackets is evaluated using values from the previous iteration, as indicated by the superscript 'old' [19]. The diffusive terms are discretized by the central difference method. Overall, the second order accuracy is achieved for time and space.

The detailed discretization is illustrated as follows.

By using the finite volume method, Eq. (3.16) could be written as:

$$\frac{3(\rho\phi)_P^{n+1} - 4(\rho\phi)_P^n + (\rho\phi)_P^{n-1}}{2\delta t} + (J_e - J_w) + (J_n - J_s) = S_c + S_P\phi_P \qquad (3.18)$$

where S_c and S_P are the results of source term linearization, $J_e = F_e - D_e$, $J_w = F_w - D_w$, $J_n = F_n - D_n$, $J_s = F_s - D_s$ are the convection-diffusion fluxes at each of the four interfaces of the control volume P.

The notations of spatial discretization in Eq. (3.18) is illustrated in Fig. 3.3 (A), where the uppercase letters indicate the center of the control volumes, and the lowercase letters indicate the interfaces between neighboring control volumes. Using deferred correction [19], the convection flux can be written as a mixture of upwind and central difference schemes. The convection flux in the axial direction could be

written as:

$$(F_e - F_w)^n = (F_e^u - F_w^u)^n + \lambda((F_e^c - F_w^c) - (F_e^u - F_w^u))^{n-1}$$

in which

$$F_e^u = \max\left((\rho u)_e \delta r_j, 0\right)\phi_P + \min((\rho u)_e \delta r_j, 0)\phi_E$$

$$F_w^u = \max((\rho u)_w \delta r_j, 0)\phi_W + \min((\rho u)_w \delta r_j, 0)\phi_P$$

$$F_e^c = (\rho u)_e \delta r_j (1 - \alpha_e)\phi_P + (\rho u)_e \delta r_j \alpha_e \phi_E$$

$$F_w^c = (\rho u)_w \delta r_j (1 - \alpha_w)\phi_W + (\rho u)_w \delta r_j \alpha_w \phi_P$$

where $\lambda = (0 \sim 1)$ is a parameter, and the superscripts ^{n} and $^{n-1}$ indicate taking the value from the current and previous iterations, respectively, α_e and α_w are the interpolation factors, and are defined as: $\alpha_e = \frac{x_e - x_P}{x_E - x_P}$, $\alpha_w = \frac{x_P - x_w}{x_P - x_W}$. For uniform mesh, $\alpha_e = \alpha_w = 1/2$.

Thus, we have:

$$F_e^c = (\rho u)_e \delta r_j (\phi_P + \phi_E)$$

$$F_w^c = (\rho u)_w \delta r_j (\phi_W + \phi_P)$$

The convection flux in the radial direction could be applied in a similar way. In this research, the velocity in the radial direction v is totally ignored, therefore, no convection flux is considered.

The diffusion fluxes are defined as:

$D_e = D\frac{r_j(\phi_E - \phi_P)}{x_E - x_P}$, $D_w = D\frac{r_j(\phi_P - \phi_W)}{x_P - x_W}$, $D_n = D\frac{r_i(\phi_N - \phi_P)}{r_N - r_P}$, $D_s = D\frac{r_i(\phi_P - \phi_S)}{r_P - r_S}$.

where D is the diffusion coefficient, and is treated as a constant.

Substituting everything into Eq. (3.18), a set of algebraic equations are obtained in the following form:

$$A_S\phi_S + A_W\phi_W + A_P\phi_P + A_E\phi_E + A_N\phi_N = b \tag{3.19}$$

The coefficients of Eq. (3.19) consist of a pentadiagonal matrix, and are given by:

$$A_N = -D\frac{\delta x_i r_n}{r_N - r_P}$$
$$A_S = -D\frac{\delta x_i r_s}{r_P - r_S}$$
$$A_E = \min((\rho u)_e \delta r_j, 0) - D\frac{\delta r_j r_P}{x_E - x_P}$$
$$A_W = -\max((\rho u)_w \delta r_j, 0) - D\frac{\delta r_j r_P}{x_P - x_W}$$
$$A_P = \frac{3\rho r_P \delta x_i \delta r_j}{2\delta t} - (A_W + A_S + A_E + A_N)$$

The right hand side vector is given by:

$$b = (S_c + S_P) r_P \delta x_i \delta r_j + (\frac{2\rho\phi_P^n}{\delta t} - \frac{\rho\phi_P^{n-1}}{2\delta t}) r_P \delta x_i \delta r_j - \lambda(F_e^c - F_e^u - F_w^c + F_w^u)$$

The matrix of the equations can be solved by Stone's SIP [80] solver, or some other suitable solver, such as BiCGStab solver. Stone's SIP solver is preferred due to its faster convergence and simpler implementation.

The North Boundary Condition Discretization

The north boundary condition discretization is worth mentioning, because the binding kinetics occurs on the north boundary or cell surfaces of the wall. Fig. 3.3 (B) shows the north boundary control volume.

Based on Fick's first law, diffusive flux in one dimension is expressed as $J = K_d \frac{\partial \phi}{\partial r}$, where K_d is the diffusive coefficient or diffusivity of the growth factor (FGF-2) in the solution, and regarded as a constant here. The north boundary condition is:

$$\frac{\partial \phi}{\partial r} = f = \frac{q}{K_d} \tag{3.20}$$

where q is the boundary flux.

By using one-side difference, then:

$$(\frac{\partial \phi}{\partial r})_n = \beta\frac{\phi_N - \phi_P}{r_N - r_P} + (1-\beta)\frac{\phi_P - \phi_S}{r_P - r_S} \tag{3.21}$$

where $\beta = \frac{\alpha+2}{\alpha+1}$, and $\alpha = \frac{r_P - r_S}{r_N - r_P} = 2$, so $\beta = \frac{4}{3}$. By using finite volume method [19], Eq. (3.20) can be discretized as:

$$\frac{4}{3}\frac{\phi_N - \phi_P}{r_N - r_P} - \frac{1}{3}\frac{\phi_P - \phi_S}{r_P - r_S} = \frac{q_N}{K_d}$$

or

$$\phi_N = (1 + \frac{1}{4}\frac{r_N - r_P}{r_P - r_S})\phi_P - \frac{1}{4}\frac{r_N - r_P}{r_P - r_S}\phi_S + \frac{3}{4}\frac{r_N - r_P}{K_d}q_N$$

Therefore:

$$\begin{aligned}
A_N\phi_N &= A_N(1 + \frac{1}{4}\frac{r_N - r_P}{r_P - r_S})\phi_P - A_N\frac{1}{4}\frac{r_N - r_P}{r_P - r_S}\phi_S + A_N\frac{3}{4}\frac{r_N - r_P}{K_d}q_N \\
A_P &= A_P + A_N(1 + \frac{1}{4}\frac{r_N - r_P}{r_P - r_S}) \\
A_S &= A_S - A_N\frac{1}{4}\frac{r_N - r_P}{r_P - r_S} \\
b &= A_N\frac{3}{4}\frac{r_N - r_P}{K_d}q_N
\end{aligned}$$

where, subscripts N, P, S indicate the northern interface, the cell center, and the southern interface of a control volume, respectively.

To solve the mass transport equations correctly, the unit of the growth factor (FGF-2) should be appropriate. In binding kinetics equations described in the next section, the unit of growth factor is mol/L, which is a very small value, even less than the stopping criteria. Obviously, this unit is inappropriate. Instead, to solve the equations, the unit of ng/ml is used, which is much larger than the stopping criteria. Thus, a unit conversion is required between calculating mass transport equations PDEs and binding kinetics equations ODEs.

A transient solution is pursued. The linear system is solved by using Stone's SIP method [80].

3.3.3 Binding Kinetics Equations

The binding kinetics model is adopted from Forsten-Williams et al. [27], as shown in Fig. 3.4. It involves a series of molecular activities, including the growth factor

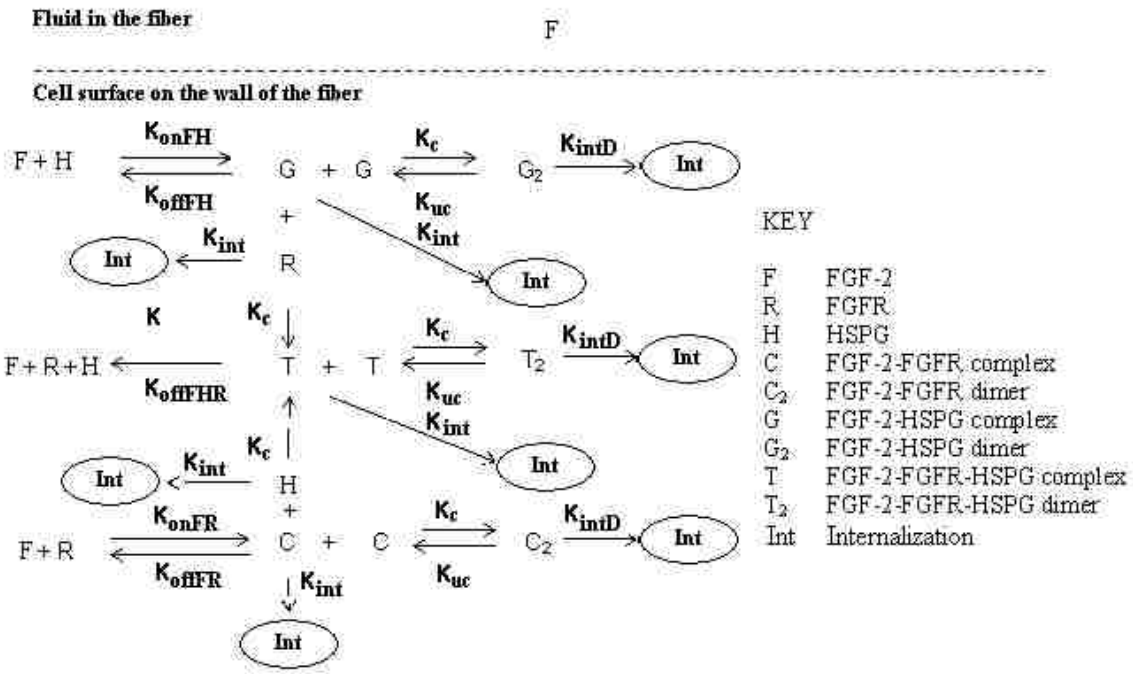

Figure 3.4: The diagram of binding kinetic pathway.

(FGF-2) binding to its receptors (FGFR and HSPG), some intermediate complexes and dimers are created, and internalization of those complexes and dimers. Nine chemical reactions and species are involved [27, 71]. The computational model is expressed as a set of ODEs shown in Table 3.1 and in Appendix A [20, 27]. Some key parameters used in simulation are listed in Table 3.2.

These coupled nonlinear ODEs can be solved by the CVODE solver with user-supplied Jacobian matrix [6]. Readers are referred to Chapter 1 for details.

3.4 Numerical Algorithm

In order to solve those coupling equations (PDEs and ODEs), a numerical algorithm for simulation has been designed. A schematic algorithm is given in Algorithm 8.

Inside the while loop, first, it computes the velocity u in each grid for the whole mesh by calling Eq. (3.12); then, solves the binding kinetics ODEs on the north boundary grids by calling the CVODE solver since the boundary conditions of mass

Table 3.1: Equations describing the binding reactions in the model.

No	Binding Equations
1	$\frac{dR}{dt} = -k_{onFR}FR + k_{offFR}C + K_{offFHR}T - k_cRG - k_{int}R + k_{int}R_0$
2	$\frac{dC}{dt} = k_{onFR}FR - k_{offFR}C - k_cCH - k_cC^2 + 2k_{uc}C_2 - k_{int}C$
3	$\frac{dC_2}{dt} = 0.5k_cC^2 - k_{uc}C_2 - k_{intD}C_2$
4	$\frac{dT}{dt} = k_cRG + k_cCH - k_{offFHR}T - k_cT^2 + 2k_{uc}T_2 - k_{int}T$
5	$\frac{dT_2}{dt} = 0.5k_cT^2 - k_{uc}T_2 + k_{intD}T_2$
6	$\frac{dH}{dt} = -k_{onFH}FH + k_{offFH}G + k_{offFHR}T - k_cCH - k_{int}H + k_{int}H_0$
7	$\frac{dG}{dt} = k_{onFH}FH - k_{offFH}G - k_cRG - k_cG^2 + 2k_{uc}G_2 - k_{int}G$
8	$\frac{dG_2}{dt} = 0.5k_cG^2 - k_{uc}G_2 - k_{intD}G_2$
9	$V\frac{dF}{dt} = -k_{onFR}FR + k_{offFR}C + k_{offFHR}T - k_{onFH}FH + k_{offFH}G$

Cells line the walls of the hollow fiber tube in the model and growth factor can bind to both receptors FGFR (R) or HSPG (H) to form complexes (C or G, respectively). These complexes can dimerize (C_2 or G_2,) or form heterodimers (T) that can then form higher order complexes (T_2). The equations that describe the binding reactions are listed as well as the parameters (Table 3.2) and initial conditions used for the simulations. The initial condition for the FGF-2 concentration (F) was based on the amount of FGF-2 injected. The concentration is assumed to be uniform across the entrance. The receptor FGFR and HSPG densities were the initial conditions for R and H respectively. All other variables had an initial value of zero.

Table 3.2: Parameter values used in simulation.

Parameter	Value	Meaning(Ref.)
k_{onFR}	$4.2 \times 10^8 M^{-1}min^{-1}$	ARC for FGF-2 and FGFR [77]
k_{offFR}	$0.79min^{-1}$	DRC for FGF-2 and FGFR [77]
k_{onFH}	$1.2 \times 10^8 M^{-1}min^{-1}$	ARC for FGF-2 and HSPG [77]
k_{offFH}	$1.37min^{-1}$	DRC for FGF-2 and HSPG [20]
k_{offFHR}	$0.038min^{-1}$	DRC for FGF-2 and HSPG and FGFR [77]
k_c	$0.001(\#/cell)^{-1}min^{-1}$	coupling rate constant [33]
k_{uc}	$1.0min^{-1}$	uncoupling rate constant [33]
k_{int}	$0.005min^{-1}$	IRC for complexes [77]
k_{intD}	$0.078min^{-1}$	IRC for dimers [77]
R_0	$10^4\#/cell$	initial FGFR density [17, 20, 40]
H_0	$10^6\#/cell$	initial HSPG density [17, 20, 40]
K_d	$1.57 \times 10^{-10}m^2/s^A$	FGF-2 diffusivity at $37°C$ [20]
μ	$0.001Pa \cdot s^B$	viscosity of aqueous solution
ρ	$1000kg/m^3$	density of aqueous solution

^{A} Filion & popel (2004), but aqueous solution this study used has different viscosity ^{B}. The relationship between viscosity and diffusivity can be expressed by Stokes-Einstein-Sutherland equation, that is,$K_d = \frac{kT}{6\pi\mu a}$, where K_d is the diffusion coefficient, k is the Boltzmann's constant, T is absolute temperature, μ is viscosity, and a is molecular radius. ARC = association rate constant, DRC = dissociation rate constant, IRC = internalization rate constant.

Algorithm 8 Numerical algorithm for simulation system

```
Initialization
t = 0
while t ≤ t_end do:
    Compute velocities by solving medium flow equations
    Solve binding kinetics equations by using CVODE solver
    Solve mass transport equation by using finite volume method
    Compute growth factor binding(captured, exited, etc.) if user needs
    Output results for analysis and visualization if needed
    t = t + Δt
end while
```

transport equations depend on those ODEs; at last, solves the mass transport equations in the whole mesh domain by calling SIP or BiCGStab solver, an inner iterative loop. At this point, it computes the binding information (bound, internalized, exited, etc.) and outputs those results for analysis and visualization if user needs. At the end, it moves forward to the next time step and loops again until the target simulation time is reached.

Since the unit of the growth factor (FGF-2) should be in the unit of mol/L during the calculation of kinetics binding equations, a very small value. For example, 2.54 ng/ml of the growth factor (FGF-2) equals to 1.411×10^{-10} mol/L. It is too small to be used to solve mass transport equations. Instead, the unit of ng/ml is used for the precision of calculation.

In the algorithm above, the coupled equations of three parts actually can be solved separately, which means different parts can be calculated independently in a given order. That is why different binding kinetics models can be easily implemented into the system with trivial efforts. Also, it is possible to make it support more complicated binding kinetics models, for example, more growth factors and receptors involved.

Due to its intensive computation, it is desirable to make the simulation system running quickly and efficiently. The current system is implemented with Open Multi-Processing (OpenMP) and multi-threading techniques to take advantage of multi-core processors of computers. If the binding occurs in the whole fiber (i.e., there are

competitive bindings in the fluid and on cell surfaces as well), some kind of parallel algorithm needs to be implemented by using OpenMP or message passing interface (MPI) techniques.

3.5 Some Implementation Details

In order to achieve accurate simulation results compared to those obtained from experiments, several issues have to be addressed, such as: (1) What type of mesh should be used? uniform or non-uniform? and how large the mesh size is appropriate? (2) What is the concentration of the growth factor (FGF-2) flowing into the fibers at a specific time? Obviously, it is a function of time and related to the amount of the growth factor (FGF-2) injected at inlet reservoir, but what the concentration function should be with respect to time? (3) How to measure the amount of the growth factor (FGF-2) or other molecules (bound, internalized, or remained within the fibers) ? (4) How to calculate the amount of the growth factor (FGF-2) exited?

3.5.1 Mesh Size Selection

Because the binding reactions occur only on the cell surfaces on the wall of the fibers, a thin layer of the growth factor (FGF-2) near the surface of the hollow-fibers binds to its receptors (FGFR and HSPG, etc.) on cell surfaces. This cross sectional area is illustrated in Fig. 3.5 and can be estimated as:

$$\delta v = \pi(R^2 - r_n^2)\delta x = \pi\delta r(2R - \delta r)\delta x \tag{3.22}$$

where δv is the volume of this area, δx is the length in the axial direction, r_n is the radius of the nth grid and δr is the grid size in the radial direction, respectively.

Supposing the cells are distributed evenly on the surface of the wall and packed tightly, and the cell shape is round with the radius of r_c, the total number of cells in each fiber can be estimated as:

$$N_{cell} \approx \frac{2\pi RL}{\pi r_c^2} \tag{3.23}$$

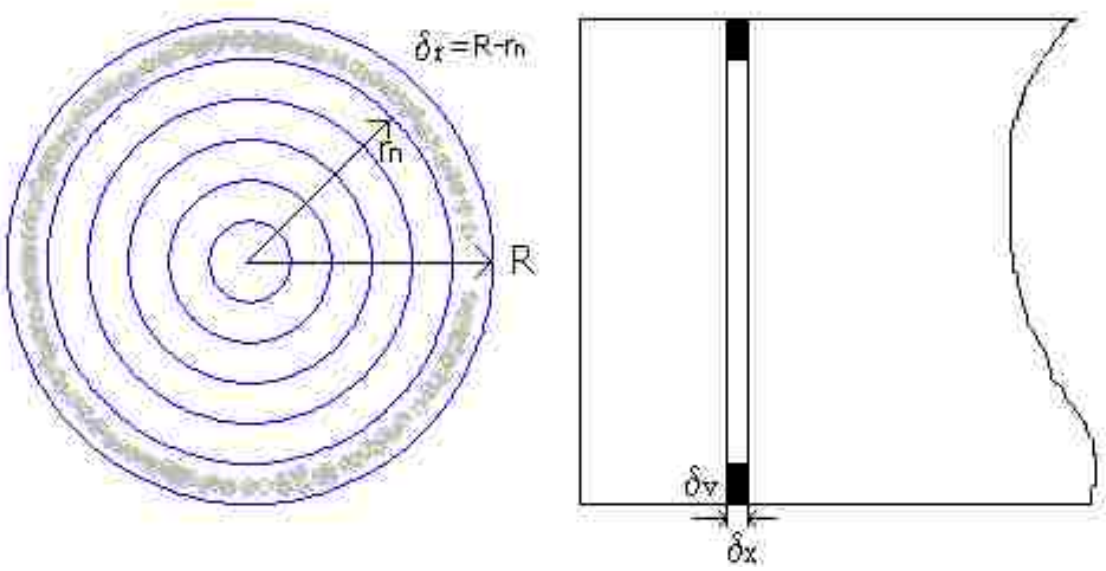

Figure 3.5: The cross section of a fiber and the mesh schematic diagram.

where $R = 0.035cm$ is the radius of the fiber, and $L = 12cm$ is the length of the fiber.

If a cell size is around $10um$ in radius, or $r_c = 10um$, then, $N_{cell} \approx 8.4 \times 10^5$. Let $N_{cell} = 8 \times 10^5$, which is the same as the estimation of the experiment. Thus, the total number of cells in the cartridge is about 16 millions. If $\delta x = 20um$ is used, the number of grids in the axial direction $N = L/\delta x$, which is around 6000. The number of grids in the radial direction is set to be 24, that is $M = 24$ or $\delta r = R/M \approx 0.001458cm$.

The major interest of this study is calculating the mass of proteins (such as FGF-2) captured. It is appropriate to calculate those values on cell-by-cell basis. Therefore, a uniform mesh is a better choice, and the mesh could be 6000×24 if the mesh size is equivalent to the size of cells in the axial direction. So, $\delta v = \pi \delta r(2R - \delta r)\delta x \approx 6.279 \times 10^{-10}\ L$. There are about 133.33 cells in each δv. Let $v = \delta v/133.33 \approx 4.721 \times 10^{-12}\ Lcell^{-1}$. ($v$ is the volume of space corresponding to one cell.) The parameter V in Eq. 9 of Table 3.1 can be calculated by the formula:

$$V = v \times Na \approx 2.835 \times 10^{12} \#Lcell^{-1}mol^{-1} \tag{3.24}$$

where Na is the Avagodro's number.

It is worth mentioning that the unit of the growth factor (FGF-2) concentration

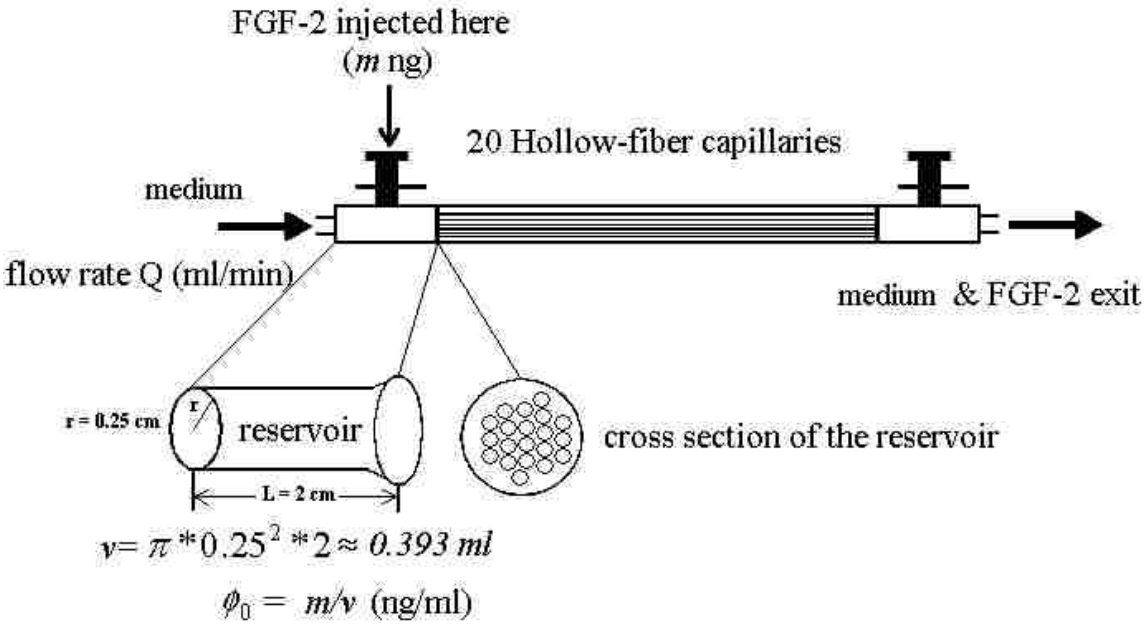

Figure 3.6: The diagram of inlet reservoir.

in Table 3.1 should be in mol/L, but it is normally given in the unit of ng/ml (also preferred in solving mass transport equations). The unit conversion is necessary, and we simply multiply it by a constant (For FGF-2, it is 5.556×10^{-11}).

Other possible meshes could be 3000×24, 1500×24, etc. V is kept as a constant. Another variable K_{gf} is used as a grid factor. K_{gf} is equal to the number of cells per fiber divided by the number of grids in the axial direction.

3.5.2 The Concentration of Growth Factor at Inlet

To more closely link the simulations to the experimental model system, several additional assumptions were made. For simplicity, all the 20 fibers are assumed to have the same concentration function of growth factor at entrance or inlet. In the experimental system, the growth factor (FGF-2) is injected into the inlet reservoir, as shown in Fig. 3.6.

It is assumed that the initial concentration of the growth factor (FGF-2) in the whole reservoir is uniform, and then distributed into the individual hollow-fiber capillaries by the pump. The concentration of the growth factor (FGF-2) in the reservoir

is assumed to decrease gradually at each time step as:

$$\phi_{ent}^{n} = \phi_{ent}^{n-1} \times \frac{v - \delta v}{v} \tag{3.25}$$

where v is the volume of the inlet reservoir, which is around 0.393 ml (refer to Fig. 3.6), δv is the volume of fluid flowing into the fibers at each time step, ϕ_{ent}^{n-1} is the previous and ϕ_{ent}^{n} is the current concentration of the growth factor (FGF-2) in the reservoir, and $\phi_{ent}^{0} = \frac{F_0}{v}$, in which F_0 is the amount of the growth factor (FGF-2) injected in the unit of ng.

3.5.3 The Mass of Growth Factor Bound

The kinetics binding is assumed to occur on the cell surfaces only, and the amount of the growth factor (FGF-2) bound to its receptors (FGFR and HSPG) within the fibers includes two parts: bound on cell surfaces and internalized. Let M_n be the amount of the growth factor (FGF-2) bound, M_n^{int} be the internalized part, and $M_n^{surface}$ be the bound on cell surfaces at the nth time step, we have:

$$M_n = M_n^{int} + M_n^{surface} \tag{3.26}$$

First, the number of molecules of the growth factor (FGF-2) bound is determined, then we multiply it by a constant to obtain the amount of the growth factor (FGF-2) bound.

Based on deterministic approach and uniform mesh, the number of molecules of the growth factor (FGF-2) bound at the nth time step F_n can be determined by the following formulas:

$$F_n = F_n^{int} + F_n^{surface} \tag{3.27}$$

$$F_n^{int} = F_{n-1}^{int} + N_f K_{gf} dt \sum_{i=1}^{N} (k_{int}(C_i^n + T_i^n + G_i^n) + 2k_{intD}(C_{2,i}^n + T_{2,i}^n + G_{2,i}^n)) \tag{3.28}$$

$$F_n^{surface} = N_f K_{gf} \sum_{i=1}^{N} (k_{int}(C_i^n + T_i^n + G_i^n) + 2(C_{2,i}^n + T_{2,i}^n + G_{2,i}^n)) \tag{3.29}$$

where C_i^n, T_i^n, G_i^n are the number of the growth factor (FGF-2) complexes, and $C_{2,i}^n$, $T_{2,i}^n$, $G_{2,i}^n$ are the number of the growth factor (FGF-2) dimers at the ith grid in the axial direction (see Fig. 3.4), k_{int} is the internalization rate constant of complexes, k_{intD} is the internalization rate constant of dimers, Superscript ^{n} means the nth time step, N_f is the number of fibers in the cartridge, and K_{gf} is the grid factor.

Supposing the cell density is 800,000 cells per fiber, or 16 millions cells per cartridge, if the mesh of 1500 grids in the axial direction is selected, there are about 533 cells in each grid cross sectional area of each fiber. This number is the grid factor, i.e., $K_{gf} \approx 533$.

Since the molecular weight of the growth factor is w kDa, once the above molecular number is obtained, to convert the number of molecules to its weight in the unit of ng, just multiply it by a constant ($K = w \times 10^{12}/6.022 \times 10^{23}$), that is:

$$M_n = F_n \times K(ng) \tag{3.30}$$

Based on the deterministic approach, the mass of any kind of molecule in biochemical reactions can be calculated in a similar way. Generally, the method can be illustrated as follows:

Supposing two kinds of molecules A and B can be associated to C with the association rate constant k_{on} and dissociation rate constant k_{off}, in the meantime, C may be internalized with rate constant k_{int}, the kinetics equation can be expressed as:

$$\frac{dC}{dt} = k_{on}AB - k_{off}AB - k_{int}C \tag{3.31}$$

In a 2D case, if the uniform mesh is used and the mesh size is $N \times M$, and the binding reaction occurs in all 2D domain, the number of molecules of A bound to B can be calculated by the formula:

$$A_n = k \times \sum_{j=1}^{M} \sum_{i=1}^{N} C_{i,j}^n + A_n^{int} \tag{3.32}$$

and

$$A_n^{int} = A_{n-1}^{int} + k \times \sum_{j=1}^{M} \sum_{i=1}^{N} (\Delta t \times k_{int} \times C_{i,j}^n) \tag{3.33}$$

where A_n is the number of molecules of A bound to B in the nth time step, Δt is the time step of numerical simulation, $C_{i,j}^n$ is the number of molecules of C in grid (i,j) at the nth time step, N and M are the mesh sizes in the axial and the radial directions, respectively, k is the number of cells in each grid, A_n^{int} and A_{n-1}^{int} are the internalized components at the nth and the $(n-1)$th time step, respectively.

Again, internalized component is accumulated at each time step.

To calculate the mass of A, we just multiply it by a constant if its molecular weight is known. To the best of the author's knowledge, there is no such formula in the literature before.

3.5.4 The Mass of Growth Factor Flowing Into or Out of the Fibers

In order to control the amount of the growth factor (FGF-2) flowing into the fibers or calculate the amount of the growth factor (FGF-2) exited, or calculate the total amount of the growth factor (FGF-2) inside the fibers, it is necessary to figure out how to calculate the amount of the growth factor (FGF-2) flowing through a cross section of a fiber at a given time span.

The mass of the growth factor (FGF-2) moving through a fiber at location x in the axial direction in δt can be integrated by the following formula:

$$M_{FGF-2}(x) = 2 \times \pi \int_0^{\delta t} \int_0^R u(r,t)\phi(r,x,t) r dr dt \tag{3.34}$$

Numerically, it can be estimated in a similar way by:

$$M_{FGF-2}(x_i) \approx \pi \times \sum_{j=1}^{M} (r_j^2 - r_{j-1}^2) u_j(x_i)\phi_j(x_i)\delta t \tag{3.35}$$

where δt is the time step, $u_j(x_i)$ is the axial velocity, $\phi_j(x_i)$ is the concentration of the growth factor (FGF-2) on the jth grid in the radial direction and at location x_i

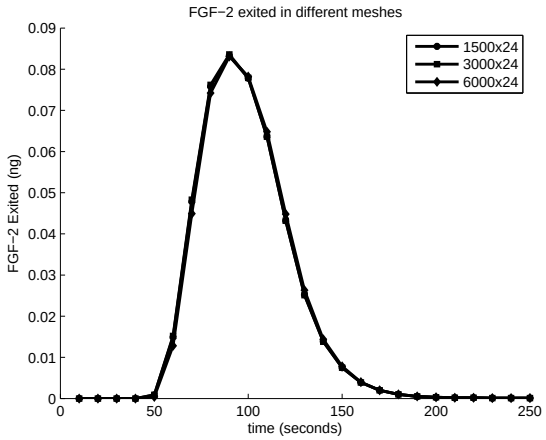

Figure 3.7: Comparison of the growth factor (FGF-2) exited in different mesh sizes.

in the axial direction, and M is the number of grids in the radial direction of the current mesh.

Eq. (3.35) can be used to estimate the mass of the growth factor (FGF-2) flowing into or out of a fiber. To calculate the mass of the growth factor (FGF-2) inside one fiber, the following formula is used:

$$M_{inside} \approx \sum_{i=1}^{N} M_{gf}(x_i) \tag{3.36}$$

To obtain the mass of the growth factor (FGF-2) inside the whole cartridge, M_{inside} is multiplied by $N_f(=20)$, the total number of fibers in the cartridge.

3.5.5 Some Considerations for the Simulation

Choose an Appropriate Mesh Size for the Simulation

Generally speaking, larger mesh sizes mean less computational costs. It is desirable to find larger mesh size without sacrificing accuracy. Three different meshes 1500×24, 3000×24, and 6000×24 were evaluated. Fig. 3.7 is the comparison of the growth factor (FGF-2) exited using different mesh sizes. There are only slight differences between these three cases. Other binding parameters, such as the amount of bound, internalized, and inside the fibers are also quite close between these three mesh sizes.

Conclusion: The coarsest grid 1500×24 is appropriate for the simulation and is selected for all the subsequent simulations to save computational costs.

Choose an Appropriate Time Step for the Simulation

Generally, a smaller time step usually leads to more accurate results but longer simulation time, and a larger time step may sacrifice accuracy, but could save simulation time. It is a trade off. For the current simulations, it is desirable for the fluid to move forward no more than one grid point within a time step since the simulation is working on a cell by cell basis. The cells however are only localized on the wall of the fibers where the velocity in the axial direction u approaches zero. A relatively larger time step therefore could possibly be used without sacrificing the binding accuracy. However, large time steps may influence the accuracy of calculating the amount of the growth factor (FGF-2) flowing into and out of the fibers or the mass transport equations.

For example, with a flow rate of 0.67 ml/min, or 0.145 cm/s on average, if a time step of 0.05 second is selected, the fluid would only move forward 0.00725 cm on average per time step. This is close to the value of one grid size (0.008 cm) in the axial direction when a 1500×24 uniform mesh is used. Therefore, time step = 0.05 second is appropriate in this case. Even doubling the time step to 0.1 second, there is no significant impact on the simulation results. Therefore, 0.1 or 0.05 second is considered an acceptable time step for slower flow rates, such as 0.67 ml/min. For higher flow rates, time steps should be smaller accordingly. If the time step is too big, it will cause computational stability issue for higher flow rates.

3.6 Simulation

3.6.1 Flow Rate Impact on Growth Factor Binding

By intuition, people may think that higher flow rates would result in less binding due to lower residence time in the cell environment. Table 3.3 shows the quantitative

Table 3.3: The relationship between flow rate and binding.

Flow rate(ml/min)	FGF-2 exit(ng)	FGF-2 bound(ng)
0.6	3.96	0.016
0.7	4.12	0.0012
0.8	4.26	0.0009
0.9	4.37	0.0007

Initial FGF-2 injected 5.47ng, diffusivity 1.57×10^{-10} m2/s, heparinase treated cells, total simulation time 643 seconds.

relationship between flow rate and the growth factor (FGF-2) binding. Identical simulation parameters except the flow rate were used. Fig. 3.8 shows the relationship between flow rate and the amount of binding. The simulation results show that the higher flow rate, more growth factor exited, less growth factor bound, and more growth factor bound at the entrance part of the fiber than at other parts.

3.6.2 Diffusivity Impact on Growth Factor Binding

Generally, larger diffusivity or smaller viscosity values will lead to more molecules of the growth factor (FGF-2) dissipating toward the wall, where cells are located. More binding will likely occur resulting in less growth factor exiting. Several simulations were conducted with the same parameters except the diffusivity or viscosity to find out the quantitative relationship between the two, as shown in Table 3.4.

Diffusivity affects the distribution of the growth factor (FGF-2) bound along the fiber, as shown in Fig. 3.9. Larger diffusivity will cause more bound in the middle of the fiber, but a slightly more bound at the entrance or exit of the fiber. Thus, diffusivity affects the amount of the growth factor (FGF-2) bound and larger diffusivity values will lead to more growth factor (FGF-2) bound to its receptors (FGFR and HSPG).

Table 3.4: The relationship between diffusivity and binding.

Diffusivity(cm^2/s)	Viscosity(cP)	FGF-2 exited(ng)	FGF-2 bound(ng)
5.22×10^{-7}	3^A	0.72	0.13
1.57×10^{-6}	1^B	0.55	0.22
1.75×10^{-6}	0.89^C	0.53	0.23
2.18×10^{-6}	0.72^D	0.48	0.25

Initial FGF-2 injected 0.92ng, flow rate 0.63 ml/min, total simulation time 715 seconds. ^{A}blood at 25°C, ^{B}The solution this research used, ^{C}water at 25°C, ^{D}Filion & Popel(2004) [20].

3.7 Summary

This chapter presents a numerical solution to describe growth factor-receptor binding under flow through hollow fibers of a bioreactor. The fluid flow, the kinetics of the growth factor (FGF-2) binding to its receptors (FGFR and HSPG) and the growth factor mass transport is modeled by a set of coupled nonlinear partial differential equations (PDEs) and coupled nonlinear ordinary differential equations (ODEs). A finite volume method is used to discretize the PDEs. The ODEs are solved by a stiff ODE solver, the CVODE solver. Overall, second order accuracy in time and space is achieved with the second order implicit Euler scheme. In order to obtain a reasonable accuracy of the binding and dissociation from cells, a uniform mesh is used. To handle pulsatile flow, several assumptions are made including neglecting any entrance effects, and an analytical approximate solution for axial velocity within the fibers is obtained.

A computer simulation program has been developed for the simulation of a growth factor binding to its receptors within the FiberCell Bioreactor Systems, an *in vitro* flow cell culture system. Some simulation results have been obtained based on the basic model [27], such as (1) the current coarsest gird (1500×24) is appropriate for the simulation; (2) the amount of binding of FGF-2 is proportional to the diffusivity of the solution and roughly linear proportional to the flow rate; (3) different flow rates

or diffusion coefficients will affect the profile of the growth factor (FGF-2) outflow and the distribution of the growth factor (FGF-2) bound on the wall along the fiber at different time.

The simulation package can be used for any kinetics binding analysis in a similar flow environment, as long as only one growth factor is injected in the flow. Next, this simulation package is used to investigate growth factor-receptor binding and compared with the experiments.

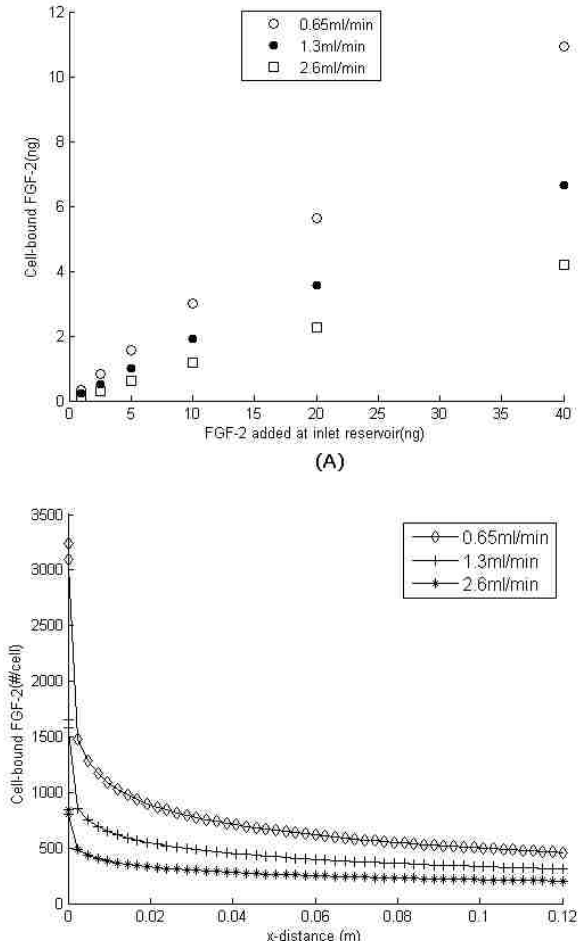

Figure 3.8: The relationship between flow rate and the amount of FGF-2 binding. (A) Cell-bound FGF-2 is shown after 5 min of simulation for various amount of FGF-2 injected and various flow rates. (B) Cell-bound FGF-2 is shown along the fiber. 1ng FGF-2 was injected at time 0 under different flow rates. Each cell expressed 10^4 FGFRs and 5×10^5 HSPGs initially.

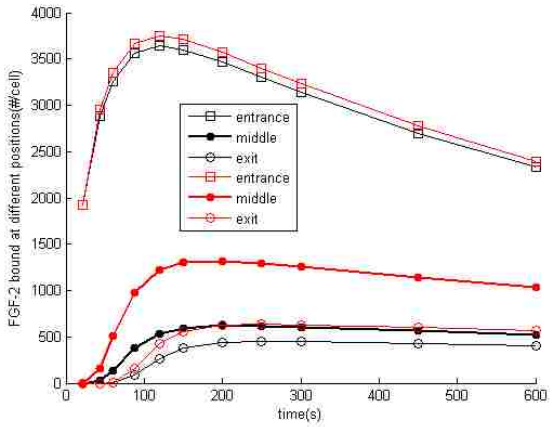

Figure 3.9: Plot of FGF-2 bound to FGFR and HSPG versus time at the entrance , middle and exit of the fiber when FGF-2(1ng) is introduced into the fiber under pulsatile flow at 0.67ml/min with FGF-2 having a diffusivity of $1.67 \times 10^{-10} m^2/s$ (black) or $1.67 \times 10^{-9} m^2/s$(red).

4 Endothelial Cell Capture of Heparin-Binding Growth Factors under Flow

4.1 Introduction

The bioavailability of molecules as they circulate through the bloodstream is a crucial factor in their signaling capability. Halflife in circulation can determine the effectiveness of a drug simply by regulating the opportunities a molecule has to interact with the vessel wall. Although *in vivo* measurements are routinely made by researchers to monitor serum levels of molecules and to determine half-lives, interactions in the microenvironment are not easily measured or observed. While some molecules may have a long circulation life, many may have only a single opportunity to interact with the blood vessel walls before being filtered through the liver or kidneys. In addition, even molecules with a long circulation life may still face impediments to direct interaction with the endothelium. This, for example, is the case with vascular endothelial growth factor (VEGF) when bound to bevacizumab, a monoclonal antibody to VEGF [37, 45]. Bevacizumab has been shown to increase the circulating concentration of VEGF in cancer patients when compared to patients not undergoing therapy because of the increased half-life of the growth factor-antibody complex; however the complex is unable to bind to VEGF receptors [31] making delivery of the VEGF questionable. In order to better understand the vessel microenvironment and to accurately monitor drug interactions in the context of that microenvironment, better tools are needed to provide meaningful measurements that can predict the fate of molecules in circulation. Many important measurements have and continue to be made using *in vitro* mammalian tissue culture methods but there are obvious limitations to the traditional two-dimensional culture approach. In circulation, the influence of flow on whether a molecule remains in the fluid phase or binds to the vessel wall can be a dominant factor. This influence cannot be ascertained in static tissue culture studies. For example, the velocity of blood in the aorta is 400 mm/sec while at the capillary

level it is less than 1 mm/sec [83]. This reduction in velocity allows the exchange processes at the capillary level to take place more efficiently [83] and it likely also affects the activity of molecules in circulation that rely on cell surface binding in order to fulfill their roles. While direct measurement of this binding process is difficult, the computer model of this study makes use of a commercial bioreactor with endothelial-lined hollow tubes operating under pulsatile flow to mimic the vascular environment architecture and to directly measure the loss of molecules as they pass through these hollow fibers. A single pass method is used to allow better assessment of the effect of flow in either retaining molecules in the circulation or permitting their interaction with vessels. This approach also makes use of a bolus administration, since this is a typical way in which drugs would be delivered in a clinical setting. The binding of fibroblast growth factor-2 (FGF-2) to its cell surface receptor (FGFR) and the role of heparan sulfate proteoglycans (HSPG) in regulating the process have been of research interest for many years because of their role in angiogenesis, the growth of new blood vessels from existing vessels. Knowledge of how these processes work could aid in the development of new therapeutics to control tumor growth and assist clinically in the treatment of chronic wounds. In order to understand the mechanism of FGF-2-mediated cell proliferation, a multitude of experimental studies have been undertaken [3] and, in the past two decades, several computational models of FGF-2 binding to its receptor FGFR and HSPG have been proposed [17, 20, 27, 38, 48, 55]. Insight can be gained through experiment-coupled modeling that could not otherwise be readily obtained. Nugent and Edelman [55] were among the earliest researchers to develop a simple model that includes three species, FGF-2, FGFR and HSPG. They measured kinetic binding rate constants experimentally and used their model to analyze the data thereby providing a foundation for investigating the complexity of FGF-2 binding. A similar approach was used by Ibrahimi et al. [38] to investigate stepwise assembly of a ternary FGF-2-FGFR-HSPG complex in conjunction with

their surface plasmon resonance measurements. Forstern-Williams et al. introduced more complexity into the FGF-2 binding model with the inclusion of heparin binding [26], receptor dimerization [27], and formation of alternative HSPG-FGFR species [28]. Recent models have moved towards including intracellular signaling [29]. With the exception of work by Filion and Popel [20, 21], which included diffusive transport, previous simulation work has been based on a static tissue culture environment that may be quite different from the dynamic *in vivo* environment of blood vessels. A computational model based on a flow environment was introduced, in which the competitive binding of FGF-2, FGFR, and HSPG in a pulsatile flow environment was addressed to mimic blood vessel-like hollow fibers [71, 96].

In this chapter, the model is used to explore how specific parameters such as flow rate impact FGF-2 capture and receptor binding, and compare simulation results with experimental studies. Insights with regard to the importance of surface coupling and ligand depletion zones within the fluid phase were found. The described simulation package provides a new and valuable way to investigate growth factor capture and can be easily extended to other biologically relevant molecules and drugs.

4.2 Materials and Methods

4.2.1 Preparation of Bovine Aortic Endothelial Cells (BAECs)

BAECs (passage 10), cryopreserved in liquid nitrogen, were cultured in Dulbecco's modified Eagle's medium (DMEM-low glucose, phenol red-free, Invitrogen Corporation, Grand Island, NY), supplemented with penicillin (100U/mL, Invitrogen Corporation, Grand Island, NY), streptomycin (100mg/mL, Invitrogen Corporation, Grand Island, NY), glutamine (2mM, Invitrogen Corporation, Grand Island, NY), and 5% newborn calf serum (Invitrogen Corporation, Grand Island, NY). When a sufficient number of cells were grown (passage 11,13), they were transferred to the hollow fiber cartridge.

4.2.2 Preparation and Maintenance of Endothelial Cartridges

The FiberCell polysulfone plus endothelial cartridges (C2025, FiberCell Systems Inc., Frederick, MD), also called hollow fiber bioreactors, contain 20 capillaries which are 12 cm long, 700 mm I.D., 300 mm wall, 0.1 mm pore size, 53 cm2 lumen surface area (Fig. 3.1). They were activated with 70% ethanol (Fisher Scientific, Houston, TX), followed by multiple washes with sterile distilled water. The cartridges were then coated using 5 mg/mL fibronectin (Sigma Aldrich, St. Louis, MO) in phosphate buffered saline (PBS, Invitrogen Corporation, Grand Island, NY). BAECs (passage 11,13) were inoculated into the cartridges ($0.7-1\times10^7$ cells/cartridge) 24 hours after the coating and placed in an incubator for 4 hours (rotated 180° after 2 hours) without flow in order to promote cell attachment. The BAEC culture cartridges were then linked to the FiberCell pump system (FiberCell Systems Inc., Frederick, MD) and medium circulated through the system at ,2.6 mL/minute (5.2 mm/sec). The flow system was maintained in the incubator (37°C,5% CO2) at all times except during the experiment periods. Cell growth and viability was monitored by measurement of the cell glucose consumption from the medium once a day with OneTouch UltraSmart blood glucose monitoring system (Lifescan, Inc., Milpitas, CA).

4.2.3 Growth Factor Flow Studies

The flow system and cell-lined cartridges were removed from the incubator, gently washed once with warmed (37°C) PBS (60 mL), and then maintained in circulating 125 mL serum-free medium (DMEM-low glucose, phenol red-free, supplemented with 0.05% gelatin in PBS) in a sterile room-temperature tissue culture hood (Thermo Scientific, Waltham, MA). After establishing flow at the desired rate (low rate: 0.60,0.68 mL/min (1.2-1.36 mm/sec); high rate: 1.6-1.8 mL/min (3.2-3.6 mm/sec) or 2.9-3.0 mL/min (5.8- 6.0 mm/sec)) with a CellMax Quad pump (Spectrum Laboratories, Inc.) for about 2 minutes, flow was stopped to allow the growth factor of interest

(FGF-2 (Sigma Aldrich, St. Louis,MO), EGF (R&D Systems Inc., Minneapolis, MN) and VEGF (R&D Systems Inc., Minneapolis, MN)) (0.11 mL) to be injected into the inlet. After the injection, the flow was resumed and the flow medium collected (two drops/fraction) for the desired time period. The flow pattern was assumed to be sigmoidal based on previous studies [7, 14]. The cartridges were then gently washed with warmed PBS supplemented with 0.3 MNaCl (10 mL) followed by one wash with 10 mL PBS and a wash of the whole flow system with PBS (60 mL). The system was returned to the same culture medium and flow rates as described under Preparation of BAECs, allowing at least 24 hours before the next experiment. The medium fractions collected during the binding experiments were stored at 4°C and analyzed with ELISA kits (R&D Systems Inc., Minneapolis, MN) within the next 24,48 hours.

4.2.4 Viscosity Measurements

Dynamic viscosity of the test cell culture medium was measured using a DV-II++ Pro Programmable cone-plate viscometer (cone #CPE-40; Brookfield Engineering Laboratories; Boston, MA) according to the manufacturers instructions. Viscosity measurements were made for a range (375 to 750 sec^{-1}) of shear rates (to confirm Newtonian fluid behavior) at room (i.e., 25°C) and physiologic (i.e., 37°C) temperatures.

4.2.5 Enzymatic Treatment

Heparan sulfate expression was measured in static tissue culture dishes and in the flow cartridge by heparinase treatment of cells, collection of the cleaved glycosaminoglycans, and quantitation using a dimethylene blue colorimetric assay [5, 18]. Cells in static culture contained $4.3 \pm 0.31 \times 10^{-6} \mu g$ of heparan sulfate/cell and cells in cartridge hollow fibers contained $1.1 \pm 0.09 \times 10^{-6} \mu g$ of heparan sulfate/cell, reflecting an 75% reduction in cell surface heparan sulfate under flow (0.63 mL/min (1.26 mm/sec)). Heparinase III (0.01 unit/0.11mL, Seikagaku Corp., Japan; 0.2unit/0.11mL, Sigma

Aldrich, St. Louis, MO), chondroitinase ABC (0.2 unit/0.11mL, Seikagaku Corp., Japan) and keratanase (0.33unit/0.11mL, Sigma Aldrich, St. Louis, MO) were utilized to observe their effect on growth factor flow and binding. In some experiments, the enzymes (heparinase III, chondroitinase ABC and keratanase) were mixed together as an enzymatic cocktail solution at the above concentrations. Cartridges were treated for 20 minutes at 37°C,washed with warmed PBS (10 mL), and growth factor studies performed as described above.

4.2.6 Determination of Non-specific Binding

In addition to binding to receptors of interest, growth factors (such as FGF-2) may also bind to other sites, such as plastic wall of a fiber. Binding to the receptors of interest is called specific binding, while binding to the other sites is called nonspecific binding. Non-specific binding of FGF-2 in the system was determined to be primarily due to the inlet reservoir. The reservoir chamber was removed from the cartridge, growth factors were injected into the inlet of the cartridges with a syringe, and flow was initiated. Fractions were collected as they exited the reservoir. Growth factors were measured before injection and compared to the sum of the collected fractions. The difference between the input amount and the amount collected constituted the nonspecific binding in the experiments. For FGF-2 (1.0±0.1 ng), the amount retained in the reservoir was 29±2.8% of the FGF-2 added (SD, n= 3). Additional nonspecific binding within the hollow fibers was assumed to be minimal.

4.2.7 Determination of Growth Factor Concentration in Outflow

The concentrations of FGF-2, EGF, and VEGF in the collected fractions were measured by ELISA. The flow rate of each experimental run was determined from the total volume collected divided by the total flow time.

4.3 Model Development

The computational model is based on the physical dimensions of the bioreactor although the system is scalable to other desired dimensions. The domain of the simulation is the hollow-fiber portion of the cartridge (Fig. 3.1). The computational model has three coupled parts: (1) the medium flow equations; (2) the convective mass transport equations of growth factor in the flow; (3) the binding kinetics equations on the wall of the fibers [27, 71]. In order to solve the coupled equations numerically and efficiently, the following assumptions are made: (1) the walls of the hollow fibers are rigid and nonporous; (2) the flow is axisymmetric and laminar; (3) the fluid is incompressible, Newtonian and isothermal; (4) all of the hollow-fiber capillaries within the cartridge have the same dimensions, flow rate, cell densities and entrance conditions; and (5) the cells are packed tightly and distributed evenly on the wall of the hollow-fiber capillaries. Entrance effects of the flow are ignored [35, 89] and, consequently, the flow within the fibers is treated as fully developed flow in which the radial velocity is neglected. A uniform mesh is used. The kinetic pathways are shown in Fig. 3.4 and the equations and parameter values are included in Table 3.1 and Table 4.1, respectively.

In the experimental system, FGF-2 is injected into the inlet reservoir where it is assumed to quickly reach a uniform concentration. The concentration of FGF-2 in the reservoir is assumed to decrease gradually as fluid is pumped into the reservoir prior to distribution into the capillaries with each time step as:

$$\phi_{ent}^{n} = \phi_{ent}^{n-1} \times \frac{v - \Delta v}{v} \tag{4.1}$$

where, v is the volume of the reservoir, Δv is the volume of fluid flowing into the fibers at each time step and is time dependent due to pulsatile flow, ϕ_{ent}^{n} is the current and ϕ_{ent}^{n-1} is the previous concentration of FGF-2 in the reservoir. $\phi_{ent}^{0} = \frac{F_0}{v}$, where, F_0 is the amount of FGF-2 injected.

Table 4.1: Parameter values used in simulation.

Parameter	Value
k_{onFR}	$3.2 \times 10^8 M^{-1} min^{-1*}$
k_{offFR}	$0.28 min^{-1*}$
k_{onFH}	$1.2 \times 10^8 M^{-1} min^{-1*}$
k_{offFH}	$0.56 min^{-1\&}$
k_{offFHR}	$0.018 min^{-1\&}$
k_c	$0.0024 (\#/cell)^{-1} min^{-1\bigstar}$
k_{uc}	$0.6 min^{-1\bigstar}$
k_{int}	$0.005 min^{-1*}$
k_{intD}	$0.078 min^{-1*}$
R_0	$10^4 \#cell^{-1\&}$
H_0	$2.5 \times 10^5 \#cell^{-1\%}$
D	$1.67 \times 10^{-10} m^2/s^{\&}$
μ	$0.00094 Pa \cdot s^{\%}$
ρ	$1000 kg/m^3$
ρ_{cell}	$800,000 \#fiber^{-1\%}$

* [78] but scaled to 25°C except for k_{int} and k_{intD}. $^{\&}$ [20] but scaled to 25°C except for R_0. $^{\bigstar}$ [49]. $^{\%}$ measured.

The pump pulse cycle was measured experimentally and determined to be 36 strokes/min at a flow rate of 1.4 mm/sec. Pulsatile flow is treated in the following manner. A pulse of fluid volume enters the pre-pump inlet reservoir (0.4 mL volume), from which a continuous flow of fluid having an axial velocity greater than or equal to zero enters the cell-lined fibers in the cartridge. The axial velocity is oscillatory but with only positive terms. Entrance effects are considered negligible [89]. The velocity of the fluid in the axial direction is determined with the following formula [96]:

$$u(r,t) \approx \frac{2q_s}{N_f \pi R^2}(1 - \frac{r^2}{R^2})(1 + cos\omega t) \tag{4.2}$$

where q_s is the average volumetric flow rate, N_f is the number of fibers inside the cartridge, R is the radius of a fiber, $\omega = 2\pi/T$ is the angular frequency of the pulsatile flow, and T is the pump pulse cycle.

4.3.1 Criteria for Comparison Between Simulation and Experiment

Good agreement between the simulation and experimental results was determined based on two criteria: an amount criterion and a curve-matching criterion.

Amount Criterion

The amount criterion is defined as:

$$\frac{|M_{exp} - M_{sim}|}{M} < 1\% \tag{4.3}$$

where M_{exp} is the outflow amount of protein determined experimentally, M_{sim} is the outflow amount determined within the simulations and M is the amount of FGF-2 entering the capillary.

Curve-matching Criterion

The FGF-2 exit profile curve is not a continuous curve but is a series of discrete values at different time intervals. This makes use of traditional curve matching algorithms difficult. The curve-matching criterion is calculated in the following way: (1) Align the initial exit times for the simulations and experiments; (2) Calculates the distance between points on the two outflow curves using the following formula:

$$D = \sqrt{\frac{\sum_{i=1}^{N}(a_i - b_i)^2}{N}} \tag{4.4}$$

where N is the total number of time intervals. a_i and b_i is the amount of FGF-2 exited at the ith time interval in experiment and simulation, respectively. (3) The curve-matching criterion is defined as:

$$\frac{D}{M} < 2\% \tag{4.5}$$

Considering possible errors when recording the time during the experiment and the second order accuracy of the numerical simulation, it is appropriate to set 2% for the curve matching and 1% for the amount criteria.

In the simulations, there are 800,000 cells/fiber or 16,000,000cells/cartridge, a value which was obtained from the experimental system. The tolerance for solving the mass transport PDEs was set at 10^{-12}. The relative tolerance for solving the kinetic ODEs was set at 10^{-8} and the absolute tolerance was set at 10^{-12}.

4.4 Results

4.4.1 Endothelial Cells Form a Uniform and Confluent Monolayer in Cartridge Capillaries

Endothelial cells line blood vessels and are the initial entry point for access of blood-borne proteins to the underlying tissue. The investigations of this study focused on flow and the impact it has on endothelial cell capture of growth factors, which are important regulators of cell and tissue activity. To better approximate the microenvironment of a blood vessel, this research seeded bovine aortic endothelial cells into the FiberCell cartridge system and cultured the cells under flow (Fig. 3.1). Cell viability was confirmed for up to eight weeks and cell density was around $0.3 \times 10^6 \#/cm^2$. The geometry is clearly more similar to *in vivo* than typical cell culture dishes but it was important to obtain a uniform and confluent monolayer of cells within the cartridge system to correctly perform and analyze experiments. To confirm this, cartridges were treated with a high salt wash to extrude the cell-based vessel and the cells were fixed and imaged (Fig. 4.1). An incision was made at one end to expose the lumen and demonstrate the continuity of the cell layer.

4.4.2 There is Significant Capture of FGF-2 Under Low Flow Rates

The average fluid velocity in human capillaries is 1 mm/sec [83]. This research hypothesized that capture of regulatory growth factors from solution would be significant at these flow rates thereby facilitating growth factor activity. Using the lowest velocity setting with the standard pulsatile pump included with the Cellmax system (1.3 mm/sec, 0.65 mL/min), FGF-2 (5.0±0.4 ng) was injected into the cartridge inlet reservoir and flow was commenced. As shown in Figure 3, there is a delay in FGF-2 appearance in the outflow corresponding to the time for FGF-2 to travel through the cartridge and exit the system. The majority of FGF-2 added exited the cartridge as a large peak approximately 1 mL (or 1.5 min at this flow rate) after

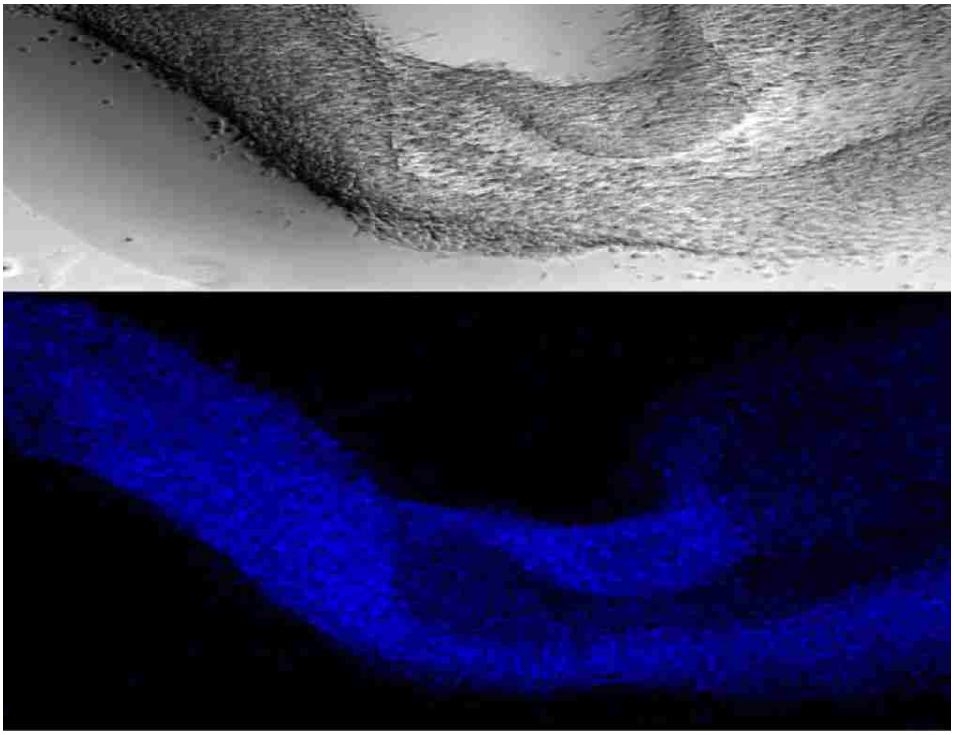

Figure 4.1: Brightfield and DAPI stained images of endothelial cells from the unit showing the continuous vessel-type architecture.

flow was initiated. Nonspecific binding within the injection cartridge reservoir was measured directly (31±2.5%). Specific binding within the celllined hollow fibers accounted for 9±2.5% of total FGF-2 added to the cartridge at this concentration and 13% of the FGF-2 entering the cell-lined fibers, after taking into account non-specific binding (Fig. 4.2). The results shown in Fig. 4.2(A) are from three independent experiments conducted using three different cartridges illustrating the reproducibility of the system. Repeated runs conducted using the same cartridge as well as runs using radiolabeled FGF-2 instead of unlabeled FGF-2 both produced similar results. The peak appearance time or volume in the outflow from the cartridge was insensitive to FGF-2 injection concentration in the range studied. However, the size of the FGF-2

peak correlated with the injection concentration with the highest peak corresponding to the highest concentration of FGF-2 added (Fig. 4.2(B)). The accuracy of the measurements took into consideration specific losses that occurred with injection (i.e., tube, syringe, needle, and reservoir). Rather than averaging datasets with variable FGF-2 reservoir values, they are presented as discrete results. A plot of total FGF-2 retained at these discrete concentration points shows a dose responsive binding curve, reflecting the linear portion of the binding curve expected at subsaturation ligand concentrations (Fig. 4.2(C)).

4.4.3 Heparinase Treatment Significantly Increases the FGF-2 Outflow

Heparan sulfate proteoglycans (HSPG) are ubiquitous molecules found on virtually all cells including endothelial cells and have been shown to regulate heparin-binding growth factor binding and activity in tissue culture [17, 16, 25, 53, 58, 92]. FGF-2 is a heparin-binding molecule associated with a number of physiologic and pathologic processes [23] and, therefore, the role of HSPG in regulating FGF-2 retention under flow was examined. Although the binding affinity of FGF-2 for HSPG has been shown to be lower than the affinity for the FGF receptor, these HSPG sites can provide up to a thousand fold more binding sites for FGF-2 [17, 16] significantly impacting the cell binding "potential" for heparin-binding growth factors. Cartridges were treated with heparinase, an enzyme specific for heparin and heparan sulfate, and FGF-2 outflow quantified. After heparinase treatment, FGF (1 ng) was injected and pumped through the cartridge. Almost 74% of the total FGF-2 added to the system was recovered in the outflow, compared to 46% of the total FGF-2 recovered from the nonheparinase treated cartridge prior to subtraction of non-specific binding. The amount of FGF-2 retained in the cartridge after heparinase treatment corresponded to the measured level of nonspecific binding and thus indicated no specific binding to cell-lined fibers in the absence of HSPGs (Table 4.2). In contrast, 25% of the FGF-2 pumped through untreated cartridges was retained after subtraction of non-

Table 4.2: Heparinase and chondroitinase but not keratanase impact FGF-2 output.

Treatment	FGF-2 input(ng)	% FGF-2 retained	flow rate(mL/min)
control	0.95 ± 0.05	25 ± 1.7	0.62 ± 0.02
heparinase	0.92 ± 0.00	0.0 ± 2.9*	0.66 ± 0.02
chondroitinase	1.73 ± 0.68	16 ± 4.1*	0.65 ± 0.03
keratanase	0.95 ± 0.15	20 ± 7.5	0.62 ± 0.08

Mean ± standard deviation of at least three experimental runs. * indicates significantly (p,0.05) different from control.

specific binding. Although FGF-2 can bind to its receptor in the absence of HSPG stabilization, that binding, based on the apparent KD of the receptor for FGF-2 in the absence of heparan sulfate, the lower level of FGFR generally found, and the ligand-receptor exposure time under flow, would be expected to be at least ten-fold lower than in the presence of HSPG [16] and the data certainly support this. To ensure that the effect with heparinase under flow was due to the specific removal of heparan sulfate and not a general effect due to enzymatic treatment of the cartridge or the enzyme incubation process, the cartridges were treated with keratanase, an enzyme having no specific known target on these cells. Keratanase, as opposed to heparinase, had no significant effect on FGF-2 retention (Table 4.2). Interestingly, there was a small but reproducible reduction (9%) after chondroitinase treatment on FGF-2 retention compared to control. Chondroitin sulfate proteoglycans are typically found on vascular surfaces but FGF-2 has not been shown to bind directly to chondroitin sulfate [52, 88]. It is not known at this time what the cause for the reduced binding is, although it has been reported that both chondroitin sulfate and dermatan sulfate under certain circumstances are able to influence FGF binding [2, 75, 82].

4.4.4 VEGF but not EGF is Impacted by Heparinase Treatment

VEGF, a heparin binding protein, and EGF, which does not bind heparin, were next tested in this system. Both the initial appearance time and outflow volume for the protein as well as the general shape of the outflow peak for both VEGF and EGF were

Table 4.3: VEGF but not EGF retention is impacted by heparinase (experimental).

Treatment	Growth Factor input(ng)	% Growth Factor Retained	flow rate(mL/min)
EGF	1.4 ± 0.15	19 ± 8.1	0.61 ± 0.01
+Enzymes	1.6 ± 0.170	20 ± 7.2	0.62 ± 0.01
VEGF	1.2 ± 0.19	16 ± 5.8	0.66 ± 0.00
+Heparinase	1.0 ± 0.26	-2.5 ± 6.1*	0.66 ± 0.02

Mean ± standard deviation of at least three experimental runs. * indicates significantly (p,0.05) different from non-enzyme treated case.

similar to FGF-2 (Fig. 4.3). To ensure that the measured effects seen with heparinase-treatment on FGF-2 retention were due to specific responses of the growth factor to the removal of heparan sulfate and not a general response by all proteins, flow studies were done with VEGF and EGF following enzymatic treatment. EGF retention and outflow were unaffected by treatment with a cocktail of heparinase, chondroitinase, and keratanase (Table 4.3). Treatment with heparinase without chondroitinase or keratanase also had no effect on EGF retention or outflow. In contrast, VEGF showed a significant decrease in specific retention between control and heparinase treated cartridges (16±5.8% versus 22.5±6.1% VEGF retained) indicating the critical role HSPG can have in heparin-binding growth factor capture under flow. The lack of a change in EGF binding or outflow profile under heparinase treatment is supportive that there are no gross changes in the cell glycocalyx that might impact the shear stress in the system.

4.4.5 Simulations Capture Critical Properties of Process

Capture of FGF-2 by endothelial cells within the vasculature is a critical step in growth factor activity and the bioreactor is an excellent tool for investigating the capture process. However, it has limitations with regard to quantification of cellular binding behavior. The cartridges are expensive for short-term experiments and culture time and preparation can be relatively lengthy. Visualization of individual cell behavior within the culture is not feasible. In addition, the ability to predict the

capture of molecules by cells under flow has value across a wide range of areas and the development of a flow-based tool for the design and testing of mechanisms related to retention is desirable. The computer model of this research was designed based on medium flow equations and mass transport equations [12] with cell surface reaction equations to reflect the cell growth factor interactions (see Materials and Methods-Model development). To validate the model, simulations were performed using the variables (i.e., FGF input concentration and flow rate) specific for an experimental series and a comparison was made. Experimental trials were run in which FGF-2 (0.92 ng) was added to the reservoir, pumped through the cartridge, and outflow collected and analyzed for FGF-2. FGF-2 in the outflow showed a characteristic peak outflow approximately 100s after flow was initiated at 0.63 mL/min (1.26 mm/sec) and 17±6.3% of the input FGF-2 was retained within the cartridge after non-specific binding was subtracted (Fig. 4.4). Simulations performed using the same input FGF-2 value and flow rate were run and comparison was made between the simulations and experimental outflow from control (Fig. 4.4(A)) or heparinase-treated (Fig. 4.4(B)) cartridges. Good agreement was defined based on two criteria; the amount of FGF-2 recovered and the curve similarity. Criteria one requires the relative difference in FGF-2 outlow from the experimental and simulation studies to be less than 1% while the second criteria compares the actual amounts of FGF-2 exiting from the experimental and the simulation system (see Materials and Methods). The research did note that FGF-2 retention with the simulations was very dependent on the level of HSPGs with higher densities resulting in too much retention via HSPG-FGF-2 binding and subsequent FGFR coupling while lower HSPG densities resulted in too little retention. Comparison of simulation results with the heparinase-treated data showed fine agreement with regard to the criteria when non-specific loss in the reservoir was subtracted.

4.4.6 Pulsatile and Steady Flow Results Are Similar at Low Flow Rates

Capillary flow is generally steady, and gradually becomes pulsatile at higher flow rates. The simulations and *in vitro* experiments are conducted to compare steady and pulsatile flow at a low flow rate (0.6 mL/min, 1.2 mm/sec) to determine whether the model would predict differences between FGF-2 interactions using steady and pulsatile flow. Simulations predicted no difference in FGF-2 binding at low flow using pulsatile flow conditions versus steady flow in either the FGF-2 binding down the cell-lined hollow fiber (Fig. 4.5(A)) or in the profile of the outflow (Fig. 4.5(B)). *In vitro* experiments were performed using a syringe pump for steady flow and the bioreactor's pulsatile flow pump (Fig. 4.5(C)). FGF-2 outflow measurements indicated no overall change at 0.6 mL/min (1.2 mm/sec) suggesting that, at low rates typical of capillary flow, no significant change in FGF-2 interactions takes place.

4.4.7 Simulations Predict Peak FGF-2 Binding at Entrance to the Cell-lined Hollow Fibers

The experimental system does not allow easy separation between internalized FGF-2 and that bound to the cell surface or visualization of FGF-2 distribution within the cell-lined hollow fiber. The simulations were used to examine how FGF-2 would be distributed with respect to time after flow was initiated (Fig. 4.6). At a relatively low flow rate (0.63 mL/min, 1.26 mm/ sec), the FGF-2 in the reservoir had essentially all entered the hollow fibers by 150s and the peak outflow of FGF-2 was evident ∼200s after flow was initiated corresponding to the time when the bulk FGF-2 had exited the hollow fibers. Later times showed cellbound FGF-2 either internalized or dissociated from the cell surface with little chance to reassociate. The vast majority of binding is predicted to occur near the entrance to the cell-lined hollow fibers as opposed to the middle or end of the fibers (Fig. 4.6(B)). The impact of time was more pronounced in the front section also as fluid entering the hollow fiber after ∼150s was devoid of FGF-2 ($< 0.1\%$ of initial FGF-2). Increasing the diffusion rate for FGF-2 in

solution by increasing the diffusion coefficient by an order of magnitude is predicted to have a negligible impact on FGF-2 capture in the front of the capillary but increased significantly the FGF-2 bound down the length of the cell-lined hollow fiber. This was due to changes in the depletion zone near the cell-lined walls (Fig. 4.7). After 44 seconds, an FGF-2 depletion zone near the surface was evident which was reduced when the diffusive transport of FGF-2 was increased. The replenishment of FGF-2 near the wall promoted greater FGF-2 binding as complex formation is a second-order process and illustrates the importance of surface depletion in growth factor capture.

4.4.8 Flow Rate Impacts FGF-2 Binding

The simulations indicate that depletion near the cell surface impacts binding and suggests that residence time in the vicinity of the cell surface is important. Therefore, how flow impacted cell binding of FGF-2 was studied. Simulations predict that cell binding is significantly diminished with increased flow rate (Fig. 4.8(A)) although the basic result of high binding at the entrance and reduced binding down the cell-lined hollow fiber was consistent across flow rates examined. This difference was evident regardless of the concentration of FGF-2 introduced to the system with the difference being more pronounced at higher flow rates (Fig. 4.8(B)). Reduction in binding due to the loss of HSPG is less evident at higher flow rates where the specific binding was already greatly reduced. This inverse relationship between flow and cell binding is potentially important especially at these relatively low flow rates. The highest rate used in the simulations ($\sim$3 mL/min,$\sim$6 mm/sec) is considerably lower than average arterial flow rates (100-400 mm/sec) in larger vessels of the circulatory system [83] suggesting that, with a short half-life, retention may be relevant only in small vessels with lower velocities. Note that simulations were run to a constant time rather than volume to reduce small fluctuations in retained FGF-2 due to dissociation effects.

Experimentally, the results were consistent but not quantitatively exact with this model prediction (Table 4.4). FGF-2 retention in the hollow fibers was virtually

Table 4.4: Increased flow rate eliminates FGF-2 binding (experimental).

Treatment	FGF-2 input(ng)	% FGF-2 Retained	Flow rate(mL/min)
Control	1.1 ± 0.11	6.7 ± 4.6	1.7 ± 0.10
+Heparinase	1.1 ± 0.02	6.7 ± 1.2	1.8 ± 0.05
Control	0.91 ± 0.17	0.5 ± 9.1	2.9 ± 0.13
+Heparinase	0.95 ± 0.25	0.5 ± 10	3.0 ± 0.03

Mean ± standard deviation of at least two experimental runs.

eliminated under medium (∼1.7 mL/min, 3.4 mm/sec) and higher flow rates (3.0 mL/min, 6 mm/sec), a significant reduction compared to binding at 0.62 mL/min (1.24 mm/sec) (Table 4.2- control group). The simulations, in contrast, did show some level of binding even at the highest level but this likely reflects the idealized conditions used for the model system (i.e., uniform receptor and HPSG densities, free access to coupling between FGF-2 bound molecules). Heparinase treatment showed no significant further reduction in retention at the higher flow rates in agreement with the simulation results.

Simulations indicated no difference in FGF-2 binding under the pulsatile flow conditions versus steady flow. Additional experiments were performed using a syringe pump with steady flow rather than pulsatile flow. FGF-2 outflow measurements indicated no overall change at 0.62 mL/min (1.2 mm/sec). Qualitatively the experimental results agreed with the simulation predictions for the overall effect of flow rate on retention although the model suggested higher retention levels for the control case and closer agreement between control and heparinase at both higher flow rates.

4.4.9 Changes in FGF-2 Affinity for HSPG Are Predicted to Have a Larger Impact on Retention Than Similar Changes in Affinity for FGFR at Physiological Cell Densities

FGF-2 binding affinity and concentration, along with binding partner density, regulates the capture process for FGF-2 from the fluid phase. Therefore, the simulations were used to examine how varying the affinity of FGF-2 for either HSPG (Fig. 4.9(A))

or FGFR (Fig. 4.9(B)) while holding all other parameters at their baseline value would impact retention. Decreasing the affinity (i.e., increasing K_D) for HSPG had a dramatic effect on retention, reducing it to 40% of baseline capture at the lowest value examined. The association rate constant had a greater impact than the dissociation rate constant although both followed similar trends. Somewhat surprisingly, increasing the affinity of the interaction by reducing the value of the dissociation rate constant of FGF-2 for HSPG did not alter FGF-2 binding likely due to the strong coupling present between FGFR and HSPG in the presence of FGF-2, making strict HSPG-dissociation somewhat irrelevant. For the same reason, FGF affinity for FGFR did not have a strong impact on FGF-2 capture since the vast majority of FGF-2 interacting with FGFR was via FGF-2-HSPG coupling.

4.4.10 Simulations Predict Binding Site Density is Critical for FGF-2 Retention

Cells typically express significantly more HSPG than FGFR and the research next asked how varying the cell surface densities of these binding sites would impact FGF-2 capture. In the absence of FGFR, a typical density of HSPG in the cartridge ($2.5 \times 10^5 \#/cell$) resulted in significant binding of FGF-2 in the absence of FGFR that is essentially doubled when FGFR density is $1 \times 10^6 \#/cell$, a two-fold increase in binding sites (Fig. 4.10(A)). FGFR typically are expressed at densities of approximately $1 \times 10^4 \#/cell$ thereby keeping the primary signaling receptor at a controlled level. This is predicted to result in an order of magnitude less overall FGF-2 binding than that found at typical HSPG levels but which is increased in a similar way when HSPG are present. The combination of the two surface binding sites (FGFR and HSPG) is critical. For example, when 1.0×10^4 FGFR are present, the retained FGF-2 is increased to ~0.25ng from a value of ~0.14ng without the FGFR. Looking at cell binding at the entrance of the cell-lined hollow fiber as a function of time after FGF-2 has been introduced with constant FGFR ($1 \times 10^4 \#/cell$) and variable HSPG, this

research found that there was a significant increase in bound FGF-2 at the higher HSPG ($1 \times 10^5 \#/cell$) when compared to the lower values and that the FGFR binding was essentially all coupled to HSPG (Fig. 4.10(B)). When there are fewer HSPG, there is a lower percentage of coupled binding at least at earlier times as well as lower overall FGFR complexes.

4.4.11 Simulations Predict Coupling is Key to Effective Capture of FGF-2

The results with the FGF-2-HSPG affinity simulations and the density studies indicated the importance of coupling in facilitating effective FGF-2-FGFR interactions. Next, the research looked at how varying the coupling rate constant impacted binding and internalization using simulations (Fig. 4.11). In the absence of HSPG-FGFR coupling ($k_c = 0$), there is a reduction in peak binding of FGF-2 and the majority of FGF-2 bound is not internalized but dissociates and exits from the system in the outflow. Even with a low level of coupling, the FGF-2 binding and internalization is dramatically increased until a peak effect is seen with $k_c = 0.01(\#/cell)^{-1}min^{-1}$. Looking at later times in the simulation (Fig. 4.11(B)), it would be found that a large fraction of the FGF-2 injected is bound during the initial pass and that this bound FGF-2 is largely internalized with little exiting the system. If coupling between HSPG and FGFR is eliminated (Fig. 4.11(C)), this is not the case. In this scenario, the cells bind a smaller but still significant level of FGF-2 during the initial pass but this FGF-2 is not retained and nearly all of the FGF-2 captured ultimately exits the system in the outflow.

To further illustrate the importance of the coupling process, simulations were performed with cell-lined hollow fibers having only HSPG ($2.5 \times 10^5 \#/cell$) in the front 25% of the tube and both FGFR ($1 \times 10^4 \#/cell$) and HSPG ($2.5 \times 10^5 \#/cell$) in the back 75% of the fiber (Fig. 4.12). The entrance area (front 25%) did not include internalization of FGF-2 by HSPG modeling an ECM-like section, however,

the overall outcomes are not significantly changed when internalization is included. HSPGs in this front section were able to capture FGF-2 but there is a significant rise in retention in the back section where both HSPG and FGFR are present. This is not simply due to the increase in binding sites due to the addition of FGFR as increasing HSPG by an equivalent level to that of the HSPG plus FGFR did not lead to the same increase in retention. Moreover, this increase in retention is lost when the dissociation rate for FGF-2-FGFR-HSPG is reduced to that of FGF-2-HSPG and only nominally increased when the coupling rate is eliminated, reflecting the increased affinity of FGFR compared to HSPG for FGF-2. The effect is evident at both low and high flow rates.

Finally, The simulations were used to ask whether dissociation from HSPG in an ECM-like section could lead to increased binding downstream due to slow dissociation of the growth factor and prolonged availability of the growth factor for downstream binding. When the HSPG density in the front 25% zone was increased to 5×10^6 HSPG/cell, a large increase in overall retention of FGF-2 in the front section was evident, resulting in a decrease in FGF binding in the HSPG-FGFR section (back 75%) due to a depletion of FGF-2 in the fluid zone near the cells. This was evident at both 5 (Table 4.5) and 10 min. In contrast, a low level of HSPG (5×10^4 or less) in the entrance section did not lead to significant binding in this zone and results in increased binding of FGF-2 in the final 75% section. FGF-2 in the fluid phase was at a higher concentration at later times after FGF-2 injection when there were more HSPG in the front section due to dissociation from the HSPGs; however, under flow conditions, this dissociated FGF-2 is not predicted to grow to a high enough concentration to meaningfully impact downstream receptor binding. This is an important difference between flow and static culture studies.

Table 4.5: Simulations predict effect of entrance HSPG zone on FGF-2 capture at 5 min.

HSPG Density in front 25% of Cell-lined Hollow Fiber			
	5×10^6	5×10^5	5×10^4
Total FGF-2 Retained(ng)	0.39	0.34	0.31
FGF-2 Bound(ng) (Front 25%)	0.16	0.063	0.0022
FGF-2 Bound(ng) (Back 75%)	0.17	0.24	0.28
FGF-2 Internalized(ng) (Back 75%)	0.013	0.017	0.022
FGF-2 in Fluid Phase(ng)	0.029	0.022	0.008

4.5 Discussion

Circulation is an obligatory process for the maintenance of human life. The proper balance of solid and fluid components, flow and pressure, and chemical content are all tightly regulated to maintain homeostasis. Within these limits, however, wide fluctuations can occur. The effects of the regulatory processes that are in place to deal with these fluctuations are not well characterized. Often the overall effects can be easily measured but not the changes in the microenvironment that come together to drive these effects. Although traditional tissue culture studies have added a wealth of knowledge in such areas, they often lack the capability to emulate the *in vivo* environment. In the study of the effect of flow in regulating vessel wall interactions, for example, three-dimensional studies can provide valuable information. Three-dimensional studies have been used previously to measure the effects of flow on cell populations [7, 54, 79, 34, 59]. Such an approach has been chosen in this study to measure the effect of flow on heparin binding protein delivery. By employing a single pass method to focus on the initial growth factor-vessel wall interaction, it was able to more directly measure the effect of flow on the bioavailability of these growth factors. Substantial binding of all growth factors (FGF-2, VEGF, and EGF) were measured at the lowest flow rate tested (0.61-0.66 mL/min, 1.22-1.32 mm/sec). Had a traditional two-dimensional approach been used instead, these factors would have had few limitations on their rebinding potential since in a closed system they would not

be subject to the flow that would remove them from the vessel as is typical of normal circulation. In the case of the heparin binding proteins (FGF-2 and VEGF), removal of heparan sulfate sites via enzyme digestion resulted in a significant increase in growth factor outflow (i.e., non-retention within the vessel), suggesting an important regulatory role for these proteoglycans in ligand capture. This is not necessarily surprising given the large number of binding sites these proteoglycans provide on normal cell surfaces. Certainly, it has been shown by many researchers that HSPGs are important regulators of FGF-2 binding to FGF receptors in tissue culture [92], although not essential for the interaction [17, 16, 58]. Their importance with regard to capture under flow has, however, not been shown previously and suggests a critical role in the circulation.

An equally significant influence on FGF-2, VEGF, or EGF binding, regardless of heparin binding characteristics however, was the flow rate. By increasing the flow rate by less than a factor of three (∼1.8 mL/min, 3.6 mm/sec) a significant increase was seen in growth factor outflow, reflecting the absence of specific binding taking place on vessel surfaces. A higher flow rate (∼3.0 mL/min, 6 mm/sec) showed no further increase in FGF-2 outflow above that observed at the medium flow rate with both showing retention levels equivalent to that evident in the absence of heparan sulfate. This correlation of flow rate and outflow of growth factors suggests a strong regulatory effect and an environment in the bloodstream that reduces the probability of capture significantly at flow rates typically measured in arteries [83]. Although pulsatile flow is undoubtedly important in increasingly larger vessels and higher flow rates, both simulations and experiments showed that at the low flow rate typical of capillaries it had no significant effect on FGF-2 interactions when compared to steady flow.

The removal of chondroitin sulfate created a small but significant increase in FGF-2 outflow. This is interesting since a number of published findings found no significant

affinity between FGF-2 and chondroitin sulfate [52, 88]. It is possible that under flow conditions subtle changes in chondroitin sulfate modifications allow for some weak interaction. Others have reported the ability of FGF-2 to bind chondroitin sulfate under certain circumstances [2, 75, 82]. EGF binding was, however, unaffected by treatment with a heparinase, chondroitinase and keratanase cocktail suggesting the chondroitinase effect was not universal. How this effect is manifest is currently under further study.

The minimum size of capillaries has been shown to be relatively fixed across species regardless of size [69] and is a basic assumption in the general model of allometric scaling laws proposed by West et al. [90]. This suggests an optimum environment for the exchange of gases, nutrients, and the removal of waste products that is likely rooted in fundamental physical laws. In order to best make use of these environmental conditions blood flow must also be optimal. The data demonstrate an inverse correlation between flow rate and probability of capture. Although the presence of heparan sulfate is crucial to FGF-2 capture at low flow rates, at higher flow rates the overriding regulator seems to be the flow rate itself which, based on the results, would all but preclude efficient FGF-2 binding to vessel walls in a single pass under all but the slowest flow conditions. The expectation of lower binding at increasingly higher flow rates might be somewhat expected but the relatively small increase in flow rate required to ablate binding was surprising.

Other influences, such as viscosity, and the presence of competing molecules were not addressed in this work. These are ongoing studies as the research begins to add complexity to the system so as to form even more accurate models of circulation. The advantage of this method is that the conditions can be monitored and controlled much as two dimensional culture systems can be but include the three dimensional architecture and flow characteristics that are part of normal blood flow. This approach has obvious potential in the testing of both endogenous molecules and

pharmaceuticals in order to provide a better perspective of molecular interactions in the microenvironment of blood vessels.

The importance of HSPGs in FGF-2 binding and signaling has been shown in many systems [17, 20, 27, 38, 48, 55], and is a generally accepted feature for heparin-binding growth factors. The research work builds upon those studies and shows the critical importance of HSPGs in FGF- 2 capture under flow (Fig. 4.2). In this chapter, the impact of this critical component is explored in detail using the computational model and show the parameters that regulate this process. In particular the study shows that the two-step coupling process and the accompanying decrease in dissociation are essential for effective retention of FGF-2 in a flow situation.

HSPG can mediate both the heparin-binding growth factor-receptor interaction at the cell surface and the accumulation and storage of these growth factors in the extracellular matrix [63, 84]. Removal of HSPG from the cell surface by enzymatic digestion greatly impairs FGF-2 activity in vitro and inhibits neo-vascularization *in vivo* [58, 92, 67]. HSPG interacts with FGFR directly [41, 68] and FGF-2 binding to cell surface HSPG can facilitate FGF-2 binding to FGFR, which in turn can result in activation of intracellular signaling cascades. Using the simple model under flow, the study shows in several ways that the coupling step is critical for FGF-2 retention. Elimination of coupling or decreasing the rate constant describing that interaction has a dramatic effect on both FGF-2 bound and internalized with essentially no internalization or effective binding when coupling is eliminated (Fig. 4.11). Reducing the density of HSPG (Fig. 4.10) or the affinity of FGF-2 for HSPG (Fig. 4.8) significantly reduces the amount of FGF-2 bound to both the cell surface and to FGFR. In addition, simulations with only low levels of HSPG (Fig. 4.10, 4.11 - entrance zone) or FGFR do not exhibit high retention but, when both HSPG and FGFR are present (Fig. 4.12), the combination of both increases retention. This is evident independent of flow rate. The ability of flow to regulate the level of binding suggests how crucial

the presence of HSPG is on the vessel wall, in order to increase the probability of capture of heparinbinding molecules especially given the short half-lives of some growth factors in circulation.

Under the flow condition, simulations predict that the majority of FGF-2 binding occurs at the entrance to the cell-lined hollow fiber (Fig. 4.6). In the simulations set up to match the experimental conditions, FGF-2 enters at its highest concentration and thus is most likely to bind under those conditions. Once binding occurs, there is a depletion of FGF-2 in the fluid phase near the cell surface (Fig. 4.7). Under flow, this zone can be replenished via diffusion as increasing the diffusion coefficient increases the concentration in this zone (Fig. 4.7) and ultimately leads to higher binding down the cell-lined hollow fiber. The research had postulated that FGF-2 bound in the entrance zone of the cell-lined hollow fiber would eventually dissociate and rebind further down the tube but this does not appear to be the case. Even when binding is extremely high at the entrance, FGF-2 that dissociated from the entrance was not in high enough concentration to impact downstream binding and was eventually washed out of the system. In a non-flow system this would likely not be the case and exemplifies the importance of including flow in studies.

In conclusion, a simulation program for the specific cell investigations of FGF-2 binding under flow [71, 96] performed well when compared to the experimental endothelial cell-lined bioreactor. The simulations suggest that:

(1) The amount of FGF-2 bound to FGFR is dominated by HSPG and the coupling rate constant, and this triad (FGFR-HSPG-FGF-2) is the key to FGF-2 capture;

(2) The amount of FGF-2 bound is proportional to the diffusivity of the growth factor in solution and inversely proportional to the flow rate;

(3) Flow rate and diffusivity will affect the FGF-2 outflow profile and the distribution of FGF-2 bound along the cell-lined hollow fiber wall;

(4) The majority of FGF-2 binding occurs in the entrance zone of the cell-lined hollow

fiber;

(5) Most FGF-2 effectively bound by FGFR and HSPG will be internalized rather than dissociated.

The simulation environment can provide additional information and insight into capture of FGF-2 that is not easily accessible from experimental work. The model is applied to *in vitro* bioreactor system but it has potential to be used for other growth factors as well as other cell systems where flow and capture are pivotal such as in drug and biologicals delivery testing.

4.6 Summary

Circulation is an important delivery method for both natural and synthetic molecules, but microenvironment interactions, regulated by endothelial cells and critical to the molecule's fate, are difficult to interpret using traditional approaches. This research analyzed and predicted growth factor capture under flow using computer modeling and a three-dimensional experimental approach that includes pertinent circulation characteristics such as pulsatile flow, competing binding interactions, and limited bioavailability. An understanding of the controlling features of this process was desired. The experimental module consisted of a bioreactor with synthetic endothelial-lined hollow fibers under flow. The physical design of the system was incorporated into the model parameters. The heparin-binding growth factor fibroblast growth factor-2 (FGF-2) was used for both the experiments and simulations. The computational model was composed of three parts: (1) medium flow equations, (2) mass transport equations and (3) cell surface reaction equations. The model is based on the flow and reactions within a single hollow fiber and was scaled linearly by the total number of fibers for comparison with experimental results. The model predicted, and experiments confirmed, that removal of heparan sulfate (HS) from the system would result in a dramatic loss of binding by heparin-binding proteins, but not by proteins

that do not bind heparin. The model further predicted a significant loss of bound protein at flow rates only slightly higher than average capillary flow rates, corroborated experimentally, suggesting that the probability of capture in a single pass at high flow rates is extremely low. Several other key parameters were investigated with the coupling between receptors and proteoglycans shown to have a critical impact on successful capture. The combined system offers opportunities to examine circulation capture in a straightforward quantitative manner that should prove advantageous for biologicals or drug delivery investigations.

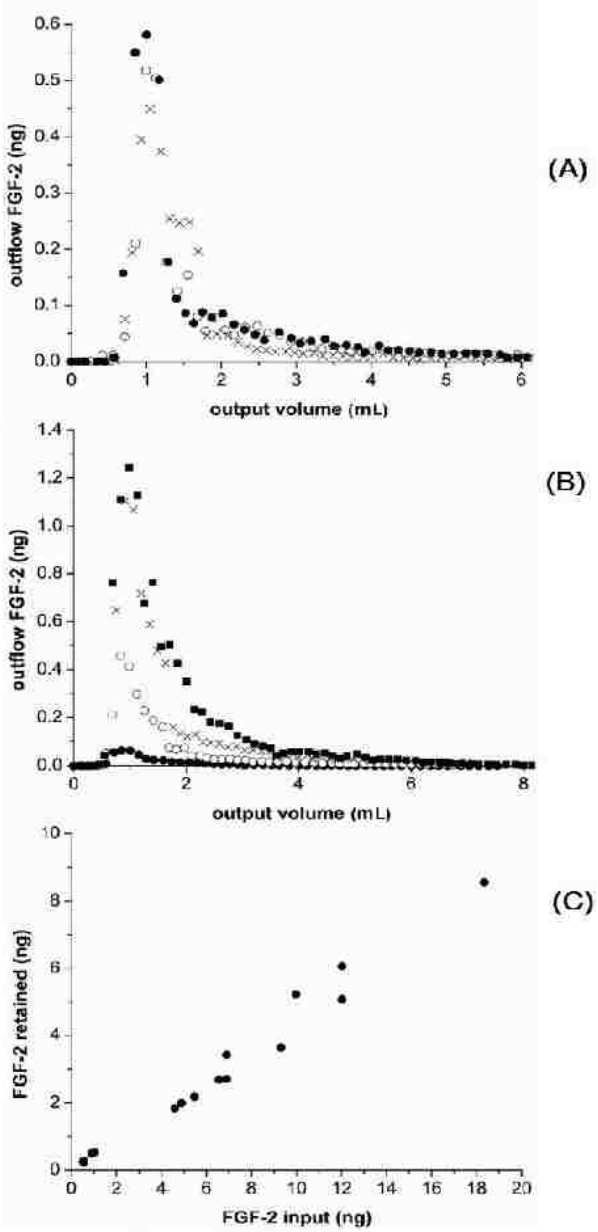

Figure 4.2: Significant retention of FGF-2 occurs under flow). (A) FGF-2 (5.0±0.4 ng) was injected into the inlet reservoir, pumped through the cartridge at 0.65±0.01 mL/min (1.3 mm/sec), and measured in the output stream samples from three independent runs on three separate cartridges. The average retention of FGF-2 within the cell-lined cartridge was 40±0.5of the three runs shown) with a specific binding of 9±2.5% (B) FGF-2 ((•) 0.92 ng , (○) 6.9 ng, (×) 12 ng, and (■) 18 ng FGF-2) was injected into the initial reservoir, run through the system at 0.64 mL/min, and the FGF-2 in the output stream measured using ELISA. Results are from individual runs with 9 independent cartridges. (C) FGF-2 (ng) retained within the cell-lined cartridge versus the FGF-2 (ng) injected into the system is shown. The flow rate for this study varied between 0.60 and 0.67 mL/min (1.2 and 1.34 mm/sec respectively).

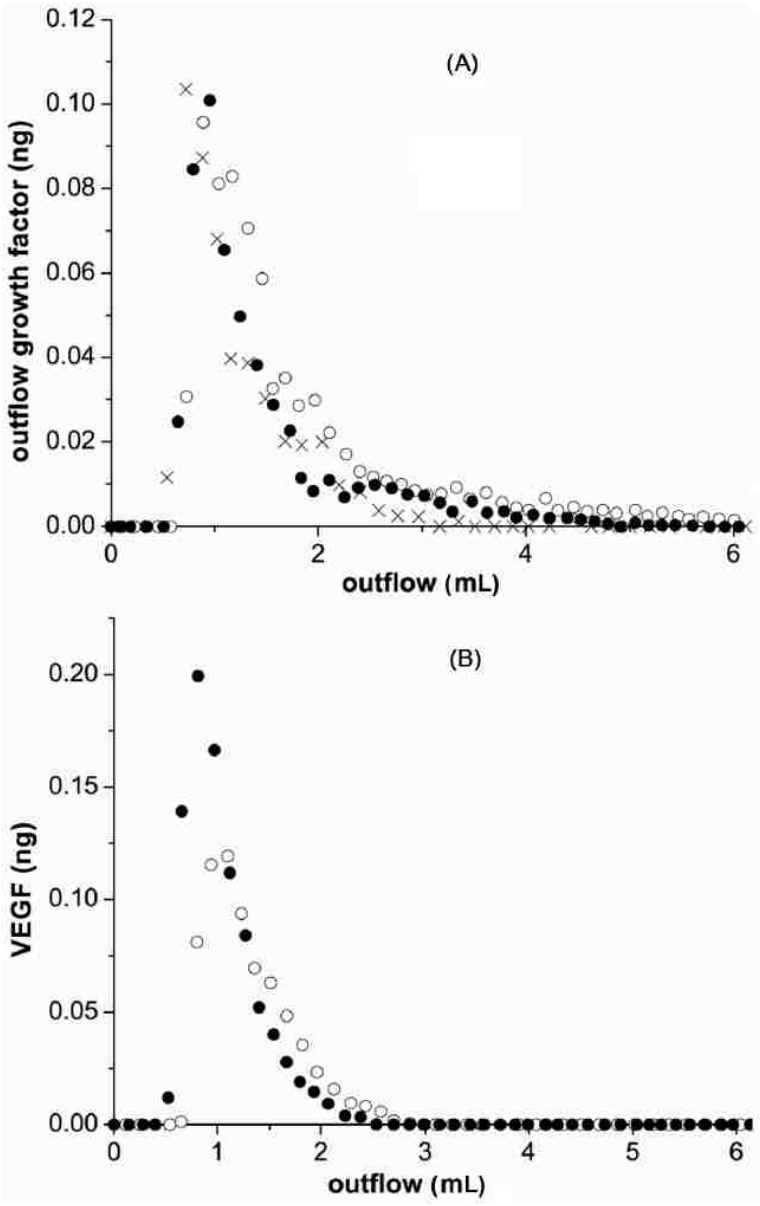

Figure 4.3: EGF and VEGF are retained under flow. (A) EGF (1.49 ng) was injected into the input reservoir, pumped through the system at 0.61 mL/min (1.22 mm/sec), and EGF quantified in the output flow by ELISA. Data shown are from the same cartridge either untreated (○) or enzyme-treated (●). FGF-2 (1.01ng - ×) is shown for comparison. (B) VEGF was injected into the input reservoir of untreated (0.95ng - ○) or heparinase-treated (0.98ng - ●) cartridges, run through the system at 0.66 mL/min (1.32 mm/sec), and VEGF quantified in the output flow by ELISA. Data are representative of at least three runs quantified in Table 4.3

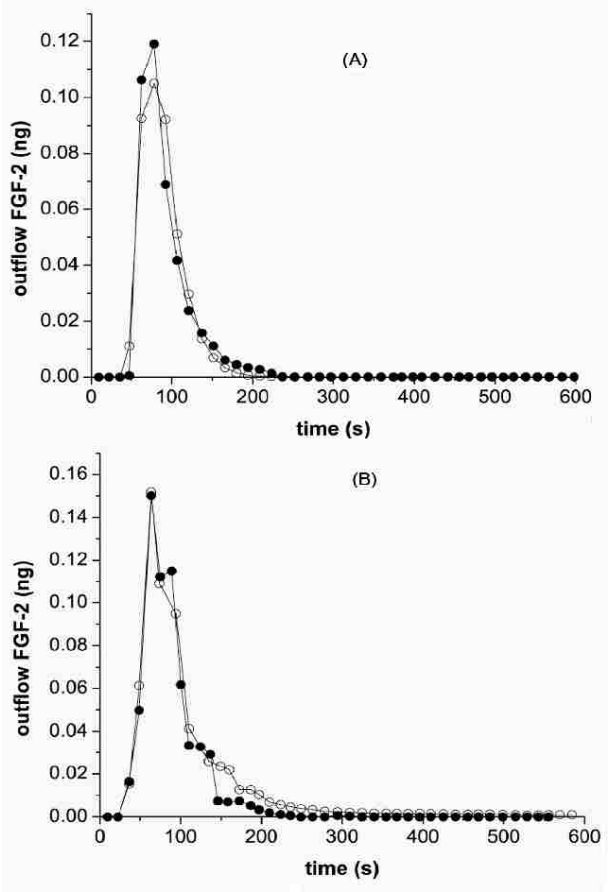

Figure 4.4: Simulations agree well with FGF-2 outflow measurements. (A) FGF-2(0.92 ng) was injected into the cartridge reservoir and then flowed through the cell-lined hollow fibers at 0.63 mL/min (1.26 mm/sec), pulsatile flow. FGF-2 collected from the exit fluid (•) is shown. Simulation results based on cells expressing 1×10^4 FGFR/cell and 2.5×10^5 HSPG/cell with 32% loss in the entrance reservoir having the same FGF-2 amount injected at the same flow rate (○) are also shown. (B) Similar outflow FGF-2 measurements are shown following FGF-2 (0.92 ng) addition for heparinase-treated (experimental - •) and simulation results with out HSPG (simulations - ○). Simulations were run with cells expressing 1×10^4 FGFR/cell and 30% loss in the entrance reservoir.

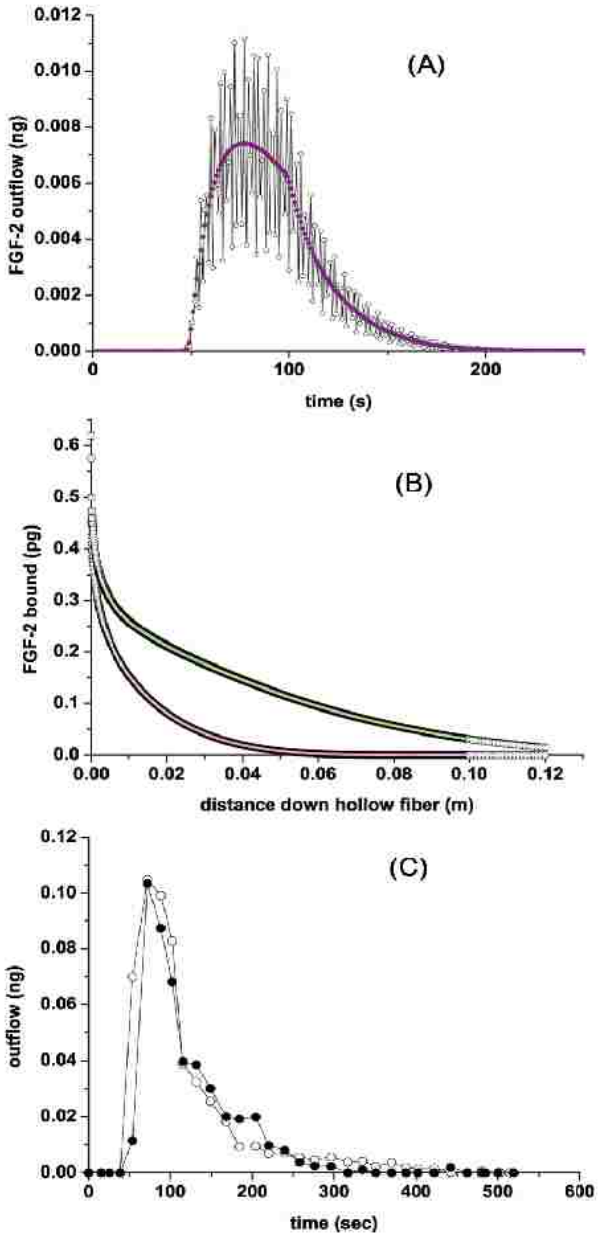

Figure 4.5: Simulation and experimental comparison between pulsatile and steady flow. (A) Simulation results of FGF-2 in the outflow as a function of time for pulsatile (○) or steady (●) flow, (B) Simulation results of FGF-2 bound along the endothelial-lined hollow fiber as a function of distance at 44 sec (pulsatile (○), steady (pink circle) flow) and at 88 seconds (pulsatile (□), steady (green square) flow) as a function of time, (C) Experimental comparison of FGF-2 in outflow using pulsatile (○) and steady (●) flow. Simulations and experiments used 1 ng of FGF-2 at a flow rate of 0.6 mL/min (1.2 mm/ sec) and pulsatile flow was set at ∼36 strokes/min.

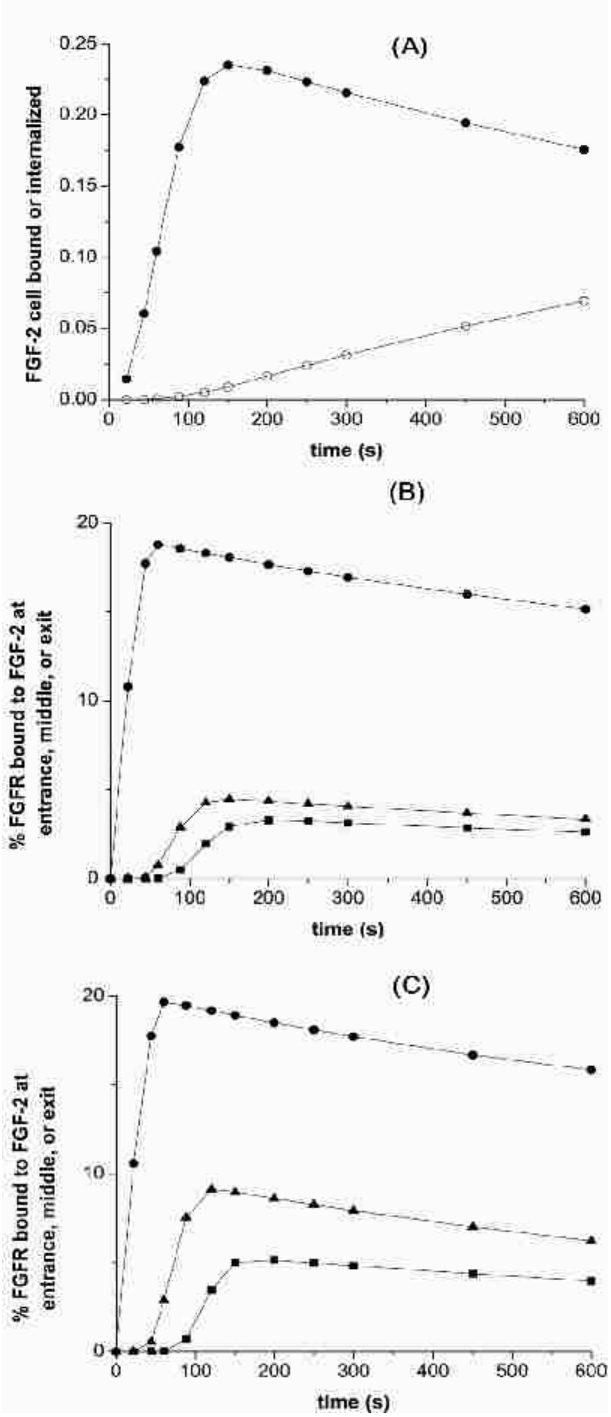

Figure 4.6: Simulations show FGF-2 binding and internalization under flow. For the simulations, FGF-2 (1 ng) was introduced into the reservoir (30% nonspecific loss) and sent into the cell-lined hollow fibers under pulsatile flow (0.63 mL/min, 1.26 mm/sec). (A) The sum of all cell surface bound FGF-2 (•) and FGF-2 internalized (○) within the celllined hollow fiber are shown. (B) and (C) Plot of % FGFR bound to FGF-2 versus time at the entrance (•), middle (▲) and at the exit (■) cell when the diffusion coefficient is 1.67×10^{-10} (B) or 1.67×10^{-9} m2/s (C). The fluid entering the system is essentially free of FGF-2 by 150s after flow is initiated.

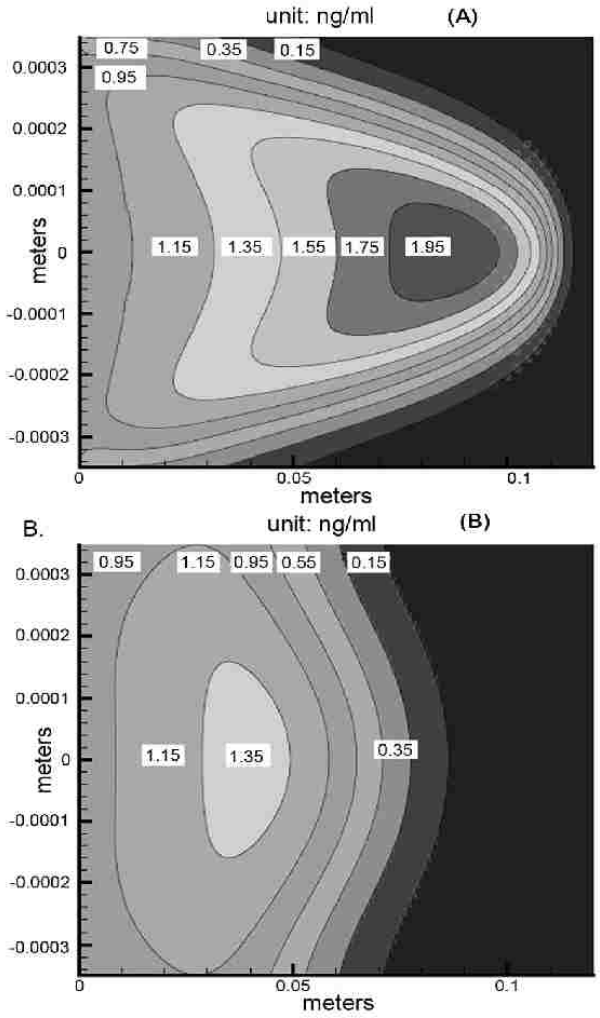

Figure 4.7: Simulations predict FGF-2 concentration profile in the cell-lined hollow fiber is impacted by diffusion. Grayscale images of FGF-2 concentration within the cell-lined hollow fiber (1×10^4 FGFR/cell and 2.5×10^5 HSPG/cell) at 44s after FGF-2 (1 ng) addition from the reservoir (30% nonspecific loss) at 0.63 mL/min (1.26 mm/sec) with FGF-2 having a diffusion coefficient of 1.67×10^{-10} (A) or 1.67×10^{-9} m2/s (B). The scale and numbers on the plots indicates the concentration of FGF-2 in ng/mL.

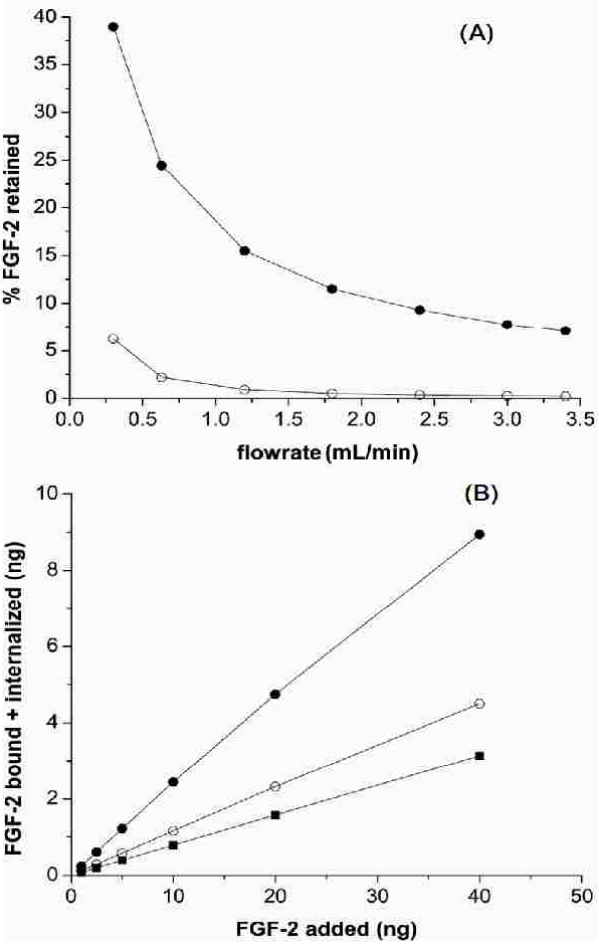

Figure 4.8: Simulations show reduced binding with increased flow rate. (A) Simulations for control (•), and HSPG-deficient cells (○), were run modeling injection of FGF-2 (1 ng) into the system and run at varied flow rate. 30% non-specific loss of FGF-2 in the reservoir was incorporated. (B) Cell-bound+internalized FGF-2 as a function of injection concentration at 5 min as a function of flow rate is shown. Simulations performed at 0.63 (•), 1.8 (○), and 3.0 (■) mL/min pulsatile flow(1.26, 3.6, and 6 mm/sec, respectively). Each cell on the cell-lined hollow fiber expressed 1×10^4 FGFR/cell and 2.5×10^5 HSPG/cell.

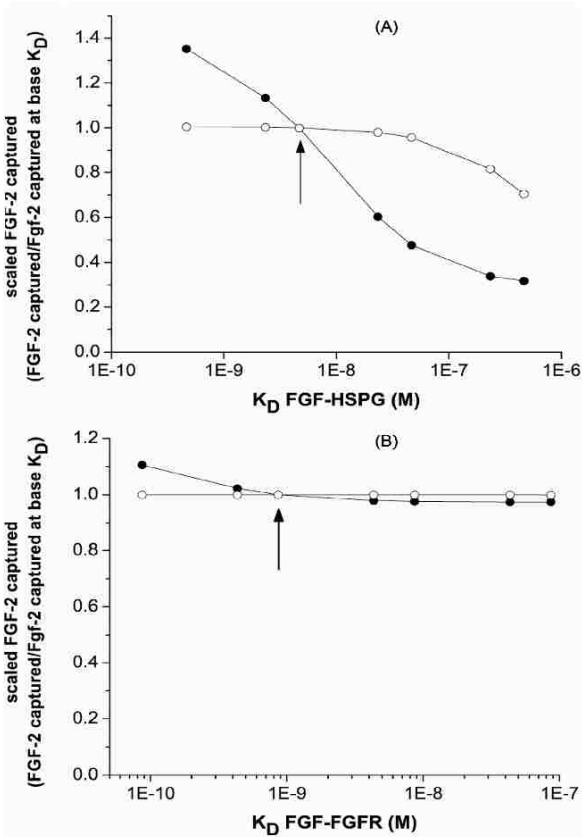

Figure 4.9: Simulations predict binding affinity of FGF-2 for HSPG impacts FGF-2 capture more than affinity for FGFR. (A) The affinity of FGF-2 for HSPG was varied in simulations by changing the association rate constant (•) or the dissociation rate constant (○). (B) The affinity of FGF-2 for FGFR was varied by changing the association rate constant (•) or the dissociation rate constant (○). The FGF-2 captured within the celllined hollow fiber (bound or internalized) at the given K_D value after 5 min. was scaled by that same value from simulations using the base case K_D value (Table 4.1). Arrow indicates base case K_D.

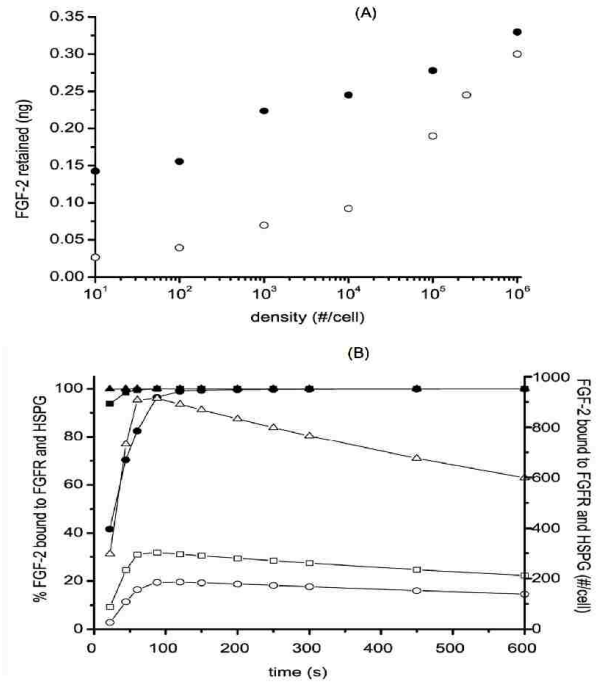

Figure 4.10: Simulations predict cell surface density impacts FGF-2 retention. Simulations were run for FGF-2 (1ng) added to the system (30% non-specific loss) at 0.63 mL/min pulsatile flow (1.26 mm/sec) for 5 min. (A) Cells expressed either 1×10^4 FGFR/cell and variable densities of HSPG ($\circ$) or 2.5×10^5 HSPG/cell and variable densities of FGFR ($\bullet$) on the cell-lined hollow fibers. The amount retained within the system (bound, internalized, and fluid phase FGF-2) is shown. (B) Cells expressed 1×10^4 FGFR/cell and 2×10^3 ($\bullet, \circ$), 2×10^4 ($\blacksquare, \square$), or 2×10^5 ($\blacktriangle, \triangle$) HSPG/cell on the cell-lined hollow fibers and simulation results correspond to entrance cell value at a given time. Filled symbols correspond to % of FGF-2 bound to FGFR which are simultaneously bound to HSPG and open symbols correspond to the $\#/cell$ of FGF-2 bound to FGFR and HSPG.

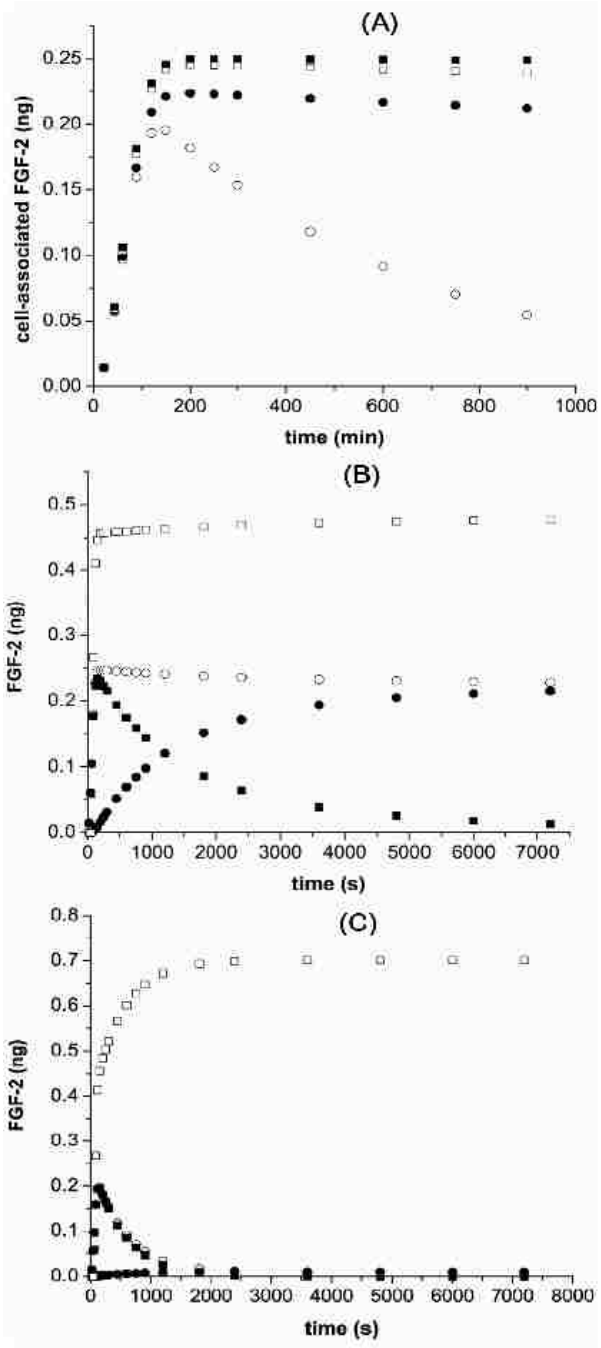

Figure 4.11: Simulations indicate coupling is critical for FGF-2 retention. (A) FGF-2 bound on cell surfaces plus internalized FGF-2 as a function of time for k_c values of 0 (○), 0.0001(●), 0.001(□), and 0.1(■)$(\#/cell)^{-1}min^{-1}$; (B) and (C) FGF-2 bound (■), internalized (●), bound plus internalized (○) and exited (□) under flow with k_c = 0.0024 (B) or 0 (C) $(\#/cell)^{-1}min^{-1}$ following addition of FGF-2 (1ng) at 0.63 mL/min (1.26 mm/sec) pulsatile flow(30% non-specific loss). Capillaries were simulated to include 1×10^4 FGFR/cell and 2.5×10^5 HSPG/cell on the cell-lined hollow fibers. 300s corresponds to the time when essentially all of the FGF-2 has entered the hollow fiber from the reservoir.

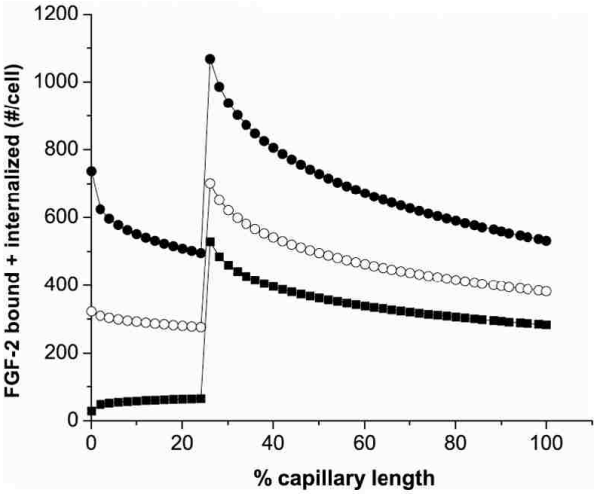

Figure 4.12: Simulations predict both FGFR and HSPG contribute to retention through FGF-2-mediated coupling. In these simulations, HSPG ($2.5\times10^5\#/cell$) were expressed on the cell-lined fibers along the entire chamber while FGFR ($1\times10^4\#/cell$) were expressed only in the cells found in the final 75% of the hollow fiber. FGF-2 (1ng) was added at time 0 (30% loss in the reservoir) at 0.65 (•), 1.3 (∘), and 2.6 (■) mL/min pulsatile flow (1.3, 2.6, and 5.2 mm/sec respectively). Cell-bound+internalized FGF-2 after 5 min of simulation time is shown.

5 Parallel Simulation of Multiple Proteins Through a Bioreactor Coupled with Biochemical Reactions

5.1 Introduction

This chapter presents a parallel system to handle complex models, in which more complexities are added into the binding model to mimic complicated binding mechanisms in human blood vessels or capillaries, as presented in Forsten-Williams recent models [28].

Instead of only one growth factor in the fluid, FGF-2, more growth factors are allowed to investigate cross regulation of different growth factors, such as heparin-binding EGF-like growth factor (HB-EGF), heparin and FGF-2, etc. Instead of occurring on cell surfaces only, competitive bindings now occur in the fluid as well, adding more complexity for calculating the mass transport equations. Also, the concentrations of different growth factors or proteins at the inlet reservoir (see Fig. 3.1) are complicated due to binding among different growth factors compared with only one growth factor in the basic model (see Chapters 3 and 4). Parallel methods are appropriate to solve the whole coupled nonlinear system effectively.

5.2 Modeling Process

Fig. 3.1 is the diagram of the hollow fiber cartridge system used in the experiments. Different growth factors or ligands are injected into the left sampling port or the inlet reservoir. The fluid is then pumped into the cartridge and proteins enter into the 20 hollow-fiber capillaries, which are coated with endothelial cells on the wall. Fluid from the capillaries is pooled in the right reservoir or the outlet reservoir and collected manually in tubes [71, 96, 99].

The geometric model is based on the experimental one (shown in Fig. 3.1) and illustrated in Fig. 5.1. The flow is pulsatile. To simplify modeling, the following assumptions are made:

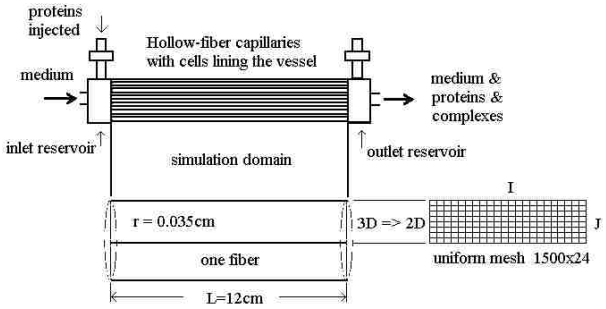

Figure 5.1: Diagram of single pass simulation geometric modeling.

(1) All of the 20 hollow-fiber capillaries have the same dimensions, flow, cell densities, and the endothelial cells are distributed evenly on the wall of the fiber capillaries and tightly packed;

(2) The fluid is incompressible, Newtonian, viscous and isothermal;

(3) The flow is steady, axis-symmetric and laminar and entrance effects are ignored [35];

(4) The walls of the hollow-fiber capillaries are rigid and nonporous.

Supposing the mass transports of different growth factors or complexes created to have the same flow. In other words, they have the same medium flow equations. The model consists of three coupled parts:

(1) the medium flow equations;

(2) the convection-diffusion mass transport equations of growth factors and their complexes;

(3) the competitive binding kinetics equations on cell surfaces and in the fluid [27, 71, 96].

The modeling is illustrated in Fig. 5.2.

5.2.1 Medium Flow Equations

Since all the proteins (growth factors plus all the intermediate complexes created in the fluid) are assumed to have the same flow, as investigated in Chapter 3, Eq. 3.12

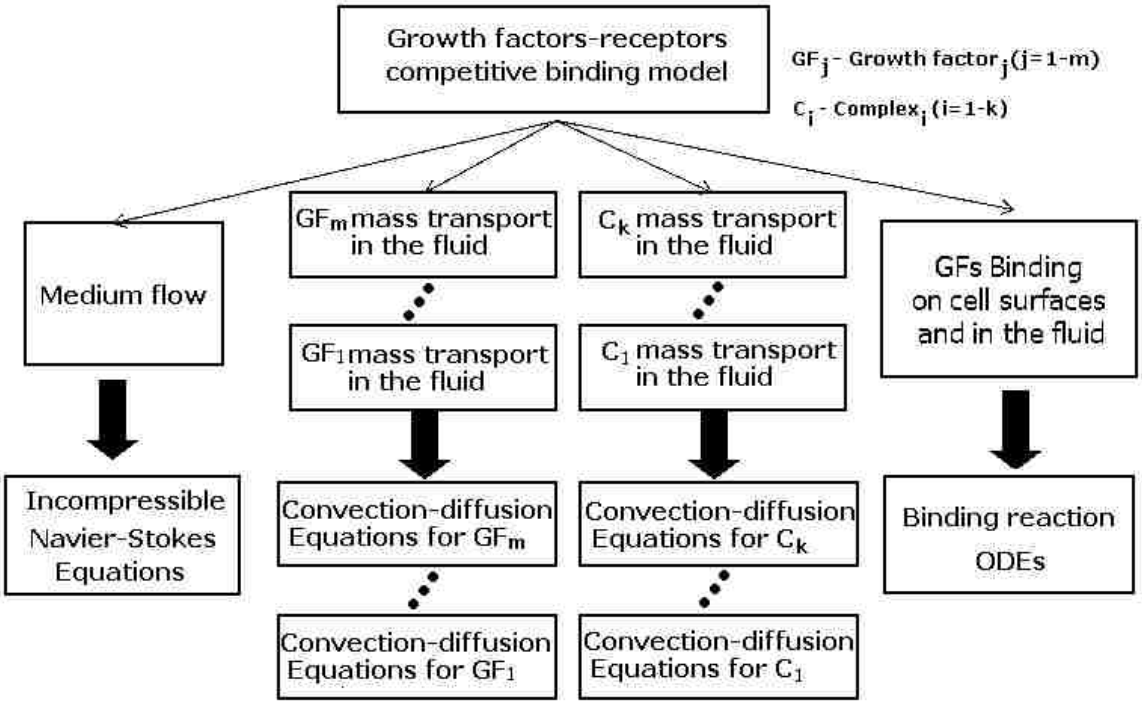

Figure 5.2: The modeling diagram of extended binding system.

is still valid and used for calculating the velocity u in the axial direction.

5.2.2 Mass Transport Equations

Due to the same flow, for each protein in the flow, the mass transport equation is the same as described in Eq. 3.16. Assuming there are m different kinds of growth factors and k different kinds of complexes formed among them, the total number of mass transport equations is S ($S = m + k$). The mass transport equations are described as:

$$\frac{\partial \phi_k}{\partial t} + \frac{\partial (u\phi_k)}{\partial x} = \frac{1}{r}\frac{\partial}{\partial r}(rK_d\frac{\partial \phi_k}{\partial x}) + \frac{\partial}{\partial x}(K_d\frac{\partial \phi_k}{\partial x}) + F(\phi_k, t, x) \ (k \in 1 \sim S) \qquad (5.1)$$

The boundary conditions of each protein in the fluid are the same, that is:

(1) $\frac{\partial \phi_k}{\partial r} = 0$ at $r = 0$, reflecting symmetry of the flow along the fiber centerline.

(2) $\frac{\partial \phi_k}{\partial r} = F(\phi_k, t, x)$ at $r = R$, reflecting binding rate of the kth protein on cell surfaces on the wall of the fiber.

(3) $\phi_k(t) = \phi_{k,ent}(t)$ at $x = 0$, assuming well mixed entrance flow, with uniform concentration along the fiber radius.

The numerical solution of Eq. 5.1 will be performed by the finite volume method described in section 3.3.2. Since all proteins in the fluid are assumed to have the same flow properties, the concentration of each protein can be expressed as the following set of algebraic equations, that is, each protein has the same scalar coefficients in its mass transport equations:

$$A_W\phi_{k,W} + A_S\phi_{k,S} + A_P\phi_{k,P} + A_E\phi_{k,E} + A_N\phi_{k,N} = b_k(k \in 1 \sim S) \qquad (5.2)$$

The coefficients in Eq. 5.2 consist of a pentadiagonal matrix [19, 71, 96] and can be expressed as (refer to section 3.3.2):

$$\begin{aligned}
A_N &= -D\frac{\delta x_i r_n}{r_N - r_P} \\
A_S &= -D\frac{\delta x_i r_s}{r_P - r_S} \\
A_E &= \min((\rho u)_e \delta r_j, 0) - D\frac{\delta r_j r_P}{x_E - x_P} \\
A_W &= -\max((\rho u)_w \delta r_j, 0) - D\frac{\delta r_j r_P}{x_P - x_W} \\
A_P &= \frac{3\rho r_P \delta x_i \delta r_j}{2\delta t} - (A_W + A_S + A_E + A_N)
\end{aligned}$$

$$b_k = ((S_{k,c} + S_{k,P})r_P\delta x_i\delta r_j + (\frac{2\rho\phi^n_{k,P}}{\delta t} - \frac{\rho\phi^{n-1}_{k,P}}{2\delta t})r_P\delta x_i\delta r_j) - \lambda(F^c_{k,e} - F^u_{k,e} - F^c_{k,w} + F^u_{k,w})$$

Considering a rectangular 2D space (see Fig. 5.1) with I and J grid points in the axial and the radius directions, respectively, Eq. (5.2) can also be expressed as:

$$A_W\phi_{k,i,j-J} + A_S\phi_{k,i,j-1} + A_P\phi_{k,i,j} + A_N\phi_{k,i,j+1} + A_E\phi_{k,i,j+J} = b_k(k \in 1 \sim S) \quad (5.3)$$

where, k is the kth protein in the flow, $j := 1, 2, ..., IJ$, and $IJ := I \times J = 1500 \times 24$, A_W, A_S, A_P, A_N, A_E, b_k are scalars. It can be expressed in a matrix form and shown in Fig. 5.3, where ϕ_k is represented by x_k.

For the solution of this nonsymmetric sparse matrix linear system, the commonly used methods are: relaxation methods, Alternating Direction Implicit (ADI) methods,

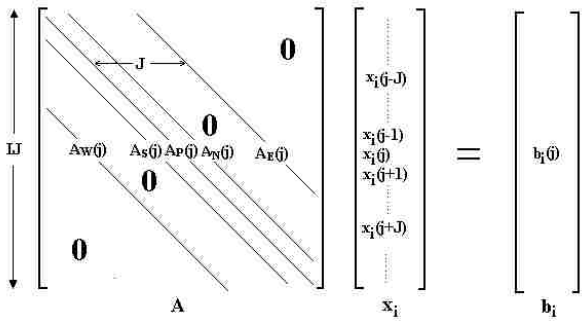

Figure 5.3: Matrix system to be solved for mass transport equations.

BiConjugate Gradient Stabilized (BiCGStab) methods, and Stone's SIP methods, etc. Compared to the above-mentioned methods, the advantages of SIP methods are: (1) fewer number of iterations for required accuracy; and (2) lower computational cost for each time step. The SIP's higher convergence rate is attributed to its more strongly implicit nature against ADI methods [80], which in turn are more strongly implicit methods than the SOR method and the point-Jacobi method. Therefore, the SIP methods are used extensively in computational fluid dynamics.

The coefficients of the matrix are time dependent, and thus the corresponding linear system must be solved separately for each time step. It is time consuming so that parallel methods are of great importance, especially when more proteins are involved. In order to solve those equations efficiently, a high performance parallel algorithm has been designed and implemented, including parallel discretization and a parallel SIP solver [19, 60, 80].

5.2.3 Binding Kinetics Equations

Similar to the basic model described in the previous chapters (Chapters 3 and 4), the complex model also involves a series of molecular activities, including proteins binding to their receptors to form some intermediate complexes and dimers on cell surfaces, and competitive binding among proteins to form some complexes in the fluid as well. Forsten-Williams 2008 models (the non-receptor coupling model and

Table 5.1: Model reactions on cell surfaces.

HB-EGF	FGF-2	EGF
$S_R^H \rightarrow R_H$	$S_R^F \rightarrow R_F$	$R_H + E \leftrightarrow C_E$
$S_P^H \rightarrow P_H$	$S_P^F \rightarrow P_F$	$C_E + C_E \leftrightarrow C_{2E}$
$S_P^C \rightarrow P^C$	same common sites HSPG	No HSPG binding
$R_H + H \leftrightarrow C_H$	$R_F + F \leftrightarrow C_F$	
$P_H + H \leftrightarrow G_H$	$P_F + F \leftrightarrow G_F$	
$C_H + C_H \leftrightarrow C_{2H}$	$C_F + C_F \leftrightarrow C_{2F}$	
$C_{2H} + P_H \leftrightarrow X_H$	$C_{2F} + P_F \leftrightarrow X_F$	
$R_H + G_H \leftrightarrow T_H$	$R_F + G_F \leftrightarrow T_F$	
$R_H + P_H \leftrightarrow T_H$	$R_F + P_F \leftrightarrow T_F$	
$T_H + T_H \leftrightarrow T_{2H}$	$T_F + T_F \leftrightarrow T_{2F}$	
$X_H + P_H \leftrightarrow T_{2H}$	$X_F + P_F \leftrightarrow T_{2F}$	
$P^C + H \leftrightarrow G_H^C$	$P^C + F \leftrightarrow G_F^C$	
$P_H^C + H \leftrightarrow G_H^C$	$P_F^C + F \leftrightarrow G_F^C$	
$P_H^C + C_H \leftrightarrow T_H^C$	$P_F^C + C_F \leftrightarrow T_F^C$	
$G_H^C + R_H \leftrightarrow T_H^C$	$G_F^C + R_F \leftrightarrow T_F^C$	
$C_{2H} + P_H^C \leftrightarrow X_H^C$	$C_{2F} + P_F^C \leftrightarrow X_F^C$	
$T_H^C + T_H^C \leftrightarrow T_{2H}^C$	$T_F^C + T_F^C \leftrightarrow T_{2F}^C$	
$T_H^C + T_H \leftrightarrow T_{HH}^C$	$T_F^C + T_F \leftrightarrow T_{FF}^C$	
$X_H^C + P_H^C \leftrightarrow T_{2H}^C$	$T_F^C + P_F^C \leftrightarrow T_{2F}^C$	
$X_H + P_H^C \leftrightarrow T_{HH}^C$	$T_F + P_F^C \leftrightarrow T_{FF}^C$	

The first part is the non-receptor-coupling model. Adding second part to the first one becomes the receptor-coupling model. h=heparin, F=FGF-2, H=HB-EGF, E=EGF, S=synthesis, R=receptors, C=ligand-receptor complexes, P=HSPG, T=ligand-receptor-HSPG complexes, C_2=dimers of C, $X = C_2$ bound to P, T_2= dimers of T. Unique receptors, proteoglycans and their ligand complexes are distinguished with a subscript H or F. The common site HSPG and their resulting complexes are designated with a subscript C.

the receptor coupling model) [28] were adopted as the simulation target, in which at most four proteins, such as FGF-2, HB-EGF, EGF, and heparin, can be injected into the system or any combination of them can be injected at the inlet reservoir simultaneously.

The model reactions on cell surfaces are listed in Table 5.1, and the model reactions in the fluid are listed in Table 5.2.

There are at most five equations in the fluid listed in Table 5.3. The non-receptor coupling model involves twenty four equations on cell surfaces listed in Table 5.4, and the receptor-coupling model involves thirty-two equations on cell surfaces listed in Table 5.5. The parameters used in simulation are listed in Table 5.6.

Table 5.2: Model reactions in the fluid.

HB-EGF	FGF-2	heparin	EGF
$h + H \leftrightarrow C_{hH}$	$h + F \leftrightarrow C_{hF}$	$h + F \leftrightarrow C_{hF}$ $h + H \leftrightarrow C_{hH}$	E no binding

h=heparin, F=FGF-2, H=HB-EGF, E=EGF

Table 5.3: Binding equations in the fluid.

1	$\frac{dF}{dt} = -k_a^{hF} hF + k_d^{hF} C_{hF}$
2	$\frac{dh}{dt} = -k_a^{hF} hF + k_d^{hF} C_{hF} - k_a^{hH} hH + k_d^{hH} C_{hH}$
3	$\frac{dC_{hF}}{dt} = k_a^{hF} hF - k_d^{hF} C_{hF}$
4	$\frac{dH}{dt} = -k_a^{hH} hH + k_d^{hH} C_{hH}$
5	$\frac{dC_{hH}}{dt} = k_a^{hH} hH - k_d^{hH} C_{hH}$

Table 5.4: Binding equations on cell surfaces in the non-receptor-coupling model.

1	$\frac{dR_F}{dt} = S_R^F - k_a^{FR_F} FR_F + k_d^{FR_F} C_F - k_c G_F R_F + k_{uc} T_F - k_{int} R_F$
2	$\frac{dC_F}{dt} = k_a^{FR_F} FR_F - k_d^{FR_F} C_F - k_c(C_F C_F + P_F C_F) + k_{uc}(2C_{2H} + T_F) - k_{int} C_F$
3	$\frac{dC_{2F}}{dt} = k_c(0.5 C_F C_F - C_{2F} P_F) + k_{uc}(X_F - C_{2F}) - k_{intD} C_{2F}$
4	$\frac{dT_F}{dt} = k_c(R_F G_F + P_F C_F - T_F T_F) + 2k_{uc}(T_{2F} - T_F) - k_{intD} T_F$
5	$\frac{dT_{2F}}{dt} = k_c(0.5 T_F T_F + X_F P_F) - 2k_{uc} T_{2F} - k_{intD} T_{2F}$
6	$\frac{dP_F}{dt} = S_P^F - k_a^{FP_F} FP_F + k_d^{FP_F} G_F - k_c(C_F P_F + C_{2F} P_F + X_F P_F)$ $+k_{uc}(T_F + X_F + T_{2F}) - k_{int} P_F$
7	$\frac{dG_F}{dt} = k_a^{FP_F} FP_F - k_d^{FP_F} G_F - k_c R_F G_F + k_{uc} T_F - k_{int} G_F$
8	$\frac{dX_F}{dt} = k_c(C_{2F} P_F - P_F X_F) + k_{uc}(T_{2F} - X_F) - k_{intD} X_F$
9	$\frac{dF}{dt} = (-k_a^{FR_F} FR_F + k_d^{FR_F} C_F - k_a^{FP_F} FP_F + k_d^{FP_F} G_F - k_a^{FP^C} FP^C + k_d^{FP^C} G_F^C)/(N_a V)$
10	$\frac{dP^C}{dt} = S_P^C - k_a^{FP^C} FP^C + k_d^{FP^C} G_F^C - k_a^{HP^C} HP^C + k_d^{HP^C} G_H^C$
11	$\frac{dG_F^C}{dt} = k_a^{FP^C} FP^C - k_d^{FP^C} G_F^C$
12	$\frac{dE}{dt} = (-k_a^{ER_H} ER_H + k_d^{ER_H} C_E)/(N_a V)$
13	$\frac{dR_H}{dt} = S_R^H - k_a^{HR_H} HR_H + k_d^{HR_H} C_H - k_a^{ER_H} ER_H + k_d^{ER_H} C_E - k_c G_H R_H + k_{uc} T_H - k_{int} R_H$
14	$\frac{dC_E}{dt} = k_a^{ER_H} ER_H - k_d^{ER_H} C_E - k_c C_E C_E + 2k_{uc} C_{2E} - k_{int} C_E$
15	$\frac{dC_{2E}}{dt} = 0.5 k_c C_E C_E - k_{uc} C_{2E} - k_{intD} C_{2E}$
16	$\frac{dH}{dt} = (-k_a^{HR_H} HR_H + k_d^{HR_H} C_H - k_a^{HP_H} HP_H + k_d^{HP_H} G_H - k_a^{HP^C} HP^C + k_d^{HP^C} G_H^C)/(N_a V)$
17	$\frac{dC_H}{dt} = k_a^{HR_H} HR_H - k_d^{HR_H} C_H - k_c(C_H C_H + C_H P_H) + k_{uc}(2C_{2H} + T_H) - k_{int} C_H$
18	$\frac{dC_{2H}}{dt} = k_c(0.5 C_H C_H - C_{2H} P_H) + k_{uc}(X_H - C_{2H}) - k_{intD} C_{2H}$
19	$\frac{dG_H}{dt} = k_a^{HP_H} HP_H - k_d^{HP_H} G_H - k_c R_H G_H + k_{uc} T_H - k_{int} G_H$
20	$\frac{dT_H}{dt} = k_c(R_H G_H + P_H C_H - T_H T_H) + 2k_{uc}(T_{2h} - T_H) - k_{intD} T_H$
21	$\frac{dT_{2H}}{dt} = k_c(0.5 T_H T_H + P_H X_H) - 2k_{uc} T_{2H} - k_{intD} T_{2H}$
22	$\frac{dX_H}{dt} = k_c(C_{2H} P_H - P_H X_H) + k_{uc}(T_{2H} - X_H) - k_{intD} X_H$
23	$\frac{dG_H^C}{dt} = k_a^{HP^C} HP^C - k_d^{HP^C} G_H^C$
24	$\frac{dP_H}{dt} = S_P^H - k_a^{HP_H} HP_H + k_d^{HP_H} G_H - k_c(C_H P_H + C_{2H} P_H + X_H P_H)$ $+k_{uc}(T_H + X_H + T_{2H}) - k_{int} P_H$

Table 5.5: Binding equations on cell surfaces in the receptor-coupling model.

1	$\frac{dR_F}{dt} = S_R^F - k_a^{FR_F} FR_F + k_d^{FR_F} C_F - k_c(G_F R_F + G_F^C R_F) + k_{uc}(T_F + T_F^C) - k_{int} R_F$
2	$\frac{dC_F}{dt} = k_a^{FR_F} FR_F - k_d^{FR_F} C_F - k_c(C_F C_F + P_F C_F + C_F P^C) + k_{uc}(2C_{2H} + T_F + T_F^C) - k_{int} C_F$
3	$\frac{dC_{2F}}{dt} = k_c(0.5 C_F C_F - C_{2F} P_F - C_{2F} P^C) + k_{uc}(X_F - C_{2F} + X_F^C) - k_{intD} C_{2F}$
4	$\frac{dT_F}{dt} = k_c(R_F G_F + P_F C_F - T_F T_F - T_F T_F^C) + 2k_{uc}(T_{2F} - T_F + T_{FF}^C) - k_{intD} T_F$
5	$\frac{dT_{2F}}{dt} = k_c(0.5 T_F T_F + X_F P_F) - 2k_{uc} T_{2F} - k_{intD} T_{2F}$
6	$\frac{dP_F}{dt} = S_P^F - k_a^{FP_F} FP_F + k_d^{FP_F} G_F - k_c(C_F P_F + C_{2F} P_F + X_F P_F + X_F^C P_F)$ $+k_{uc}(T_F + X_F + T_{2F} + T_{FF}^C) - k_{int} P_F$
7	$\frac{dG_F}{dt} = k_a^{FP_F} FP_F - k_d^{FP_F} G_F - k_c R_F G_F + k_{uc} T_F - k_{int} G_F$
8	$\frac{dX_F}{dt} = k_c(C_{2F} P_F - P_F X_F - P^C X_F) + k_{uc}(T_{2F} - X_F + T_{FF}^C) - k_{intD} X_F$
9	$\frac{dF}{dt} = (-k_a^{FR_F} FR_F + k_d^{FR_F} C_F - k_a^{FP_F} FP_F + k_d^{FP_F} G_F - k_a^{FP_C} FP^C + k_d^{FP^C} G_F^C)/(N_a V)$
10	$\frac{dP^C}{dt} = S_P^C - k_a^{FP^C} FP^C + k_d^{FP^C} G_F^C - k_a^{HP^C} HP^C + k_d^{HP^C} G_H^C$ $-k_c(C_F P^C + C_{2F} P^C + X_F P^C + X_F^C P^C + C_H P^C + C_{2H} P^C + X_H P^C + X_H^C P^C)$ $k_{uc}(T_F^C + T_{2F}^C + T_{FF}^C + X_F^C + T_H^C + T_{2H}^C + T_{HH}^C + X_H^C) - k_{int} P^C$
11	$\frac{dG_F^C}{dt} = k_a^{FP^C} FP^C - k_d^{FP^C} G_F^C - k_c G_F^C R_F + k_{uc} T_F^C - k_{int} G_F^C$
12	$\frac{dE}{dt} = (-k_a^{ER_H} ER_H + k_d^{ER_H} C_E)/(N_a V)$
13	$\frac{dR_H}{dt} = S_R^H - k_a^{HR_H} HR_H + k_d^{HR_H} C_H - k_a^{ER_H} ER_H + k_d^{ER_H} C_E$ $-k_c(G_H R_H + G_H^C R_H) + k_{uc}(T_H + T_H^C) - k_{int} R_H$
14	$\frac{dC_E}{dt} = k_a^{ER_H} ER_H - k_d^{ER_H} C_E - k_c C_E C_E + 2k_{uc} C_{2E} - k_{int} C_E$
15	$\frac{dC_{2E}}{dt} = 0.5 k_c C_E C_E - k_{uc} C_{2E} - k_{intD} C_{2E}$
16	$\frac{dH}{dt} = (-k_a^{HR_H} HR_H + k_d^{HR_H} C_H - k_a^{HP_H} HP_H + k_d^{HP_H} G_H - k_a^{HP^C} HP^C + k_d^{HP^C} G_H^C)/(N_a V)$
17	$\frac{dC_H}{dt} = k_a^{HR_H} HR_H - k_d^{HR_H} C_H - k_c(C_H C_H + C_H P_H + C_H P^C)$ $+k_{uc}(2C_{2H} + T_H + T_H^C) - k_{int} C_H$
18	$\frac{dC_{2H}}{dt} = k_c(0.5 C_H C_H - C_{2H} P_H - C_{2H} P^C) + k_{uc}(X_H - C_{2H} + X_H^C) - k_{intD} C_{2H}$
19	$\frac{dG_H}{dt} = k_a^{HP_H} HP_H - k_d^{HP_H} G_H - k_c R_H G_H + k_{uc} T_H - k_{int} G_H$
20	$\frac{dT_H}{dt} = k_c(R_H G_H + P_H C_H - T_H T_H - T_H^C T_H) + 2k_{uc}(T_{2h} - T_H + T_{HH}^C) - k_{intD} T_H$
21	$\frac{dT_{2H}}{dt} = k_c(0.5 T_H T_H + P_H X_H) - 2k_{uc} T_{2H} - k_{intD} T_{2H}$
22	$\frac{dX_H}{dt} = k_c(C_{2H} P_H - P_H X_H - P^C X_H) + k_{uc}(T_{2H} - X_H + T_{HH}^C) - k_{intD} X_H$
23	$\frac{dG_H^C}{dt} = k_a^{HP^C} HP^C - k_d^{HP^C} G_H^C - k_c G_H^C R_H + k_{uc} T_H^C - k_{int} G_H^C$
24	$\frac{dP_H}{dt} = S_P^H - k_a^{HP_H} HP_H + k_d^{HP_H} G_H - k_c(C_H P_H + C_{2H} P_H + X_H P_H + X_H^C P_H)$ $+k_{uc}(T_H + X_H + T_{2H} + T_{HH}^C) - k_{int} P_H$
25	$\frac{dT_H^C}{dt} = k_c(G_H^C R_H + P^C C_H - T_H^C T_H^C - T_H^C T_H) + k_{uc}(2T_{2H}^C + T_{HH}^C - 2T_H^C) - k_{int} T_H^C$
26	$\frac{T_{2H}^C}{dt} = k_c(0.5 T_H^C T_H^C + X_H^C P^C) - 2k_{uc} T_{2H}^C - k_{intD} T_{2H}^C$
27	$\frac{T_{HH}^C}{dt} = k_c(T_H^C T_H + X_H^C P_H + X_H P^C) - 3k_{uc} T_{HH}^C - k_{intD} T_{HH}^C$
28	$\frac{X_H^C}{dt} = k_c(C_{2H} P^C - X_H^C P_H - X_H^C P^C) + k_{uc}(T_{HH}^C + T_{2H}^C - X_H^C) - k_{intD} X_H^C$
29	$\frac{dT_F^C}{dt} = k_c(G_F^C R_F + P^C C_F - T_F^C T_F^C - T_F^C T_F) + k_{uc}(2T_{2F}^C + T_{FF}^C - 2T_F^C) - k_{int} T_F^C$
30	$\frac{T_{2F}^C}{dt} = k_c(0.5 T_F^C T_F^C + X_F^C P^C) - 2k_{uc} T_{2F}^C - k_{intD} T_{2F}^C$
31	$\frac{T_{FF}^C}{dt} = k_c(T_F^C T_F + X_F^C P_F + X_F P^C) - 3k_{uc} T_{FF}^C - k_{intD} T_{FF}^C$
32	$\frac{X_F^C}{dt} = k_c(C_{2F} P^C - X_F^C P_F - X_F^C P^C) + k_{uc}(T_{FF}^C + T_{2F}^C - X_F^C) - k_{intD} X_F^C$

Table 5.6: Parameter values used in simulation.

Para.	Value	Meaning
$k_a^{FR_F}$	$3.24 \times 10^8 M^{-1}/min$	ARC for F & R_F
$k_d^{FR_F}$	$0.281 min^{-1}$	DRC for F & R_F
$k_a^{FP_F}$	$1.19 \times 10^8 M^{-1}/min$	ARC for F & P_F
$k_d^{FP_F}$	$0.556 min^{-1}$	DRC for F & P_F
$k_a^{FP^C}$	$7.35 \times 10^6 M^{-1}/min$	ARC for F & P^C
$k_d^{FP^C}$	$0.398 min^{-1}$	DRC for F & P^C
k_c	$0.0024(\#/cell)^{-1}/min$	coupling rate const
k_{uc}	$0.6 min^{-1}$	uncoupling rate const
k_{int}	$0.005 min^{-1}$	IRC for complexes
k_{intD}	$0.078 min^{-1}$	IRC for dimers
$k_a^{HR_H}$	$9.7 \times 10^7 M^{-1}/min$	ARC for H & R_H
$k_d^{HR_H}$	$0.6887 min^{-1}$	DRC for H & R_H
$k_a^{HP_H}$	$1.45 \times 10^7 M^{-1}/min$	ARC for H & P_H
$k_d^{HP_H}$	$0.398 min^{-1}$	DRC for H & P_H
$k_a^{HP^C}$	$2.01 \times 10^6 M^{-1}/min$	ARC for H & P^C
$k_d^{HP^C}$	$0.398 min^{-1}$	DRC for H & P^C
$k_a^{ER_H}$	$9.7 \times 10^7 M^{-1}/min$	ARC for E & R_H
$k_d^{ER_H}$	$0.24 min^{-1}$	DRC for E & R_H
k_a^{hF}	$4.2 \times 10^5 M^{-1}/min$	ARC for h & F
k_d^{hF}	$0.01 min^{-1}$	DRC for h & F
k_a^{hH}	$4.2 \times 10^5 M^{-1}/min$	ARC for h & H
k_d^{hH}	$0.01 min^{-1}$	DRC for h & H
R_{F0}	$10^4 \#/cell$	initial R_F density
R_{H0}	$10^4 \#/cell$	initial R_H density
P_{F0}	$17600 \#/cell$	initial P_F density
P_{H0}	$4200 \#/cell$	initial P_H density
P_0^C	$232400 \#/cell$	initial P^C density
K_d	$1.67 \times 10^{-10} m^2/s$	F diffusivity at $25°C$
μ	$0.00094 Pa \cdot s$	viscosity of fluid
ρ	$1000 kg/m^3$	density of fluid

ARC = association rate constant, DRC = dissociation rate constant, IRC = internalization rate constant, h = heparin, F = FGF-2, H = HB-EGF, E = EGF, R_F = FGFR, R_H = EGFR, P_F = unique FGF-2 binding HSPG, P_H = unique HB-EGF binding HSPG, P^C = common HB-EGF and FGF-2 binding HSPG, rate constants are scaled to $25°C$.

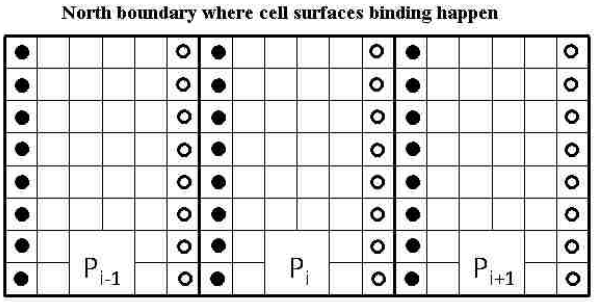

Figure 5.4: Column-wise stripping for processors domain partition. (○) and (●) points are boundary points between processors. P_0 has no (●) points and P_{N-1} has no (○) points.

5.3 Parallel Design and Implementation

5.3.1 Parallel Discretization

After discretization, a set of algebraic equations are obtained, as shown in Eq. 5.3. In the whole domain (see Fig. 5.1), the coefficients of Eq. 5.3 should be recalculated or updated at each time step.

This research takes the advantage of the mesh shape (1500×24), that is, the number of rows is much less than that of columns, to allocate the processors using column-wise stripping as shown in Fig. 5.4 to keep the total communication costs low and the load balanced among processors compared to other domain decomposition techniques, such as block checker-board processor partitions, where both row and column boundary data need to be exchanged between processors and also some processors do not have cell surfaces binding due to its position only on the north boundary or the wall of fibers.

In the above partition, each processor has no boundary rows and just has two boundary columns, the first and the last columns, except the left most and the right most processors P_0 and P_{N-1} (assuming N processors). Thus, each processor needs two boundary columns of data from the left and the right neighboring processors, except P_0 and P_{N-1}.

A_N, A_S, and A_E are not related to the grids on neighboring processors, and can be computed concurrently among processors.

A_W, A_P and the second part of source term b_k or $b_k(2) = \lambda(F^c_{k,e} - F^u_{k,e} - F^c_{k,w} + F^u_{k,w})$ are related to boundary points and need special treatments. First, A_W and $b_k(2)$ are computed in each processor concurrently, then, A_W at ($\circ$) points of P_i are replaced with the A_W values of P_{i-1}, and $b_k(2)$ at ($\circ$) points in P_{i-1} are added to that of P_i. Once A_W and $b_k(2)$ are obtained by each processor, A_P and source term b_k can be computed in each processor simultaneously. The parallel algorithm is shown in the following algorithm.

Algorithm 9 Parallel discretization of mass transport equations

Compute A_N and A_S in each processor in its subdomain simultaneously.
Compute A_E, A_W and $b_k(2)$ in each processor in its subdomain concurrently.
Exchange boundary data as follows:
  P_{i-1} sends A_W at ($\circ$) points to P_i as the new A_W values.
  P_{i-1} sends $b_k(2)$ at($\circ$)points to P_i,adding to P_i values.
Compute A_P and b_k in each processor in its subdomain concurrently.

5.3.2 Parallel SIP solver

Stone's strongly implicit procedure (SIP) algorithm has three parts: (a) LU factorization; (b) forward substitution; (c) backward substitution. The sequential SIP algorithm (refer to 6.2) is illustrated as follows.

For a sparse matrix linear system $Ax = b$ with a pentadiagonal nonzero coefficient matrix A, shown in Fig. 5.3, Stone proposed an incomplete LU factorization method [80], that is $A + E = LU$. E is an error matrix. L and U are lower and upper triangle matrix, respectively, as shown in Fig. 5.5.

The coefficient matrix A is augmented by an error matrix E, which has two diagonals lying inside and adjacent to the outer diagonals of A (see Fig. 5.5). Stone's SIP algorithm is designed so that terms in Ex are very small [80]. An iteration parameter α ($0 \leq \alpha < 1$) is used to calculate L and U. The parameter α may be a

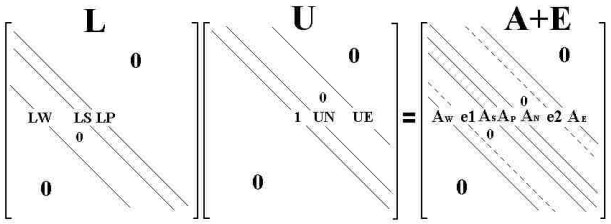

Figure 5.5: LU factorization of A+E.

function of the mesh. For simplicity, α is treated as a constant parameter, i.e., users can set its value before simulation. In Algorithm 10, ϵ is the convergence criteria, r is

Algorithm 10 Stone's SIP(A, L, U, b, ϵ, $maxloop$)

1: LU factorization:
for i=1 to I, j=1 to J, do
$L_W[i,j] = A_W[i,j]/(1 + \alpha U_N[i,j-J])$
$L_S[i,j] = A_S[i,j]/(1 + \alpha U_E[i,j-1])$
$P1 = \alpha L_W[i,j]U_N[i,j-J]$
$P2 = \alpha L_S[i,j]U_E[i,j-1]$
$L_P[i,j] = A_P[i,j] + P1 + P2 - L_W[i,j]U_E[i,j-J] - L_S[i,j]U_N[i,j-1]$
$U_N[i,j] = (A_N[i,j] - P1)/L_P[i,j]$
$U_E[i,j] = (A_E[i,j] - P2)/L_P[i,j]$
2: initialization: $k = 1$
3: **while** $\|r\|_2 > \epsilon\|InitialResidual\|_2$ and $k < maxloop$ **do**
4: forward substitution:
for i=1 to I, j=1 to J, do
$r[i,j] = b[i,j] - (A_S[i,j]x[i,j-1] + A_W[i,j]x[i,j-J] + A_P[i,j]x[i,j] + A_E[i,j]x[i,j+J] + A_N[i,j]x[i,j+1])$
$Y[i,j] = (r[i,j] - L_S[i,j]Y[i,j-1] - L_W[i,j]Y[i,j-J])/L_P[i,j]$
5: backward substitution:
for i=I to 1, j=J to 1, do
$\delta[i,j] = Y[i,j] - U_N[i,j]\delta[i,j+1] - U_E[i,j]\delta[i,j+J]$
6: update solution:
$x[i,j] = x[i,j] + \delta[i,j]$
7: $k = k + 1$
8: **end while**

the residual, $maxloop$ is the maximum number of iterations, and δ is the correction. The same array is used for r, Y and δ to save memory cost.

Based on the domain partition scheme (refer to Fig. 5.4), there is a boundary dependency between processors in LU factorization and forward substitution, as shown

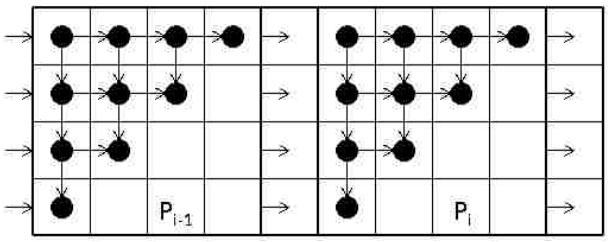

Figure 5.6: Boundary dependency between processors in factorization and forward substitution.

in Fig. 5.6. Only after the left processor finishes calculating the boundary points and sends them to the right processor, the right one can start to compute. This process continues up to the last processor [60, 80]. Backward substitution has similar fashion but in the reverse order. Basically, by using the pipeline technique, it is trivial to implement a naive parallel Stone's SIP solver. Reeve et al. proposed a parallel SIP algorithm, in which a red-black approach for forward and backward substitutions is presented [60]. This study proposed an overlapped Jacobi iteration method. Instead of using the red-black approach for forward and backward substitutions, let each processor do forward and backward substitutions concurrently in each iteration and use previous boundary values of neighboring processors. After each iteration, boundary data are exchanged among processors. In forward substitution, only (∘) points of Y(i,j) are transferred, while in backward substitution, only (•) points of Y(i,j) are transferred (see Fig. 5.4 and Algorithm 10). The $Y(i,j)$ can also be used for $\delta(i,j)$ to save memory cost.

After forward and backward substitutions, the boundary points of current solution should be exchanged among processors. If the relative error is still larger than the preset stopping criteria in the inner loop, it will loop until reaching the preset maximum number of loops or the relative error is less than the preset stopping criteria.

The overall speedup is measured for forward and backward substitutions using two techniques, respectively. The results are shown in Fig. 5.7. It is found that the

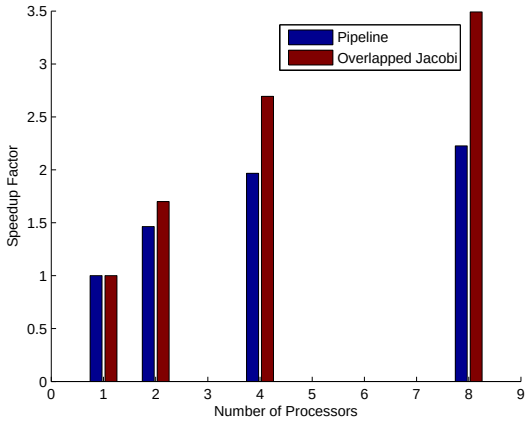

Figure 5.7: Speedup factors using the overlapped Jacobi iteration and pipeline techniques. The results are based on simulation of FGF-2 alone moving through the bioreactor for 300 seconds in single pass simulation, non-receptor-coupling model, and the software is running on the DLX high performance cluster at the University of Kentucky.

overlapped Jacobi iteration method has better speedup than the pipeline technique. The overlapped Jacobi iteration may need more iterations than the pipeline does, but actually is much faster due to simultaneous computation among processors. The overlapped Jacobi iteration method could be applied to speed up similar pipeline methods and save computational costs significantly (refer to Chapter 6 for details).

The computational cost depends mainly on the number of growth factors involved and the expected temporal goal to be simulated. It also depends on the time step used for simulation. If more growth factors are involved in the fluid, and the binding is studied for several hours, this parallel algorithm can be used to shorten the overall simulation time by more than sixty percent if four processors are used. Due to heavy boundary data exchanges among processors in each time step, simulations with more than eight processors do not yield better performance in the current DLX cluster settings at the University of Kentucky, as shown in Fig. 5.8.

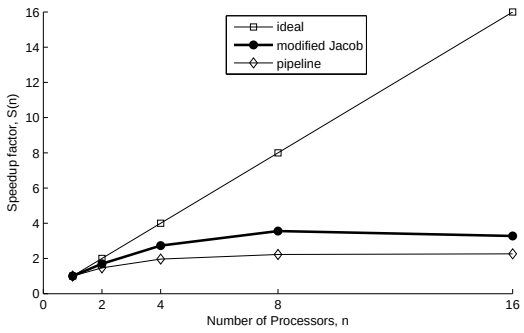

Figure 5.8: Speedup factors comparison between the overlapped Jacobi iteration and pipeline techniques, and ideal linear. The results are based on the same simulation settings shown in Figure 5.7.

5.3.3 Parallel Algorithm

Since the whole system is composed of a series of coupled nonlinear PDEs and ODEs, the order of calculation of those equations is important. First, ODEs in the fluid (equations shown in Table 5.3) are calculated by the CVODE to update the concentrations in each grid. Second, binding ODEs on cell surfaces (equations shown in Table 5.4 or Table 5.5) are calculated , and the solution in each grid on north boundary is used as the boundary condition for mass transport equations of each protein in the fluid. At this point, mass transport equations of each protein in the fluid are calculated to get the new concentration of each protein in each grid. A sequential CVODE solver combined with a parallel scheme obtains an efficient solution for mass transport equations in the whole domain. The parallel algorithm for the whole system is illustrated in Algorithm 11.

In the while loop, the flow velocity equations are calculated first, then the binding ODEs in the fluid are calculated followed by the calculation of binding ODEs on cell surfaces. Actually, the sequence of calculation of the above three kinds of equations is not critical, and they can be calculated in any order without noticeable differences. After the solutions of the above equations are obtained, the mass transport equations of different proteins in the fluid are solved iteratively in parallel. A for loop is used

Algorithm 11 Parallel algorithm of the simulation system

```
1: Initialization
2: t = 0
3: while t < t_end do
4:    Each processor computes velocity u in its subdomain
5:    Each processor solves binding ODEs in fluid in its subdomain
6:    Each procesor solves binding ODEs on cell surfaces in its subdomain
7:    for (i = 1 to W)
8:       Solve M_i(mass transport PDEs) for each protein in parallel
9:          Perform parallel discretization of mass transport PDEs
10:         Update boundary conditions in subdomain concurrently
11:         Call parallel Stone's SIP solver
12:         Exchange boundary mass transport data among processors
13:   Each processor does calculations for outputting binding information in its sub-
      domain if user needs
14:   All reduce those binding information to P_0 for output
15:   P_0 saves those output data for analysis and visualization
16:   P_0 recalculates the concentration of each protein at entrance
17:   t = t + Δt
18: end while
```

to calculate mass transport equations of each protein in the fluid one after another. For each one, first perform discretization of mass transport equations; second, update boundary conditions; third, call parallel Stone's SIP solver; and last, exchange boundary data among processors. All these four steps are performed in subdomain by each processor in parallel. Once the mass transport equations of all proteins in the fluid are solved, each processor only has solutions in its subdomain. At this point, if needed, the binding information can be calculated by each processor and all reduced to P_0, and P_0 saves the data for analysis and visualization. Then, P_0 recalculates the concentration of each protein at the inlet reservoir. In the end, it moves forward one time step and loops again until reaching the target simulation time.

5.3.4 Time Analysis

If a sequential algorithm is used, the total simulation time can be expressed in the following formula:

$$T_1 = T_{init1} + \sum(T_v + T_b + T_m + T_{o1} + T_{o2}) \approx \sum(T_v + T_b + T_m + T_{o1} + T_{o2}) \quad (5.4)$$

For the parallel algorithm, the total simulation time can be expressed as following:

$$T_p = T_{init2} + \sum(T_v + (T_b + T_m + T_{o1})/p + T_{o2} + T_c) \approx \sum(T_v + (T_b + T_m + T_{o1})/p + T_{o2} + T_c) \quad (5.5)$$

where, T_{init1} and T_{init2} are the initialization time for sequential and parallel algorithms, respectively, T_v is the time for calculating velocities of the fluid, T_b is the time for solving binding ODEs on cell surfaces and in the fluid, T_m is the time for solving mass transport PDEs in the fluid, T_{o1} is the time for calculating output data by each processors, T_{o2} is the time for saving output data for analysis and visualization by P_0, T_c is the time for inter communications between processors, and p is the number of processors used.

Therefore, the speedup of parallel algorithm is expressed as:

$$S_p = T_1/T_p \approx \sum(T_v + T_b + T_m + T_{o1} + T_{o2}) / \sum(T_v + (T_b + T_m + T_{o1})/p + T_{o2} + T_c) \quad (5.6)$$

Normally, the simulation time is in minutes or hours, therefore, T_v,T_{o1},and T_{o2} are very small compared to T_b and T_m. Speedup can be further simplified as:

$$S_p \approx \sum(T_b + T_m) / \sum((T_b + T_m)/p + T_c) \quad (5.7)$$

T_c is a dominant factor for the optimization of speedup.

5.4 Some Implementation Details

5.4.1 The Concentration of Proteins at Entrance

Supposing that different proteins are injected into the inlet reservoir at the same time and bioreactions are known among these proteins, the concentrations of proteins in the fluid can be calculated in two steps as follows:

Calculate Concentrations of Proteins by Solving Binding Kinetics ODEs

Method: suppose two proteins p_1 and p_2 are injected into the inlet reservoir at the same time with the amount of m_1 and m_2, respectively. p_1 and p_2 will form complex p_3 with association rate constant k_a. Meanwhile, p_3 will dissociate into p_1 and p_2 with dissociation rate constant k_d. Let $\phi_1(t)$, $\phi_2(t)$, $\phi_3(t)$ be the concentration of p_1, p_2, and p_3 in the reservoir at time t, respectively. They can be calculated by the following ODEs:

$$\frac{d\phi_1(t)}{dt} = -k_a\phi_1(t)\phi_2(t) + k_d\phi_3(t) \tag{5.8}$$

$$\frac{d\phi_2(t)}{dt} = -k_a\phi_1(t)\phi_2(t) + k_d\phi_3(t) \tag{5.9}$$

$$\frac{d\phi_3(t)}{dt} = k_a\phi_1(t)\phi_2(t) - k_d\phi_3(t) \tag{5.10}$$

with the initial values of $\phi_1(0) = m_1/v$, $\phi_2(0) = m_2/v$, $\phi_3(0) = 0$, and v is the volume of the inlet reservoir.

If more than two proteins are injected with different binding kinetics, the method is similar. The difference is the above ODEs.

Adjust the Concentration of Each Protein

The concentration of each protein needs to be adjusted due to the fluid flowing in and out of the inlet reservoir at each time step. The following formula is used:

$$\phi_i(n) = \phi_i(n-1) \times \frac{v - \Delta v_n}{v} \tag{5.11}$$

where, v is the volume of the inlet reservoir, Δv_n is the volume of the fluid flowing into the fibers at the nth time step, $\phi_i(n-1)$ is the previous concentration, and $\phi_i(n)$ is the current concentration of the ith protein (growth factor or complex) in the inlet reservoir.

5.4.2 The Mass of Proteins Bound

Protein (growth factor or complex) binding could occur on cell surfaces or in the fluid. Thus the amount of the ith protein bound in the nth time step $M_i(n)$ includes three parts: (1) bound on cell surfaces; (2) bound in the fluid; (3) internalized, as shown in the following formula:

$$M_i(n) = M_i^{fluid}(n) + M_i^{surface}(n) + M_i^{int}(n) \tag{5.12}$$

Based on a deterministic approach and the uniform mesh, the number of molecules of the ith protein bound in the nth time step $F_i(n)$ could be determined by the formulas, accordingly:

$$F_i(n) = F_i^{int}(n) + F_i^{surface}(n) + F_i^{fluid}(n) \tag{5.13}$$

$$F_i^{fluid}(n) = N_f K_{gf} \sum_{k=1}^{N} \sum_{l=1}^{M} C_{i,j}(k,l,n) \tag{5.14}$$

$$F_i^{surface}(n) = N_f K_{gf} \sum_{k=1}^{N} (\sum C_{i,j}(k,M,n) + 2 \sum G_{i,j}(k,M,n)) \tag{5.15}$$

$$F_i^{int}(n) = F_i^{int}(n-1) + N_f K_{gf} dt \sum_{k=1}^{N} (k_{int} \sum C_{i,j}(k,M,n) + 2k_{intD} \sum G_{i,j}(k,M,n)) \tag{5.16}$$

where, $C_{i,j}(k,M,n)$ is the number of complexes of the ith growth factor binding to the jth receptor in the (k,M)th grid (on cell surfaces), at the nth time step, if the binding exists, and $G_{i,j}(k,M,n)$ is the number of dimer of the ith protein binding to the jth receptor in the (k,M)th grid (on cell surfaces), at the nth time step. $C_{i,j}(k,l,n)$ is the number of complexes of the ith protein binding to the jth protein in the (k,l)th grid (in the fluid), at the nth time step, if the binding exists, M and N are the number of grids in the radius and the axial directions, respectively, k_{int} is the internalization rate constant of complexes and k_{intD} is the internalization rate constant of dimers, N_f is the number of fibers in the cartridge, dt is the time step, and K_{gf} is the grid factor.

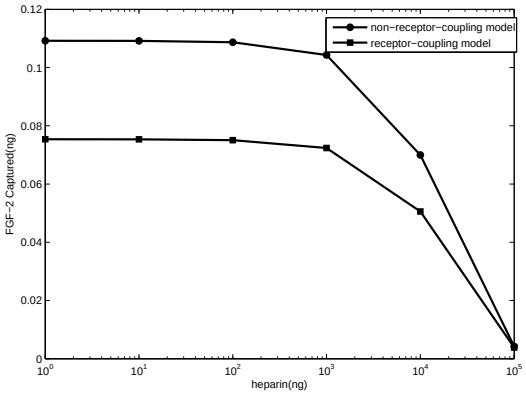

Figure 5.9: Plot with varied heparin impact on FGF-2 cell surface capture. (1ng FGF-2, at 600 seconds, 30% loss at inlet, non-receptor-coupling and receptor-coupling models [28]).

The mass of the ith proteins bound can be calculated by multiplying a constant K_i if its molecular weight is known [96], that is:

$$M_i(n) = K_i \times F_i(n) \tag{5.17}$$

5.5 Simulations

The purpose of these simulations is to predict whether competitors for proteoglycans impact FGF-2 binding in a solution based on both models (non-receptor-coupling and receptor-coupling models) (see section 5.2.3). The study will look at: (1) soluble traps, such as heparin; (2) surface competitors, such as HB-EGF; (3) multi-pass simulations. The conclusions are drawn from the simulation results, which need further experimental verifications.

5.5.1 Effect of Heparin on FGF-2 Capture

Heparin will bind to FGF-2 directly in the fluid, limiting the available amount of FGF-2 binding to its receptors on cell surfaces. Fig. 5.9 shows heparin impact on FGF-2 capture under different amounts of heparin. Fig. 5.10 shows FGF-2 captured along the endothelial-lined hollow fiber as a function of distance under different amounts of

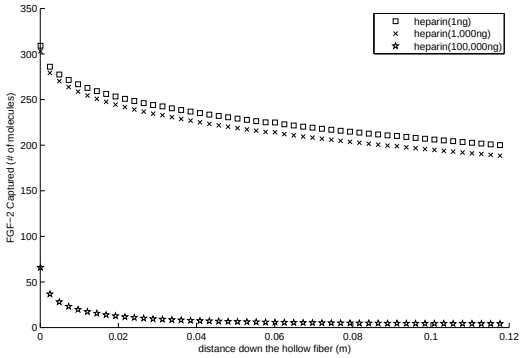

Figure 5.10: Simulation results of FGF-2 captured along the endothelial-lined hollow fiber as a function of distance under different amount of heparin. (1ng FGF-2, at 600 seconds, 30% loss at inlet, non-receptor-coupling model [28]).

heparin at 600 seconds. In Fig. 5.9 and Fig. 5.10, it has been found that heparin (or possibly other solution binding agents) can prevent FGF-2 capture under flow, but it occurs only at high concentrations ($> 100ug$).

5.5.2 Effect of HB-EGF on FGF-2 Capture

FGF-2 and HB-EGF can cross regulate receptor binding of the other despite having unique receptors [28]. Is this conclusion still correct in the flow condition? Also, the research wants to find out how large the impact would be? In Fig. 5.11, the amount of FGF-2 are captured under different amounts of HB-EGF, supposing FGF-2 and HB-EGF are injected simultaneously. Fig.5.12 shows FGF-2 captured along the endothelial-lined hollow fiber as a function of distance under different amounts of HB-EGF at 600 seconds. It is shown that the addition of HB-EGF has only a slight effect on FGF-2 capture and it occurs when HB-EGF is at high concentrations.

5.5.3 HB-EGF Has Only a Minor Impact on Heparin Regulation of FGF-2 Binding

Fig. 5.13 shows that the addition of HB-EGF has only a minor impact on heparin regulation of FGF-2 binding.

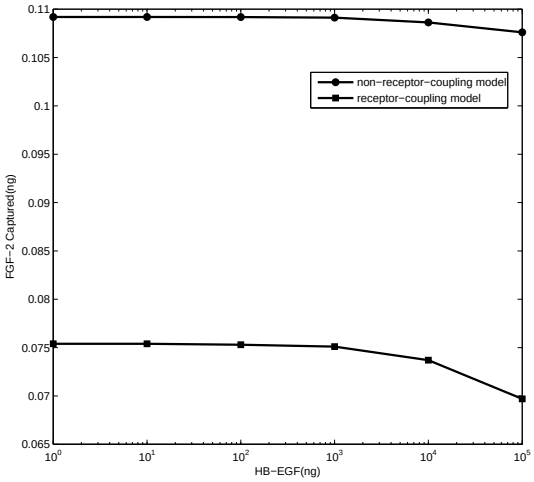

Figure 5.11: Plot with varied HB-EGF impact on FGF-2 cell surface capture. (1ng FGF-2, at 600 seconds, 30% loss at inlet, non-receptor-coupling and receptor-coupling models [28]).

The research concludes that HB-EGF or other proteoglycan-competitors has very little effect on FGF-2 capture under a single pass flow.

5.5.4 Multi-pass Simulation

The human blood system is constantly in circulation, which means that when injecting some drugs into human blood vessels, some of them may bind somewhere in each circulation, leaving the remaining part to circulate. It is very hard to do experiments to study a mechanism of this kind. However, by using computer simulation, it is fairly easy to implement different strategies to simulate this situation, called a multi-pass simulation.

The multi-pass simulation is designed as follows:

Step 1: In the first few minutes, before all the injected growth factor enters the entrance port of fibers, the single pass simulation is used, but the growth factor moving out of the fibers at the outlet is saved in a FIFO queue in each time step.

Step 2: Once all the growth factor has entered the fibers, lets say after 10 minutes,

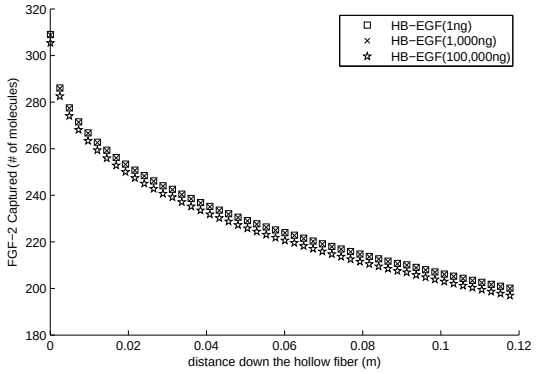

Figure 5.12: Simulation results of FGF-2 captured along the endothelial-lined hollow fiber as a function of distance under different amount of HB-EGF. (1ng FGF-2, at 600 seconds, 30% loss at inlet, non-receptor-coupling model [28]).

the growth factor will be dequeued and enters into the fibers again in each time step. There is no mixing. In the meantime, the growth factor moving out of the fibers at the outlet is queued.

The process is illustrated in Fig. 5.14.

The concentration of a growth factor at the inlet reservoir after switching to queue is:

$$q_{inlet}(t+i) = q_i \tag{5.18}$$

where, t is the time when all the initial injected growth factor has entered the fibers and it is a parameter for user to set up before simulation, and i is the ith time step after t.

This is one strategy for some special purposes. Generally, some actions on the growth factor can be applied in the queue, for example, the growth factor in the queue could be mixed or some kinds of attenuation could be applied to simulate functions of kidneys or liver if their mechanisms were known, etc. Then, the concentration of the growth factor at the inlet reservoir after switching to queue becomes:

$$q_{inlet}(t+i) = f(q_i, t) \tag{5.19}$$

where f is a function applying on the concentration of the growth factor in the queue,

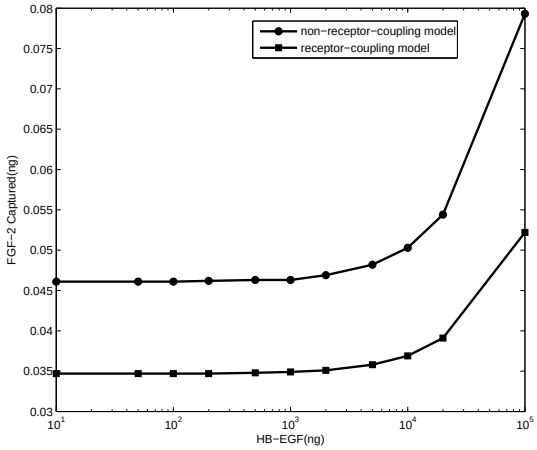

Figure 5.13: Plot with varied HB-EGF impact on heparin regulation of FGF-2 cell surface capture. (1ng FGF-2, 20 ug heparin, at 600 seconds, 30% loss at inlet, non-receptor-coupling and receptor-coupling models [28]).

and it is time dependent.

5.5.5 Effect of Time on FGF-2 Capture Under Multi-pass

Some multi-pass simulations were conducted based on strategy illustrated in Fig. 5.14 to study the effect of time on FGF-2 capture. Both non-receptor-coupling model and receptor-coupling model are used. The results are shown in Fig. 5.15. The results show that the FGF-2 captures are increased with the time in both models and there is a tendency that most of the FGF-2 will be captured eventually if no attenuation exists.

5.5.6 Effect of Different Radiuses of Fibers on FGF-2 Capture

The human blood vessels or capillaries are in different sizes of radius, which may have some critical effects on the growth factor capture. Some simulations were conducted in different radiuses with the same cell density on the wall of fibers. Some additional simulation values are listed in Table 5.7 and other parameters are the same as listed in Table 5.6. Fig. 5.16 shows the simulation results in different radiuses of fibers under

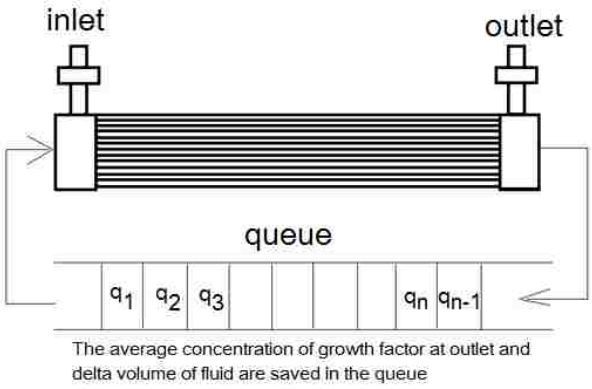

Figure 5.14: The diagram of a multi-pass simulation design. The average concentration of the growth factor at outlet is saved in a FIFO queue along with the delta volume of fluid in each time step. Once the original growth factor at inlet is depleted, switching to the queue, forming a simulation loop, but without mixing the growth factor in the queue.

Table 5.7: Some values used in simulations of different radiuses.

radius	Cell/fiber	Ave. flow rate	Ave. flow velocity
(um)	$(\#)$	(ml/min)	(mm/s)
2.5	5000	0.0000235	1.0
5.0	10000	0.000094	1.0
10	20000	0.000376	1.0
25	50000	0.00235	1.0
50	100000	0.0094	1.0
100	200000	0.0376	1.0
200	400000	0.1504	1.0
350	700000	0.4606	1.0

two models. The simulation results reveal that when average velocity is 1 mm/s, similar to blood flow in human capillaries, almost all FGF-2 entered are captured when the radius is small, such as 2.5, 5 or 10 um. The relative capture (captured /entered) decreases as the radius increases.

It is worth mentioning that in the simulation, the viscosity is treated as a constant, but in human capillaries, the viscosity of blood flow depends on the radius of the capillary it flows through. The Poiseuille's relationship for viscosity doesn't hold for blood flow in capillaries, at least in a range of capillary radiuses (15 μm < r < 150

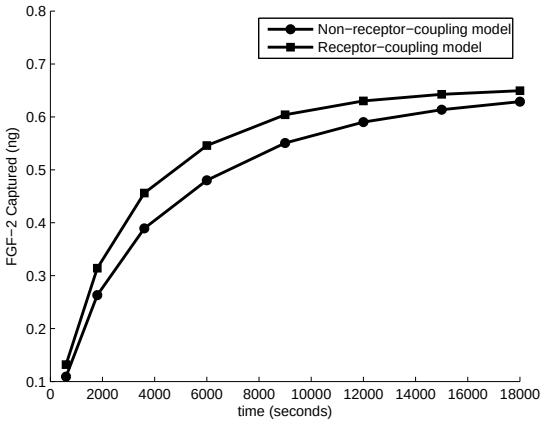

Figure 5.15: The effect of time on FGF-2 capture under multi-pass simulation. 1ng FGF-2 injected at t=0 and 30% loss at inlet as non-specific binding. After 600 seconds almost all FGF-2 entered the fiber(0.7ng), and the FGF-2 at inlet uses the saved values at queue.

μm). This is called the Fahraeus-Lindqvist effect [15]. This effect would be considered in the future when conducting *in vitro* human blood simulations.

5.6 Summary

Since all proteins are assumed to have the same flow, the multi-physics of fluid flow is modeled by the same incompressible Navier-Stokes equations. The kinetics of biochemical reactions occurs in the fluid and on cell surfaces as well, so they are modeled by two separate sets of coupled nonlinear ordinary differential equations (ODEs). The mass transport of different proteins in the fluid is modeled by a distinctive set of coupled nonlinear partial differential equations (PDEs) for each of them.

To solve this computationally intensive system efficiently, a novel parallel algorithm is devised, in which all the numerical computations are solved in parallel, including parallel discretization of those mass transport equations PDEs and a parallel linear system solver. A novel parallel SIP solver is designed. For solving binding equations ODEs in the whole domain efficiently, a parallel scheme combined with a sequential CVODE solver is used for the purposes of high performance and simplicity

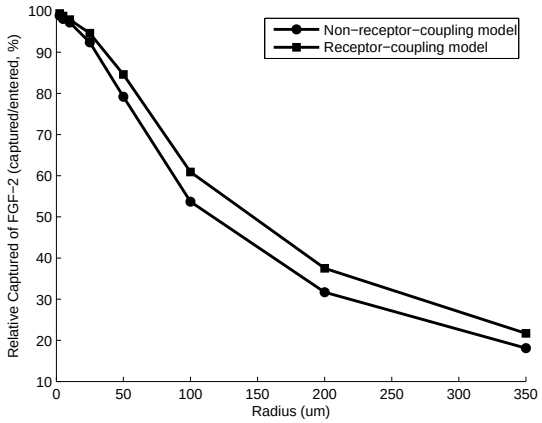

Figure 5.16: The effect of different radiuses of fibers on FGF-2 capture under two models. simulation were run with 1ng FGF-2 injected at t=0, 30% loss at inlet,an average flow velocity = 1mm/s for all radiuses.

[98].

Some predictions have been obtained based on the parallel system. The research has found that: (1) heparin or possibly other solution binding agents can effectively prevent FGF-2 capture under the flow, but it occurs only at high concentrations ($\geq 100\mu m$); and (2) FGF-2 cross regulating receptor binding agents, such as HB-EGF or possibly other proteoglycan-competitors, have little effect on FGF-2 capture in single pass flow even at high concentrations. The experiments also confirmed this conclusion. Further experiments need to be conducted to verify the predictions of the parallel simulation system. This parallel modeling system can be used to analyze any other biochemical reactions in a similar flow environment with trivial effort.

6 Parallel Stone's Strongly Implicit Procedure Solver

6.1 Introduction

The modeling of mass transport equations in the flow condition is very important in binding kinetics analysis. Normally, the finite volume method is appropriate for discretization of those PDEs. The corresponding system of linear algebraic equations is represented by a pentadiagonal nonsymmetric matrix. The coefficients of the matrix are time dependent, and thus the corresponding linear system must be solved separately for each time step. It is time consuming so that parallel methods are of great importance, especially considering that more species are involved. For the solution of the nonsymmetric sparse matrix linear system in computational fluid dynamics, SIP methods are used extensively due to their fewer number of iterations for required accuracy and lower computational costs for each time step (see Chapter 2). There are several parallel SIP methods proposed [32, 60]. For example, Ladislav, et al. proposed a parallel algorithm for calculating a 3D diffusion process of the underground water, including a specific parallel SIP for their problems. Reeve, et al. also proposed a parallel SIP method for solving sparse linear equations arising from the finite difference approximation to partial differential equations. They investigated the sequential SIP method, and proposed wavefront and red-black MPI-based algorithms; and they concluded that their red-black MPI-based algorithm is more efficient due to half values updated simultaneously in each pass before exchanging edge values [60]. This study proposed an overlapped Jacobi iteration algorithm, where, instead of waiting for new edge values to proceed, the previous edge values are used and all the other values in its subdomain are updated by each processor simultaneously. Compared to the pipeline method, the overlapped Jacobi iteration method has higher speedup with the same accuracy. The study did not compare the red-black algorithm proposed by Reeve, et al. Based on the overlapped Jacobi iteration method, a general parallel SIP

solver is built.

6.2 Analysis of Sequential Strongly Implicit Procedure

Stone's SIP method solves a set of linear equations obtained from the discretization of some arbitrary elliptic problems using a five point stencil. The matrix system obtained is shown in Fig. 5.3, and Eq. 6.1.

$$Ax = b \tag{6.1}$$

Stone's SIP method uses the implicit iteration procedure:

$$(A + E)x^n = (A + E)x^{n+1} - (Ax^n - b) \tag{6.2}$$

where $A + E = LU$ has a sparse LU factorization. E is an error matrix, which has two diagonals lying inside and adjacent to the outer diagonals of A (see Fig. 5.5). Stone's algorithm is designed so that terms in Ex are very small [80]. An iteration parameter α $(0 \leq \alpha < 1)$ is used to calculate L and U. α may be a function of mesh.

Stone's SIP algorithm consists of the following steps:

step 1. Initial factorization of matrix A into lower and upper triangular matrices L and U;

step 2. Forward substitution;

step 3. Backward substitution and correction;

step 4. Maximum relative error check.

Steps 2, 3, and 4 are repeated until the maximum relative error difference between the old and the new solution is within the defined tolerance or the maximum number of iterations has been reached [60].

6.2.1 LU Factorization

Considering a rectangular 2D space with I, J grid points in the axial and the radius directions, the code of LU factorization can be expressed as:

$L_W(i,j) = A_W(i,j)/(1 + \alpha U_N(i, j - J))$

$L_S(i,j) = A_S(i,j)/(1 + \alpha U_E(i, j - 1))$

$t1 = \alpha L_W(i,j)U_N(i, j - J)$

$t2 = \alpha L_S(i,j)U_E(i, j - 1)$

$L_P(i,j) = A_P(i,j) + t1 + t2 - L_W(i,j)U_E(i, j - J) - L_S(i,j)U_N(i, j - 1)$

$U_N(i,j) = (A_N(i,j) - t1)/L_P(i,j)$

$U_E(i,j) = (A_E(i,j) - t2)/L_P(i,j)$

The calculation of L_W, L_S, L_P, U_N, and U_E depends on its left neighboring point of U_N and/or north neighboring point of U_E.

6.2.2 Forward Substitution

Similarly, the code of forward substitution can be expressed as:

$r(i,j) = b(i,j) - (A_S(i,j)x(i, i-1) + A_W(i,j)x(i, j-J) + A_P(i,j)x(i,j) + A_E(i,j)x(i, j+J) + A_N(i,j)x(i, j+1))$

$Y(i,j) = (r(i,j) - L_S(i,j)Y(i, j-1) - L_W(i,j)Y(i, j-J))/L_P(i,j)$

The calculation of r depends on its left, right, upper and lower neighboring points of x. Thus, x needs to be updated in each iteration. The calculation of Y depends on its left and upper neighboring points of Y. The pipeline technique is appropriate.

6.2.3 Backward Substitution and Correction

The code of backward substitution and correction can be expressed as:

$\delta(i,j) = Y(i,j) - (U_N(i,j)Y(i, j+1) + U_E(i,j)Y(i, j+J))$

$x(i,j) = x(i,j) + \delta(i,j)$

The calculation of δ depends on its right and upper neighboring points of Y. Again, the pipeline technique is appropriate.

6.3 Parallel SIP Algorithms

Based on the analysis of the sequential code in the previous section and the domain partition scheme used (refer to Fig. 5.4), a parallel algorithm can be designed as follows: For LU factorization, the pipeline technique is used in order to get the exact solution as the sequential algorithm for L and U.

For forward and backward substitutions, two algorithms are designed: one algorithm uses a pipeline method, the other one uses an overlapped Jacobi iteration method.

6.3.1 Pipeline Algorithm

For forward substitution, each processor has to wait for its left side processor to finish doing the calculation in order to obtain the new values of Y in left neighboring points to start the calculation. P_i has to send the boundary values of Y to P_{i+1}, and only after P_{i+1} receives the data, it can start calculation. A blocking send or receive is used.

The solution values of x in boundary points are updated in each iteration, so the calculation of r is the same as the sequential algorithm. Maximum relative error is calculated by each processor and then the algorithm does a reduction to obtain the final value.

Similarly, for backward substitution, each processor has to wait for its right side processor to finish doing the calculation in order to obtain the new values of Y in right neighboring points to start the calculation. P_{i+1} has to send the boundary values of Y to P_i, and only after P_i received the data from P_{i+1}, it can start the calculation. A blocking send or receive is used.

The algorithm is shown below.

Algorithm 12 Parallel SIP algorithm using pipeline techniques

1: LU factorization by using pipeline technique
2: (P_i starts LU calculation after P_{i-1} finishes and P_i receives the left boundary data sent by P_{i-1})
3: **while** $||R^{n+1}||_2/||x^{n+1}||_2 > \varepsilon$ **do**
4: Forward substitution by using pipeline technique
5: (P_i starts calculation after P_{i-1} finishes and P_i receives the left boundary data sent by P_{i-1})
6: Backward Substitution by using pipeline technique
7: (P_{i-1} starts calculation after P_i finishes and P_{i-1} receives the right boundary data sent by P_i)
8: Update residual $R^{n+1} = R^n + A\Delta x^n$
9: Update solution $x^{n+1} = x^n + \Delta x^n$
10: **end while**

6.3.2 Overlapped Jacobi Iteration Algorithm

For forward substitution, each processor uses the previous values of Y in left neighboring points to calculate Y instead of waiting for its left side neighboring processor to send those values, allowing each processor to process concurrently. When all processors finish the calculation, the boundary points of Y are updated among processors, i.e., processor P_i sends the boundary values of Y to processor P_{i+1}. Blocking send and receive are used.

The solution values of x in boundary points are updated in each iteration, so the calculation of r is the same as the sequential algorithm. Maximum relative error is calculated by each processor and then the algorithm does a reduction to obtain the final value.

For backward substitution, each processor also uses the previous values of Y in right neighboring points to calculate δ instead of waiting for those neighboring points to be sent by its right neighboring processor, allowing each processor to process concurrently. The solution x is corrected based on the δ value. After all the processors finish the calculation, the boundary points of Y are updated among processors, i.e., processor P_{i+1} sends the boundary values of Y to processor P_i. Again, blocking send

and receive are used.

In each iteration, the left and right boundary points of solution x are updated among processors. That is, processor P_{i+1} sends the boundary values of x to processor P_i, and vice versa.

The algorithm is shown below:

Algorithm 13 Parallel SIP algorithm using overlapped Jacobi iteration technique

1: LU factorization by using pipeline technique
2: (P_i starts LU calculation after P_{i-1} finishes and P_i receives the left boundary data sent by P_{i-1})
3: **while** $||R^{n+1}||_2/||x^{n+1}||_2 > \varepsilon$ **do**
4: Forward substitution by using overlapped Jacobi iteration technique
5: (All processors start calculation at the same time, the left boundary data use the previous values)
6: Exchange left boundary data between processors
7: Backward Substitution by using overlapped Jacobi iteration technique
8: (All processors start calculation at the same time, the right boundary data use the previous values)
9: Update residual $R^{n+1} = R^n + A\Delta x^n$
10: Update solution $x^{n+1} = x^n + \Delta x^n$
11: Exchange right boundary data between processors
12: Exchange solution boundary data among processors
13: **end while**

6.4 Results

Different runs were conducted up to eight nodes on the same supercomputer using the above two algorithms. Problem size is fixed to be 1500 × 24. The results are shown in Fig. 5.7. It shows that the overlapped Jacobi iteration method has better speedup than the pipeline does. The overlapped Jacobi iteration method may need more iterations than the pipeline, but it is much faster.

6.5 Summary

A novel parallel SIP solver is designed and two techniques (pipeline and overlapped Jacobi iteration) are implemented. The simulation results show that the overlapped

Jacobi iteration method has better speedup. This method could be used to replace the pipeline technique in similar situations to obtain a better performance.

7 Conclusion, Contribution and Future Work

7.1 Conclusion

This dissertation presents the research work in computer modeling and simulation of biochemical reactions in a flow environment using the deterministic method. The whole simulation procedure includes: the mathematical modeling, the discretization of partial differential equations, the solutions of linear and nonlinear systems, and the scientific visualization. Several typical simulation models are discussed, such as a basic binding model and a complex binding model. The dissertation work is summarized as follows.

- First, it introduces a basic novel convection-diffusion-reaction model to simulate fibroblast growth factor (FGF-2) binding to cell surface molecules of its receptor and heparan sulfate proteoglycan (HSPG) and MAP kinase signaling under flow condition. This model includes three parts: the flow of medium using incompressible Navier-Stokes equations, the mass transport of FGF-2 using convection-diffusion transport equations, and the binding and signaling of growth factors-receptors using chemical kinetic equations. The whole model consists of a set of coupled nonlinear partial differential equations (PDEs) for flow and mass transport, and a set of coupled nonlinear ordinary differential equations (ODEs) for binding kinetics. In order to obtain a reasonable accuracy of the binding and dissociation from cells, a uniform mesh is used. To handle pulsatile flow, several assumptions are made including neglecting any entrance effects and an analytical solution for axial velocity within the fibers is obtained. To solve the time-dependent mass transport PDEs, a second order implicit Euler method is used by finite volume discretization. The ODE system is stiff and solved by an ODE solver CVODE using backward differencing formulation (BDF). The spatial distribution of FGF-2, FGFR, HSPG and their

binding complexes are obtained and presented.

- After the basic simulation system is built, the growth factor (FGF-2) capture under flow is analyzed and predicted using this computer modeling and experimental approach that includes pertinent circulation characteristics such as pulsatile flow, competing binding interactions, and limited bioavailability. The experimental module consisted of a bioreactor with synthetic endothelial-lined hollow fibers under flow. The physical design of the system was incorporated into the model parameters. The heparin-binding growth factor FGF-2 was used for both the experiments and simulations. The model is based on the flow and reactions within a single hollow fiber and was scaled linearly by the total number of fibers for comparison with experimental results. The model predicted, and experiments confirmed, that removal of heparan sulfate (HS) from the system would result in a dramatic loss of binding by heparin-binding proteins, but not by proteins that do not bind heparin. The model further predicted a significant loss of bound protein at flow rates only slightly higher than average capillary flow rates, corroborated experimentally, suggesting that the probability of capture in a single pass at high flow rates is extremely low. Several other key parameters were investigated with the coupling between receptors and proteoglycans shown to have a critical impact on successful capture. The combined system offers opportunities to examine circulation capture in a straightforward quantitative manner that should prove advantageous for biologicals or drug delivery investigations.

- The biochemical mechanism in human blood vessels and capillaries is very complicated, where different kinds of growth factors, receptors and different cells are involved. A complex model system is proposed to handle such cases, in which more growth factors, receptors and even different cells are allowed. The

binding kinetics are not only allowed to occur on cell surfaces, but in the fluid as well. The complex model also includes three major parts similar to the basic model, but mass transport equations and chemical kinetics are different. First, the complex model has more types of proteins in the fluid, and thus, more sets of mass transport equations are included. Next, the binding kinetics occurs in the fluid as well as on cell surfaces. Therefore, two different sets of ODEs are needed to handle this situation. In order to solve this coupled nonlinear system to obtain simulation results within a reasonable waiting period, a special parallel simulation program is created based on message passing interface(MPI), in which a parallel discretization and a parallel linear solver are designed. For simplicity, a parallel scheme combined with a sequential ODE solver CVODE is used to solve binding kinetics in the fluid and on cell surfaces. Overall, the parallel system is stable and some simulation results are obtained. This research has found that: (1)heparin (or possibly other solution binding agents) can prevent FGF-2 capture under flow, but only at high concentrations ($> 100ug$); (2) HB-EGF or other proteoglycan-competitors can have an effect on FGF-2 capture but it is small under single pass. In the future, more experiments need to be conducted to verify the correctness and effectiveness of the parallel simulation system.

7.2 Contribution

The contribution of the author can be summarized in the following:

(1) designed an interactive multi-threading software package running on Windows operating systems to simulate growth factor-receptor binding and dissociation processes in a bioreactor flow environment, in which several issues are solved, such as: a) deduced an approximate analytical solution for pulsatile flow; b) provided a general quantitative formula to calculate growth factor binding and internalization on

cell surfaces within a fiber based on a uniform mesh and the deterministic method; c) provided a reasonable formula to calculate the concentration of growth factors at inlet reservoir; d) solved the nonspecific binding issue based on experimental measurements.

(2) conducted massive simulations based on experimental results and provided two criteria: the amount criterion and the curve-matching criterion, to determine a correlation between the simulation and experimental results. Based on the two criteria, the simulation and experimental results have good agreements, indicating the software package is trustworthy.

(3) designed a parallel distributed software package with MPI technique running on cluster machines to simulate multiple growth factors-receptors competitive binding and dissociation processes in a bioreactor flow environment, in which competitive bindings can occur on cell surfaces and in the fluid as well, and all the calculations are parallelized including the parallel discretization and a parallel linear solver. This parallel software package can be used for any complex binding system in a similar flow environment. The idea has hints for simulation of binding processes in human blood vessels or capillaries with multiple proteins and irregular geometry.

(4) parallelized Stone's SIP solver in two methods: the pipeline and the overlapped Jacobi iteration method, and found that the latter method has better speedup. This parallel SIP solver can be used for solving the linear system of sparse matrix with similar structures.

7.3 Future Work

Some fundamental work has been done that relates to the simulation and modeling of biological processes in a flow environment. In-depth research needs to be done to make the simulation as close to human blood vessels or capillaries as possible. Possible future research directions in protein transport are listed below.

- Develop a multiphysics mathematical model for simulating ligand-receptor binding, dissociation and transport in blood circulation using a group of nonlinear differential equations. In the one phase model of ligand transport presented in the dissertation, the blood stream is considered as a single phase, and the proteins are transported passively and their effect to blood flow is neglected.

  In the multiphase model, the blood stream may be considered a mixture of several phases, in which plasma is considered the continuous phase, while protein molecules are regarded as dispersed phases. The multiphase model allows people to take a closer look at the motion of protein molecules in the blood stream and its influence on the fluid dynamic behavior of the mixture of blood and proteins. The dynamic system can be modeled by a set of partial differential equations, where each phase has its own continuity and momentum equations.

- The mathematical models and corresponding software packages for proteins transport prediction in circulation are developed for 2D applications in axisymmetric coordinates. This 2D system may be extended to 3D applications involved in some complex 3D geometries, such as human blood vessels or capillaries, to simulate blood flows in heart and lung, etc. It will be closer to *in vivo* simulations but the computational cost could be very high. Efficient parallel algorithms are still one of the major design goals in those 3D systems. Some high performance parallel techniques, such as multilevel multigrid acceleration and efficient preconditioning may be used to achieve the goal of high order accuracy and low computing cost. To be specific, adaptive multilevel multigrid method can achieve high order accuracy by mesh refinement in large gradient region and low computing cost by mesh coarsening in small gradient region.

Appendix

7.4 A

The basic model [27] studied in Chapter 3 and 4 consists of the following 9 equations, which describe the rate of components change with respect to time.

$$\frac{dR}{dt} = -k_{onFR}FR + k_{offFR}C + k_{offFHR}T - k_cRG - k_{int}R + k_{int}R_0 \tag{7.1}$$

$$\frac{dC}{dt} = k_{onFR}FR - k_{offFR}C - k_cCH - k_cC^2 + 2k_{uc}C_2 - k_{int}C \tag{7.2}$$

$$\frac{dC_2}{dt} = \frac{k_c}{2}C^2 - k_{uc}C_2 - k_{intD}C_2 \tag{7.3}$$

$$\frac{dT}{dt} = k_cRG + k_cCH - k_{offFHR}T - k_cT^2 + 2k_{uc}T_2 - k_{int}T \tag{7.4}$$

$$\frac{dT_2}{dt} = \frac{k_c}{2}T^2 - k_{uc}T_2 - k_{intD}T_2 \tag{7.5}$$

$$\frac{dH}{dt} = -k_{onFH}FH + k_{offFH}G + k_{offFHR}T - k_cCH - k_{int}H + k_{int}H_0 \tag{7.6}$$

$$\frac{dG}{dt} = k_{onFH}FH - k_{offFH}G - k_cRG - k_cG^2 + 2k_{uc}G_2 - k_{int}G \tag{7.7}$$

$$\frac{dG_2}{dt} = \frac{k_c}{2}G^2 - k_{uc}G_2 - k_{intD}G_2, \tag{7.8}$$

$$V\frac{dF}{dt} = -k_{onFR}FR + k_{offFR}C + k_{offFHR}T - k_{onFH}FH - k_{offFH}G \tag{7.9}$$

where F is FGF-2, R is FGFR, C is FGF-2-FGFR complex, H is HSPG, G is FGF-2-HSPG complex, T is FGF-2-FGFR-HSPG complex, C_2 is FGF-2-FGFR dimer, G_2 is FGF-2-HSPG dimer, and T_2 is FGF-2-FGFR-HSPG dimer.

Bibliography

[1] Anderso DA, Tannehill JC, and Pletcher RH, *Computational Fluid Mechanics and Heat Transfer*, Hemisphere Publishing Corporation, Washington, 1984.

[2] Bao X, Nishimura S, Mikami T, Yamada S, Itoh N, et al., Chondroitin sulfate/dermatan sulfate hybrid chains from embryonic pig brain, which contain a higher proportion of L-iduronic acid than those from adult pig brain, exhibit neuritogenic and growth factor binding activities, *J Biol Chem*, **279**, 9765-9776, 2004.

[3] Beenken A, Mohammadi M, The FGF family: biology, pathophysiology and therapy, *Nat Rev Drug Discov*, **8**, 235-253, 2009.

[4] Bennett BAV and Smooke MD, Local Rectangular Refinement with Application to Axisymmetric Laminar Flames, *Combust. Theory Modelling*, **2**(3), 221-258, 1998.

[5] Bjornsson S, Quantitation of proteoglycans as glycosaminoglycans in biological fluids using an alcian blue dot blot analysis, *Anal Biochem*, **256**, 229-237, 1998.

[6] Brown PN, et al., VODE: A variable-coefficient ODE solver, *SIAM J. Sci. Stat. Comput.*, **10** (5), 1038-1051, 1989.

[7] Cappadona C, Redmond EM, Theodorakis NG, McKillop IH, Hendrickson R, et al., Phenotype dictates the growth response of vascular smooth muscle cells to pulse pressure in vitro, *Exp Cell Res*, **250**, 174-186, 1999.

[8] Chapman DR, Computational Aerodynamics Development and Outlook, *AIAA Journal*, **17**, 1293-1313, 1979.

[9] Colella P and Woodward PR, The piecewise parabolic method (PPM) for gas-dynamical simulation, *Journal of Computational Physics*, **54**, 174-201, 1984.

[10] Conte SD and deBoor C, *Elementary Numerical Analysis*, McGraw-Hill, New York, 1972.

[11] Courant, R, Friedrichs K, and Lewy H, On the Partial Difference Equations of Mathematical Physics, *IBM J.*,**11**, 215-234, 1967.

[12] Dong Z, Saliganan AD, Meng H, Nabha SM, Sabbota AL, et al., Prostate cancer cell-derived urokinase-type plasminogen activator contributes to intraosseous tumor growth and bone turnover, *Neoplasia*, **10**, 439-449, 2008.

[13] Dowd CJ, Cooney CL, and Nugent MA, Heparan sulfate mediates bFGF transport through basement membrane by diffusion with rapid reversible binding, *The Journal of Biological Chemistry*, **274**, 5236-5244, 1999.

[14] Elhadj S, Mousa SA, Forsten-Williams K, Chronic pulsatile shear stress impacts synthesis of proteoglycans by endothelial cells: effect on platelet aggregation and coagulation, *J Cell Biochem*, **86**, 239-250, 2002.

[15] Fahraeus R and Lindqvist T, The viscosity of the blood in narrow capillary tubes, *American Journal of Physiology*, **96**, 562-568, 1931.

[16] Fannon M, Nugent MA, Basic fibroblast growth factor binds its receptors, is internalized, and stimulates DNA synthesis in Balb/c3T3 cells in the absence of heparan sulfate, *J Biol Chem*, **271**, 17949-17956, 1996.

[17] Fannon M, Forsten KE, Nugent MA, Potentiation and inhibition of bFGF binding by heparin: a model for regulation of cellular response, *Biochemistry*, **39**, 1434-1445, 2000.

[18] Fannon M, Forsten-Williams K, Dowd CJ, Freedman DA, Folkman J, et al., Binding inhibition of angiogenic factors by heparan sulfate proteoglycans in aqueous humor: potential mechanism for maintenance of an avascular environment, *Faseb J*, **17**, 902-904, 2003.

[19] Ferziger JH and Peric M, *Computational Methods for Fluid Dynamics*, Springer, Berlin, Germany, 1999.

[20] Filion RJ, Popel AS, A reaction-diffusion model of basic fibroblast growth factor interactions with cell surface receptors, *Ann Biomed Eng*, **32**, 645-663, 2004.

[21] Filion RJ, Popel AS, Intracoronary administration of FGF-2: a computational model of myocardial deposition and retention, *Am J Physiol Heart Circ Physiol*, **288**, 263-279, 2005.

[22] Folkman J, Langer R, Linhardt RJ, Haudenschild C, and Taylor S, Angiogenesis inhibition and tumor regression caused by heparin or a heparin fragment in the presence of cortisone, *Science*, **221**, 719-725, 1983.

[23] Folkman J, Klagsbrun M, Angiogenic factors, *Science*, **235**, 442-447, 1987.

[24] Forsten KE, and Lauffenburger DA, Probability of autocrine ligand capture by cell-surface receptors: implications for ligand secretion measurements, *J. Comp. Bio.*, **1**, 15-23, 1994.

[25] Forsten KE, Courant NA, Nugent MA, Endothelial proteoglycans inhibit bFGF binding and mitogenesis, *J Cell Physiol*, **172**, 209-220, 1997.

[26] Forsten KE, Fannon M, Nugent MA, Potential mechanisms for the regulation of growth factor binding by heparin, *J Theor Biol*, **205**, 215-230, 2000.

[27] Forsten-Williams K, Chua CC, Nugent MA, The kinetics of FGF-2 binding to heparan sulfate proteoglycans and MAP kinase signaling, *J Theor Biol*, **233**, 483-499, 2005.

[28] Forsten-Williams K, Chu CL, Fannon M, Buczek-Thomas JA, Nugent MA, Control of growth factor networks by heparan sulfate proteoglycans, *Ann Biomed Eng* **36**, 2134-2148, 2008.

[29] Gaffney EA, Heath JK, Kwiatkowska MZ, A mass action model of a Fibroblast Growth Factor signaling pathway and its simplification, *Bull Math Biol*, **70**, 2229-2263, 2008.

[30] Golub GH, and Charles F and Van Loan, Matrix Computations (3rd ed.), *John Hopkins*, 1996.

[31] Gordon MS, Margolin K, Talpaz M, Sledge GW, Jr., Holmgren E, et al., Phase I safety and pharmacokinetic study of recombinant human anti-vascular endothelial growth factor in patients with advanced cancer, *J Clin Oncol*, **19**, 843-850, 2001.

[32] Halada L, and M Lucka, A Parallel Strongly Implicit Algorithm for Solving of Diffusion Equations, *Concurrency Computat.: Pract. Exper.*, **13**, 1049-1062, 2001.

[33] Hendriks BS, Opresko LK, Wiley HS, Wells A, Lauffenburger DA, Quantitative analysis of HER2-mediated effects on HER2 and epidermal growth factor receptor endocytosis: distribution of homo- and heterodimers depends on relative HER2 levels, *J. Biol. Chem.*, **278**, 23343-23351, 2003.

[34] Herman IM, Brant AM, Warty VS, Bonaccorso J, Klein EC, et al., Hemodynamics and the vascular endothelial cytoskeleton, *J Cell Biol*, **105**,291-302, 1987.

[35] Hornbeck RW, Laminar flow in the entrance region of a pipe, *Applied Science Research*, **13**,224-232, 1964.

[36] Horowitz A, Tkachenko E, and Simons M, Fibroblast growth factor-specific modulation of cellular response by syndecan-4, *Journal of Cell Biology*, **157**, 715-725, 2002.

[37] Hsei V, Deguzman GG, Nixon A, Gaudreault J, Complexation of VEGF with bevaczumab decreases VEGF clearance in rats, *Pharm Res*, **19**, 1753-1756, 2002.

[38] Ibrahimi OA, Zhang F, Hrstka SC, Mohammadi M, Linhardt RJ, Kinetic model for FGF, FGFR, and proteoglycan signal transduction complex assembly, *Biochemistry* **43**, 4724-4730, 2004.

[39] Johnson BM, Johnston PR, Corney S, and Kilpatrick D, Non-Newtonian blood flow in human right coronary arteries: steady state simulations, *Journal of Biomechanics*, **37**, 709-720, 2004.

[40] Johnson DE, and Williams LT, Structural and functional diversity in the FGF receptor multigene family, *Adv. Cancel Res.*, **60**, 1-41, 1993.

[41] Kan M, Wang F, Xu J, Crabb JW, Hou J, et al., An essential heparinbinding domain in the fibroblast growth factor receptor kinase, *Science*, **259**, 1918-1921, 1993.

[42] Kanellos M, New life for Moore's Law, *cnet news*, 19 April 2005.

[43] Kelley CT, *Iterative Methods for Linear and Nonliear Equations*, SIAM, Philadelphia, 1995.

[44] Kholodenko BN, Demin OV, Moehren G, and Hoek JB, Quantification of short term signaling by the epidermal growth factor receptor, *Journal of Biological Chemistry*, **274**, 30169-30181, 1999.

[45] Kim KJ, Li B, Houck K, Winer J, Ferrara N, The vascular endothelial growth factor proteins: identification of biologically relevant regions by neutralizing monoclonal antibodies, *Growth Factors*, **7**, 53-64, 1992.

[46] Lew HS, Fung YC, Entry length into blood vessels at arbitrary Reynolds number, *J. of Biomechanics*, **3**, 23-38, 1970.

[47] LeVeque R, *Finite Volume Methods for Hyperbolic Problems*, Cambridge University Press, Cambridge, UK, 2002.

[48] Lovich MA, Edelman ER, Computational simulations of local vascular heparin deposition and distribution, *Am J Physiol*, **271**, 2014-2024, 1996.

[49] Mac Gabhann F, Popel AS, Dimerization of VEGF receptors and implications for signal transduction: a computational study, *Biophys Chem*, **128**, 125-139, 2007.

[50] Manuel, FiberCell Systems, Inc. *http://www.fibercellsystems.com.*

[51] Moore G. E, Cramming more componments onto integrated circuits, *Electronics*, **38(8)**, 1965.

[52] Moscatelli D, High and low affinity binding sites for basic fibroblast growth factor on cultured cells: absence of a role for low affinity binding in the stimulation of plasminogen activator production by bovine capillary endothelial cells, *J Cell Physiol*, **131**, 123-130, 1987.

[53] Moscatelli D, Basic fibroblast growth factor (bFGF) dissociates rapidly from heparan sulfates but slowly from receptors. Implications for mechanisms of bFGF release from pericellular matrix, *J Biol Chem*, **267**, 25803-25809, 1992.

[54] Neuhaus W, Lauer R, Oelzant S, Fringeli UP, Ecker GF, et al., A novel flow based hollow-fiber blood-brain barrier in vitro model with immortalized cell line PBMEC/C1-2, *J Biotechnol*, **125**, 127-141, 2006.

[55] Nugent MA, Edelman ER, Kinetics of basic fibroblast growth factor binding to its receptor and heparan sulfate proteoglycan: a mechanism for cooperativity, *Biochemistry*, **31**, 8876-8883, 1992.

[56] Ott MJ and Ballermann BJ, Shear stress-conditioned, endothelial cell-seeded vascular grafts: improved cell adherence in response to in vitro shear stress, *Surgery*, **117**, 334-339, 1995.

[57] Patankar SV, *Numerical Heat Transfer and Fluid Flow*, The McGraw-Hill Company, Inc., New York, 1980.

[58] Rapraeger AC, Krufka A, Olwin BB, Requirement of heparan sulfate for bFGF-mediated fibroblast growth and myoblast differentiation, *Science*, **252**, 1705-1708, 1991.

[59] Redmond EM, Cahill PA, Sitzmann JV, Flow-mediated regulation of endothelin receptors in cocultured vascular smooth muscle cells: an endothelium-dependent effect, *J Vasc Res*, **34**, 425-435, 1997.

[60] Reeve JS, Scurr AD and Merlin JH, Parallel version of Stone's strongly implicit algorithm, *Concurrency Computat.: Pract. Exper.*, **13**, 1049-1062, 2001.

[61] Riley BB, Savage MP, Simandl BK, Olwin BB, and Fallon JF, Retrobiral expression of FGF-2 (bFGF) affects patterning in chick limb bud, *Development*, **118**, 95-104, 1993.

[62] Roe P, Approximate Riemann Solvers, Parameter Vectors and Difference Schemes, *Journal of Computational Physics*, **27**, 1-31, 1978.

[63] Rosenberg RD, Shworak NW, Liu J, Schwartz JJ, Zhang L, Heparan sulfate proteoglycans of the cardiovascular system. Specific structures emerge but how is synthesis regulated? *J Clin Invest*, **99**, 2062-2070, 1997.

[64] Saad Y and Schultz MH, GMRES: a generalized minimal residual algorithm for solving nonsymmetric linear systems, *SIAM J. Sci. Stat. Comput.*, **7**, 856-869, 1986.

[65] Saad Y, ILUT: a dual threshold incomplete LU preconditioner. *Numer. Linear Algebra Appl.*, **1**, 387-402, 1994.

[66] Saad Y, *Iterative Methods for Sparse Linear Systems*, PWS Pub., New York, 1996.

[67] Sasisekharan R, Moses MA, Nugent MA, Cooney CL, Langer R, Heparinase inhibits neovascularization, *Proc Natl Acad Sci USA*, **91**, 1524-1528, 1994.

[68] Schlessinger J, Plotnikov AN, Ibrahimi OA, Eliseenkova AV, Yeh BK, et al., Crystal structure of a ternary FGF-FGFR-heparin complex reveals a dual role for heparin in FGFR binding and dimerization, *Mol Cell*, **6**, 743-750, 2000.

[69] Schmidt-Nielson K, *Scaling, why is animal size so important?*, Cambridge University Press, 1984.

[70] Shen WS, Zhang CJ, and Zhang J, Multiscale simulation of ligand-receptor binding and dissociation in circulation, *Proceedings The* 45th *ACM Southeast Conference*, 519-520, 2007.

[71] Shen WS, Zhang CJ, Fannon MW, Forsten-Williams K, Zhang J, A computational model of FGF-2 binding and HSPG regulation under flow, *IEEE Trans Biomed Eng*, **56**, 2147-2155, 2009.

[72] Shu CW, High-order Finite Difference and Finite Volume WENO Schemes and Discontinuous Galerkin Methods for CFD, *International Journal of Computational Fluid Dynamics*, **17** (2), 107-118, 2001.

[73] Singer MA and Pope SB, Exploiting ISAT to solve the reaction-diffusion equation, *Combustion Theory and Modelling*, **8**, 361-383, 2004.

[74] Smith JM, *Mathematical Modeling and Digital Simulation for Engineers and Scientists*, John Wiley & Sons, New Work, 1987.

[75] Smith SM, West LA, Govindraj P, Zhang X, Ornitz DM, et al., Heparan and chondroitin sulfate on growth plate perlecan mediate binding and delivery of FGF-2 to FGF receptors, *Matrix Biol*, **26**, 175-184, 2007.

[76] Sod GA, *Numerical Methods in Fluid Dynamics*, Cambridge University Press, New York, 1985.

[77] Sperinde GV and Nugent MA, Heparan sulfate proteoglycans control bFGF processing in vascular smooth muscle cells, *Biochemistry*, **37**, 13153-13164, 1998.

[78] Sperinde GV, Nugent MA, Mechanisms of fibroblast growth factor 2 intracellular processing: a kinetic analysis of the role of heparan sulfate proteoglycans, *Biochemistry*, **39**, 3788-3796, 2000.

[79] Stanness KA, Guatteo E, Janigro D, A dynamic model of the blood-brain barrier "in vitro", *Neurotoxicology*, **17**, 481-496, 1996.

[80] Stone HL, Iterative solution of implicit approximations of multidimensional partial equations, *SIAM J. Numer. Anal.*, **5**, 530-558, 1968.

[81] Sweby PK, High Resolution Schemes Using Flux Limiters for Hyperbolic Conservation Laws, *SIAM Journal of Numerical Analysis*, **21** (5), 995-1011, 1984.

[82] Taylor KR, Rudisill JA, Gallo RL, Structural and sequence motifs in dermatan sulfate for promoting fibroblast growth factor-2 (FGF-2) and FGF-7 activity, *J Biol Chem*, **280**, 5300-5306, 2005.

[83] Tortora GJ, Anagnostakos NP, *Principles of Anatomy and Physiology*, Harper and Row, New York, 1987.

[84] Tumova S, Woods A, Couchman JR, Heparan sulfate proteoglycans on the cell surface: versatile coordinators of cellular functions, *Int J Biochem Cell Biol*, **32**, 269-288, 2000.

[85] van der Vorst HA, Bi-CGSTAB: a Fast and Smoothly Converging Variant of Bi-CG for the Solution of Nonsymmetric Linear Systems, *SIAM J. Sci. Statist. Comput.*, **13** (2), 631-644, 1992.

[86] Van Leer B, Towards the ultimate conservative difference schemes, V: A second order sequel to Godunov's method, *Journal of Computational Physics*, **43**, 357-372, 1981.

[87] Venkatakrishnan V, Newton Solution of Inviscid and Viscous Problems, *AIAA Journal*, **27** (7), 885-891, 1989.

[88] Walicke PA, Interactions between basic fibroblast growth factor (FGF) and glycosoaminoglycans in promoting neurite outgrowth, *Exp Neurol*, **102**, 144-148, 1988.

[89] Welty JR, Wicks CE, Wilson RE, Rorrer LG, *Fundamentals of Momentum, Heat, and Mass Transfer*, John Wiley and Sons,USA, 2002.

[90] West GB, Brown JH, Enquist BJ, The fourth dimension of life: fractal geometry and allometric scaling of organisms, *Science*, **284**, 1677-1679, 1999.

[91] Wilkinson B and Allen M, *Parallel Programming:techniques and applications using networked workstations and parallel computers*, Prentice-Hall Inc., New Jersey, 1999.

[92] Yayon A, Klagsbrun M, Esko JD, Leder P, Ornitz DM, Cell surface,heparin-like molecules are required for binding of basic fibroblast growth factor to its high affinity receptor, *Cell*, **64**, 841-848, 1991.

[93] Young DM, Iterative methods for solving partial difference equations of elliptical type, *PhD thesis*, Harvard University, 1950.

[94] Zamir M, *The Physics of Pulsatile Flow*, Springer-Verlag New York, Inc., 2000.

[95] Zhang J and Zhao JJ, Unconditionally stable finite difference scheme and iterative solution of 2D microscale heat transport equation, *Journal of Computational Physics*, **170**, 261-275, 2001.

[96] Zhang CJ, Shen WS, Zhao B, Fannon M, Forsten-Williams K, Zhang J, A Numerical Study of Pulsatile Flow Through a Hollow Fiber Cartridge: Growth Factor-Receptor Binding and Dissociation Analysis, *Proceedings of Int'l Conf. on Bioinformatics, System Biology and Intelligent Computing*, 435-441, 2009.

[97] Zhang CJ, Forsten-Williams K, Zhao B, Fannon M, Zhang J, Coupling Between Heparan Sulfate Proteoglycans and FGF-2 Receptors is Key to FGF-2 Capture Under Flow: A Computational Study, *Proceedings of ACM Int'l Conf. on Bioinformatics, and Computational Biology*, 439-441, 2010.

[98] Zhang CJ, Forsten-Williams K, Fannon M, Shen WS, Zhang J, Parallel Simulation of Multiple Proteins Through a Bioreactor Coupled with Biochemical Reactions, *Proceedings of ACM Int'l Conf. on Bioinformatics, and Computational Biology*, 20-28, 2011.

[99] Zhao B, Zhang CJ, Forsten-Williams K, Zhang J, and Fannon M, Endothelial Cell Capture of Heparin-binding Growth Factors under Flow, *PLoS Computational Biology*, **6**(10), e1000971, 2010.

Vita

Personal Data:

Name: Changjiang Zhang

Date of Birth: 03/08/1963

Place of Birth: Anhui, China

Educational Background:

- Master of Engineering in Electrical and Computer Engineering, Donghua University, Shanghai, China, 1986.
- Bachelor of Engineering in Electrical Engineering, Donghua University, Shanghai, China, 1983.

Professional Experience:

- Research Assistant, 08/2007 - present. Department of Computer Science, University of Kentucky.
- Teaching Assistant, 08/2006 - 05/2007. Department of Computer Science, University of Kentucky.
- Financial Software Developer, 12/2002 - 08/2006. Nico Holding LLC. Chicago, USA .
- Senior Electrical Engineer, Team Leader, 08/1997 - 09/2001. Huawei Technologies Co., Ltd., Shenzhen, China.
- Electronics Engineer, 06/1996 - 07/1997. Mindray Medical International Ltd., Shenzhen, China.

- Electronics Engineer, 01/1993 - 05/1996. Shenzhen Geniture Science and Technologies INC., Ltd., Shenzhen, China.
- Research Assistant, 01/1990 - 12/1992. Image Processing Center, Donghua University, Shanghai, China.
- Teaching Assistant and Instructor, 01/1986 - 12/1989. Management Information Department, Donghua University, Shanghai, China.

Awards:

- Fellowship Award, the 9th DOE ACTS Workshop, Lawrence Berkeley National Lab, 2008.
- Student Travel Support, Graduate School, University of Kentucky, 2010-2011.
- Student Travel Support, Graduate School, University of Kentucky, 2009-2010.
- Student Travel Support, Graduate School, University of Kentucky, 2008-2009.
- Student Travel Support, Graduate School, University of Kentucky, 2007-2008.
- Student Travel Support, Graduate School, University of Kentucky, 2006-2007.
- Outstanding Graduate Student Award, Donghua University, China, 1985.

Refereed Publications:

- Changjiang Zhang, Kimberly Forsten-Williams, Michael Fannon, Wehsheng Shen, and Jun Zhang, Parallel Simulation of Multiple Proteins Through a Bioreactor Coupled with Biochemical Reactions, *Proceedings of ACM Int'l Conf. on Bioinformatics and Computational Biology*, 20-28, 2011

- Bing Zhao, Changjiang Zhang, Kimberly Forsten-Williams, Jun Zhang, Michael Fannon, Endothelial Cell Capture of Heparin-binding Growth Factors under Flow, *PLoS Computational Biology*, **6**(10), e1000971, 2010.

- Changjiang Zhang, Kimberly Forsten-Williams, Bing Zhao, Michael Fannon, and Jun Zhang, Coupling Between Heparan Sulfate Proteoglycans and FGF-2 Receptors is Key to FGF-2 Capture Under Flow: A Computational Study, *Proceedings of ACM Int'l Conf. on Bioinformatics and Computational Biology*, 439-441, 2010.

- Wensheng Shen, Changjiang Zhang, Jun Zhang and Xiaoqian Ma, Newton Method for Nonlinear Dynamic Systems with Adaptive Time Stepping, *Journal of Universal Computer Science*, **16**(6), 891-902, 2010.

- Wensheng Shen, Kimberly Forsten-Williams, Michael Fannon, Changjiang Zhang, and Jun Zhang, Multigrid accelerated computation of ligand-receptor interactions under flow condition, *Proceedings of World Congress on Eng. and Computer Sci.*, 949-954, 2009.

- Wensheng Shen, Changjiang Zhang, et al., A computational model of FGF-2 binding and HSPG regulation under flow, *IEEE Transactions on BioMed. Eng.*, **56**(9), 2147-2155, 2009.

- Michael Fannon, Bing Zhao, Changjiang Zhang, Jun Zhang, Wensheng Shen, Kimberly Forstern-Williams, Heparan Sulfate enhances Capture of Heparin-Binding Growth Factors Under flow, *Arterioscler Thromb Vasc Biol*, **29**(7), 127, 2009.

- Changjiang Zhang, Wensheng Shen, Bing Zhao, Michael Fannon, Kimberly Forsten- Williams, Jun Zhang, A Numerical Study of Pulsatile Flow Through a Hollow Fiber Cartridge: Growth Factor-Receptor Binding and Dissociation

Analysis, *Proceedings of Int'l Conf. on Bioinformatics, System Biology and Intelligent Computing*, 435-441, 2009.

- Changjiang Zhang, Wensheng Shen, Kimberly Forsten-Williams, Michael Fannon, Jun Zhang, Simulation of FGF-2 binding with receptors on cell surface on the wall in a bioreactor system, *Proceedings of Int'l. Conf. Bioinformatics and Computational Biology*, 724-727, 2008.

- Wensheng Shen, Changjiang Zhang, and Jun Zhang, Multiscale simulation of ligand-receptor binding and dissociation in circulation, *Proceedings of the 45th ACM Southeast conference*, 519-520, 2007.

- Changjiang Zhang, Design of PCMCIA interface, *China Computer Users*, **27**, 82-83, 1997.

- Changjiang Zhang, The development of general purpose high performance image adaptor based on PCI, *China Computer Users*, **9**, 22-24, 1997.

- Changjiang Zhang, and Hequn Xu, The implementation of crepe weaves design on microcomputers, *Journal of China Textile University*, **15**(1), 1989

- Changjiang Zhang, Zhongwei Hong, and Hequn Xu, A development of CAD-system software in jacquard loom, *Journal of China Textile University*, **12**(6), 43-49, 1986.

Professional Affiliations:

- ACM Student Member